Annual Report 1992

WILL

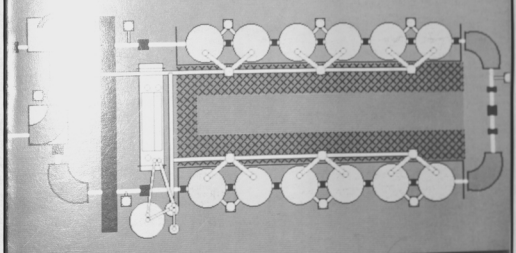

Nuclear Physics Laboratory
University of Washington

ANNUAL REPORT

Nuclear Physics Laboratory
University of Washington
April, 1992

Supported in part by the United States Department of Energy
under grant DE-FG06-90ER40537

INTRODUCTION

The University of Washington Nuclear Physics Laboratory, which is a part of the Department of Physics, operates a tandem/superconducting linac accelerator for on-campus nuclear physics research and also has an extended program of user physics at other accelerators (ATLAS, Saskatoon, SLAC, SPS/CERN, TRIUMF). Our physics program is very broad, as is traditional in our laboratory. This year the investigations range in energy from investigations of cluster-fusion effects at 300 keV bombarding energy to ultrarelativistic heavy ion collisions with 6.4 TeV sulfur ions. They also range from very basic studies which use the nucleus as a testing ground for time reversal invariance and the conservation of vector current to applications of nuclear physics and accelerator techniques to the problems of global warming, medical isotope production, and radiation damage in microelectronics.

During this last year substantial progress has been made in completing the apparatus for our precision test of the CVC, second-class current, and time reversal symmetries in nuclear β-decay. The rotating-target, rotating-catcher-foil system works as well as planned, giving us a ^{8}Li counting rate of 4000 events/sec. We have also begun measurement of the isovector M1 width in ^{8}Be, needed for the CVC comparison to the weak magnetism in A=8 β decay. We employed a technique optimized for angular distribution measurements and obtained an $E2/M1$ radio substantially different from obtained by others in an earlier experiment.

The Eöt-Wash group has continued to improve its rotating torsion-balance instrument and has a new test of the weak equivalence principle with three times the sensitivity of their previous result. The group has also just commissioned a new stationary torsion balance surrounded at close proximity by a rotating 3.0 tonne depleted uranium source. This instrument will be used to search for short-range interactions ($\lambda \leq 1\ cm$) and for macroscopic CP-violating effects.

Our studies of cluster-induced fusion have moved forward on several fronts. We have completed and published measurements with small deuterated water anions which show no collective enhancement, in disagreement with a recent report in the literature. We are also looking for enhancement with carbon clusters, following up on an observation that enhanced fusion is observed with projectile clusters which do not contain deuterons. No cluster enhancement is observed for clusters with up to nineteen carbons. In addition to experimental studies of cluster impact fusion we have developed a theoretical description for this process and a new treatment of energy loss at very low projectile energies.

Studies of sub-barrier fusion spin distributions continue on two fronts. Gamma ray multiplicity measurements have been completed for three entrance channels leading to the same compound nucleus. Rotational state populations have been measured for ^{16}O + ^{154}Sm. Slightly above the barrier the results of this latter probe confirm the mean spin obtained from multiplicity studies, and will provide more differential information about the spin distribution.

Hard photon spectra and angular distributions for 34 MeV proton-induced reactions have been measured and appear to have both nucleon-nucleon bremsstrahlung and direct-semidirect capture contributions.

Among the highlights of our giant resonance research, two items stand out. In a study of GDR decays of hot, very rapidly rotating ^{45}Sc nuclei, we have obtained evidence for an oblate $\rightarrow$ triaxial shape change at angular momentum near the limit of compound nucleus formation. This shape

change is a second-order phase transition in the mean field theory of the rotating liquid drop. The evidence for it comes from the measured spectrum shape for GDR decays to highly excited states, which indicates the presence of very large deformations in the ensemble of decaying states. In separate experiments we have obtained evidence for the restoration of isospin symmetry in highly excited compound nuclei with mass ≈ 60.

In the accelerator mass spectrometry (AMS) program, a systematic analysis of instabilities in the accelerator terminal voltage and of the properties of the high-energy beam transport system has led to the construction of a wide-aperture detector telescope and to the adoption of a wide-open mode of high energy beam transport. These changes have dramatically reduced the sensitivity of AMS measurements to terminal voltage fluctuations. First results on the dating of pollen extracted from peat and lake sediments indicate that reliable radiocarbon dates can be obtained; a two-year NSF grant under the Paleoclimatology of Arctic Lakes and Estuaries (PALE) program will support continuation and extension of this work.

Work continues on the APEX spectrometer at ATLAS. Many of the experiment subsystems have been installed and are undergoing off-line and beam tests.

The preliminary analysis of the measurement at Saskatoon of photoproduction of pions on nuclei has been completed. We are able to obtain clean pion spectra from all the targets. We will be able to determine the A-dependence of the photoproduction cross section from this experiment. A new experiment was approved for quasi-free kaon production on nuclei at CEBAF. This experiment will look for changes in the $N(\gamma, K)Y$ vertex ($Y = \Lambda, \Sigma$) embedded in a nucleus.

Despite the political and economic turmoil in the former Soviet Union, the Dubna-Seattle-Tashkent-TRIUMF collaboration has set up at TRIUMF and had its first data taking run in a new search for dibaryon resonance produced by bombarding nuclei with polarized protons.

Following a hiatus of over two years, fixed target experiments resumed in End Station A at SLAC. Experiment E140X made new measurements of σ_L/σ_T in the nucleon resonance and deep-inelastic (DIS) regimes. The resonance data will test the perturbative QCD scaling laws that have been applied to the elastic proton form factors. The deep inelastic data will contribute to our understanding of the Q^2 evolution of DIS.

As part of our participation in experiment NA35 at CERN, we have made an analysis of systematic effects in the large TPC. This has resulted in improved cluster finding techniques and recognition of the need for improved projectile trajectory definition compatible with the high- resolution TPC. We have also successfully tested 6,656 channels of new readout electronics to be installed in the NA35 TPC before the Spring-1992 run, which will greatly enhance the TPC's coverage and data rate.

As part of our contribution to the RHIC STAR detector system design, we have developed a preliminary trigger system which incorporates a combination of scintillators and gas detectors to yield both minimum bias and higher level triggers over a broad range of event configurations at low cost. As part of the development of a silicon vertex detector for STAR, we have collaborated in setting up an R&D laboratory at LBL to study prototype silicon drift detectors (SDD) and tested a prototype SDD in the M13 pion beam line at TRIUMF.

We have begun a pilot gas detector study associated with trigger development for relativistic

heavy ion detector systems. This study is focussed on the problem of achieving stable very high gain planar geometries in the presence of highly ionizing particles from pion-nucleus interactions.

The Laboratory provides beams for a wide range of uses outside of conventional nuclear physics. This year two groups from the Boeing Company studying radiation damage in electronic devices used our facility. Also a group from the Department of Radiology continued its study of target designs for a new type of production facility for radionuclides of interest in positron emission tomography.

The superconducting booster continues to operate reliably. We are currently able to operate all the resonators in the linac whenever full energy is desired. The transmission of the linac beam has been improved significantly, and it is now generally possible to tune the entire linac during an eight hour period.

As always, we welcome applications from outsiders for the use of our facilities. As a convenient reference for potential users, the table on the following page lists the vital statistics of our accelerators. For further information, please write or telephone Prof. W.G. Weitkamp, Technical Director, Nuclear Physics Laboratory, University of Washington, Seattle, WA 98195; (206) 543-4080.

We close this introduction with a reminder that the articles in this report describe work in progress and are not to be regarded as publications or quoted without permission of the authors. In each article, the names of the investigators have been listed alphabetically, with the primary author underlined.

John G. Cramer
Editor

María G. Ramírez
Assistant to the Editor

TANDEM VAN DE GRAAFF ACCELERATOR

A High Voltage Engineering Corp. Model FN purchased in 1966 with NSF funds; operation funded primarily by the U.S. Department of Energy. See W.G. Weitkamp and F.H. Schmidt, "The University of Washington Three Stage Van de Graaff Accelerator," Nucl. Instrum. Meth. **122**, 65 (1974).

Available Energy Analyzed Beams

Ion	*Max. Current* (pμA)	*Max. Practical Energy* MeV
p,d	10	18
polarized p,d	0.3	18
He	2	27
Li	1	36
C	3	63
O	2	72
Si	0.3	90
Ni	0.2	99
I	0.01	108

BOOSTER ACCELERATOR

We give in the following table maximum beam energies and expected intensities for several representative ions. "Status of and Operating Experience with the University of Washington Superconducting Booster Linac," D.W. Storm *et al.*, Nucl. Instrum. Meth. **A287**, 247 (1990).

Available Energy Analyzed Beams

Ion	*Max. Current* (pμA)	*Max. Energy (MeV)*
p	> 1	35
d	> 1	37
He	0.5	65
Li	0.3	94
C	0.6	170
N	0.03	198
O	0.1	220
Si	0.1	300
^{35}Cl	0.02	358
Ni	0.001	395

Contents

1 Astrophysics

1.1 ^{18}Ne levels above $E_x = 5$ MeV and thermonuclear ^{14}O+α reactions

E.G. Adelberger, A. García* and P.V. Magnus

We have used the ^{16}O(^{3}He,n) reaction to study high-lying levels of ^{18}Ne that could serve as resonances in stellar ^{14}O+α reactions. In the process, we also clarified some aspects of the ^{18}Ne level scheme.

Data were taken at bombarding energies of 10.9, 14.0, and 14.5 MeV, using the UW pulsed-beam time-of-flight spectrometer system. Our high-resolution results for the widths of the 5.106 and 5.153 MeV levels (50 ± 10 and ≤ 8 keV, respectively), together with the known analog levels in ^{18}O provide strong evidence for spin-parity assignments of 2^+ and 3^- respectively. We have identified a $J^\pi = (1^-)$ resonance at 6.15 MeV on the basis of angular distribution data and the calculated ^{18}O–^{18}Ne Coulomb energy shift. As this level is the lowest $J^\pi = 1^-$ resonance in ^{14}O+α, it dominates the reaction rate for $0.1 \geq T9 \geq 1.0$. Our results and analysis disagree in several respects from the previous analysis of Wiescher *et al.*[1] The extracted ^{18}Ne level properties are shown below. This work is being prepared for publication.

Table 1.1. Widths, energies and J^π of levels at $E_x \geq 5$ MeV in ^{18}Ne

previous work			our work		
E_x(MeV±keV)	J^π	Γ(keV)	E_x(MeV±keV)	J^π	Γ(keV)
5.090±8	$(2^+,3^-)$	40±20	5.106±8	2^+	50±10
5.146± 7	$(2^+,3^-)$	25±15	5.153±8	3^-	≤8
5.453± 10	(2^-)	≤50	5.454±8	2^-	≤10
			6.15±10	(1^-)	≤40
6.297±10		≤60	6.30±10		
6.353±10		≤60	6.35±10		
7.059±10		≤180	7.07±10		200±40
			7.35±18		≤50
7.713±10		≤50	7.72±10		≤30
7.950±10		≤60	7.94±10		40±10
8.086±10		≤50	8.11±10		≤30

*Now at: Lawrence Berkeley Laboratory, B-88, 1 Cyclotron Road, Berkeley, CA 94720.

[1] M. Wiescher *et al.*, AP. Jour. **316**, 162 (1987).

1.2 The structure of ^{18}Ne and break out of the hot-CNO cycle

E.G. Adelberger, A. Bacher,* N. Bateman,† G. Berg,* A. García,‡ K. Hahn,† P.V. Magnus, P. Parker† and E. Stephenson*

The $^{14}O(\alpha,p)^{17}F$ reaction plays an important role in explosive hydrogen burning as it is one of two bridges, $^{15}O(\alpha,\gamma)$ being the other, between the hot-CNO cycle and the rapid-proton (rp) process. Ideally one would study this reaction rate directly, but since ^{14}O is unstable ($t_{1/2}$=71sec.) that is very difficult. Fortunately the necessary information can be gotten from study of the structure of ^{18}Ne. The $^{14}O + \alpha$ reaction rate is dominated by resonances in the Gamow window which is at about 6 MeV of excitation in ^{18}Ne; hence the reaction rate can be determined by measuring the parameters of those resonances. The critical parameters are the resonance energy, spin, partial and total widths. Since both ^{14}O and the α-particle have $J^\pi=0^+$ only natural parity levels will contribute to the reaction rate. By comparison with the analog nucleus, a 1^- and a 3^- level are the only natural parity levels expected in the Gamow window. Since the 1^- level is a potential $\ell = 1$ resonance (the lowest ℓ resonance in the Gamow window) it is of critical importance to locate it and determine its structure as it will likely dominate the reaction rate. Little is known about the structure of ^{18}Ne in this region because only two light-ion reactions can be used to study ^{18}Ne, $^{16}O(^3He,n)$ and $^{20}Ne(p,t)$, and they selectively populate only natural-parity levels. García *et al.* studied the $^{16}O(^3He,n)$ reaction with 50 keV resolution and found 3 levels between 5.5 and 7 MeV of excitation in ^{18}Ne an isolated level at 6.15 MeV and a doublet at 6.35 MeV (see section 1.1 of this Report). They made a tentative assignment of 1^- to the level at 6.15 MeV based on its excitation energy and on its narrow (<40 keV) width, and tentatively assign $J^\pi=2^-$ and 3^- to the doublet at 6.35 MeV. The observation of the 2^- is somewhat surprising given that the $^{16}O(^3He,n)$ reaction strongly favors population of natural parity levels. We have time approved and scheduled to study this excitation energy region with the $^{20}Ne(p,t)^{18}Ne$ reaction at IUCF using the K600 spectrometer. This measurement will enable us to study the levels with better than 20 keV resolution. Data from this measurement should enable us to locate all the natural parity levels and to measure the excitation energies and the widths (or limits on widths) of any resonances we see in the region.

*Indiana University Cyclotron Facility, 2401 Milo B. Sampson Lane, Bloomington, IN 47405.
†Yale University, Dept. of Physics, PO Box 6666 Yale Station, New Haven, CT 06511.
‡Now at: Lawrence Berkeley Laboratory, B-88, 1 Cyclotron Road, Berkeley, CA 94720.

1.3 How well do we know the efficiency of ^{71}Ga solar ν detectors?

E.G. Adelberger, W.C. Haxton* and P.V. Magnus

The SAGE and GALLEX groups are currently measuring the solar neutrino capture rate on ^{71}Ga. The efficiency of ^{71}Ga ν_e detectors depends in part on the strength of ν_e captures to excited states of ^{71}Ge. The Gamow-Teller (GT) strengths of these states have been estimated from the ^{71}Ga(p,n) cross section under the assumption that (p,n) cross sections are proportional to GT strength. Recent beta decay measurements of ^{33}Ar and ^{37}Ca have raised doubts that the (p,n) data can be used to reliably extract the small $B(GT)$ strengths necessary to understand the ^{71}Ga solar neutrino capture rate (see section 6.1 of this Report), and no other technique is available to experimentally determine those strengths. Fortunately the strength of the ground state transition is known from the ^{71}Ge lifetime. We are calculating what can be inferred from the results of a ^{71}Ga measurement in light of the uncertainty in GT strength in ^{71}Ge and to what degree these uncertainties can be reduced by calibrating the detector using ^{51}Cr, ^{65}Zn, or ^{37}Ar neutrino sources.

Using the (p,n) $B(GT)$ values for the excited state transitions the expected count rate for a standard solar spectrum (no neutrino oscillations) is 129 SNU. Most of that rate comes from transitions to the ^{71}Ge ground state (whose strength is known) as it is the only level that sees a large fraction of the abundant *pp* neutrinos, and that of GT strength estimated the first excited state transition is very small. Measurements in mass 37, however, show that the (p,n) technique can underestimate such weak transitions by factors of at least six. Taking that as a range for the first excited state $B(GT)$, the standard solar model counting rate could be anywhere between 129 and 160 SNU.

If one assumes neutrino oscillations, as seems to be implied by the SAGE data, the situation is even murkier. In the range of mixing angles and mass differences consistent with results from the Homestake Mine ^{37}Cl and Kamiokande H_2O detectors, many of the low energy neutrinos do not emerge as electron type neutrinos. This greatly reduces the importance of the well-understood ground state transition and most of the rate will come from poorly-understood transitions to higher excited states whose strengths are necessarily based on (p,n) cross sections.

Calibrations using such sources as ^{51}Cr, ^{65}Zn, or ^{37}Ar can give information about the *overall* ^{71}Ga detection efficiency. If the ^{71}Ge *chemical extraction* efficiency is known independently, constraints can be placed on the strengths of the two lowest lying excited states. However, the low energy neutrinos energies from these sources do not provide any information about the strengths of higher excited states which dominate the rate for many possible mixing parameters. Comparison of the counting rates from *two* of these sources will not yield much additional information, since the neutrino spectra they produce are quite similar. In particular the chemical extraction efficiency cannot be determined in this way.

One should note that uncertainties of the kind discussed in this note would be much larger for other detector materials where transitions with $B(GT)$'s measurable in β-decay experiments account for only a small fraction (^{81}Br) or essentially none (^{98}Mo, ^{115}In, and ^{127}I) of the predicted capture rate.

*Physics Department, University of Washington, Seattle, WA 98195.

1.4 Absolute branching ratios in ^{37}Ca β-decay

E.G. Adelberger, P.V. Magnus, M. Mohar,* A. Piechaczek* and E. Roeckl*

The β-decay of ^{37}Ca provides the calibration for the ^{37}Cl neutrino detector, and a favorable case to study Gamow-Teller quenching and the relation between that strength and (p,n) cross sections (see section 6.1, this Report). We recently completed a high-resolution, high-sensitivity measurement of ^{37}Ca β-decay at ISOLDE3 at CERN. That experiment was not complete in a two senses. First, absolute branching ratios were not measured. The branching ratios were normalized to the expected strength for the isobaric analog (IAS) level, which is heavily dominated by the Fermi transition. The strength $B(GT)$ for the IAS was calculated assuming no isospin mixing in the analog level $[B(F) = 3]$ and taking a shell model calculation for the Gamow-Teller (GT) strength $[B(GT) = 0.1]$. Second, the strength of the allowed decay to the bound first excited state was not measured directly; its strength had to be determined from the requirement that the β^+ branching ratios sum to unity.

Although the above assumptions seem very robust, we intend to address these points experimentally. We proposed an experiment at GSI where ^{37}Ca from the Fragment Recoil Separator (FRS) will be implanted in a stack of solid state detectors and the subsequent proton and γ-ray decays will be detected. The experiment has been approved. The protons will be detected by the same counters into which the Ca is implanted, and the γ-rays will be detected in external Ge detectors. The run will be broken into two parts. First, ^{37}Ca ions will be implanted into the detector stack one by one and the subsequent particle decay of each ion recorded. This will enable us to determine directly the branching ratio for the population of the IAS. Second, we will implant the full intensity of ^{37}Ca (1000/sec.) into the detector stack and measure the beta-delayed proton and gamma decays in singles. Due to the electron summing from the internal source, the energy-resolution of this measurement will be much poorer than that of our ISOLDE3 data but with the full intensity (1000 ^{37}Ca per sec. at the FRS compared to 6 ^{37}Ca per sec. at ISOLDE3) and purity (<10 percent impurities at the FRS compared to 10^4 ^{37}K per ^{37}Ca at ISOLDE3) may enable us to see weaker groups in the particle channel and to detect the 1.37 MeV γ-ray with a low-efficiency Ge(Li) detector.

*GSI, Postfach 11 05 52, D-6100 Darmstadt 11, Germany.

1.5 β delayed proton decay of ^{20}Mg and the astrophysical ^{19}Ne(p,γ) reaction rate

R. Anne *et al.*,* S. Kubono *et al.*,† P.V. Magnus and E. Roeckl *et al.*‡

The ^{19}Ne(p,γ) reaction plays a critical role in breakout from the hot-CNO cycle and the ensuing synthesis of heavy ($Z > 10$) elements. The astrophysical ^{19}Ne(p,γ) reaction rate is a strong function of the spins and γ-ray widths of any low ℓ resonances near proton threshold (2.199 MeV) in ^{20}Na. The relevant region of excitation was recently studied using the ^{20}Ne(^{3}He,t) and ^{20}Ne(p,n) reactions in order to locate, and if possible identify, the spins of any possible resonances. These measurements suggest that the ^{19}Ne(p,γ) reaction is dominated by the resonant contribution of a ^{20}Na level at E_x=2.646 MeV. Kubono[1] and Wiescher[2] tentatively assigned the level $J^\pi = 1^+$ based on ^{20}Ne(^{3}He,t) and ^{20}Ne(p,n) angular distributions. As both ^{19}Ne and the proton have $J^\pi = 1/2^+$ s-wave capture can proceed through 1^+ or 0^+ resonances in ^{20}Na. Model calculations predict that the 2.646 MeV level could be the isobaric analog of either the 1^+ 3.173 MeV or the 0^+ 3.526 MeV level in ^{20}F. It is very important to find out if the E_x = 2.646 MeV level has $J^\pi = 1^+$ and not a value such as 0^-, which is also marginally consistent with the (^{3}He,t) and (p,n) studies, and what its resonance strength is.

^{20}Mg beta decay provides a beautiful tool for this task as allowed decays populate only 0^+; $T = 2$ and 1^+; $T = 1$ levels in ^{20}Na. An experiment for measuring β-delayed protons from ^{20}Mg decay has been approved at GANIL and will be performed in early April. ^{20}Mg from the LISE3 facility at GANIL will be implanted into a stack of solid state detectors. The β-delayed protons will be detected in the same detectors. If the 2.646 MeV level is populated, it will decay with nearly 100 percent branch to ^{19}Ne+p. The competing γ-ray branching ratio is estimated to be four orders of magnitude below that of the proton decay. If the 2.646 MeV level is indeed populated by ^{20}Mg decay, a firm 1^+ assignment can be made for that level. It may then be possible to measure its γ-ray branching ratio and hence to make a model independent estimate of it's resonance strength. We will try to do this by measuring γ-rays with Ge counters set up near the implantation detectors. Additionally, analog assignments between the 1^+ levels of ^{20}F and ^{20}Na may be possible by comparing the $B(GT)$'s from ^{20}Mg decay to the measured $B(GT)$'s from the decay of ^{20}O to ^{20}F. Nuclear structure information about the levels can also be obtained from the magnitudes of the $B(GT)$'s and the energy shifts of the analog levels.

If the level is not populated in ^{20}Mg decay, that will imply either that it does not have $J^\pi = 1^+$ or that it has an unusual structure. Additional information will then be necessary to determine its contribution to the reaction rate.

*GANIL, BP 5027, F-14021, Caen Cedex, France.
†Institute for Nuclear Study, University of Tokyo, Midori Cho, Tanashi, Tokyo, 188 Japan.
‡GSI, Postfach 11 05 52, D-6100 Darmstadt 11, Germany.

[1] L.O. Lamm *et al.*, Nucl. Phys. A **510**, 503 (1990).
[2] S. Kubono *et al.*, Z. Phys. A **331**, 359 (1988).

2 Giant Resonances and Photonuclear Reactions

2.1 Isospin purity of highly excited medium-mass nuclei

J.A. Behr,* Z.M. Drebi, M.S. Kaplan, K.A. Snover, D.P. Wells and D. Ye

We have continued our studies of isospin purity in highly excited compound nuclei in the A $\approx$ 60 mass region. Inclusive γ-ray cross sections at 90° have been measured for the decay of the compound nuclei ^{60}Zn, ^{59}Cu, and ^{58}Ni each at approximately 47, 63 and 80 MeV excitation energy. These three compound nuclei were formed with the fusion reactions ^{32}S +^{28}Si, ^{31}P+^{28}Si and ^{32}S +^{27}Al, and ^{31}P +^{27}Al, which have entrance channel isospins T = 0, 1/2, 1/2 and 1 respectively. The quantity of interest is the statistical γ-yield from the decay of the giant dipole resonance (GDR) built on excited states, which is sensitive to the isospin purity of the compound nucleus.[1]

The E1 GDR decays must obey the isospin selection rule $\Delta T = 0, \pm 1$, but no T = 0 to T = 0. Thus, if the entrance channel isospin purity is maintained throughout the equilibration and decay process one expects the decay of the (T = 0) $^{60}Zn^*$ compound nucleus to yield considerably fewer GDR γ-rays than the other two compound nuclei, since it can only decay to T = 1 levels whereas the non-(T = 0) compound nuclei can decay to all levels consistent with $\Delta T = 0, \pm 1$. We compare ratios of cross sections, which one expects to largely cancel experimental systematic errors. In particular, by comparing the experimental cross section ratios to the ratios of CASCADE calculations we avoid a strong dependence of our conclusions on the assumed level densities and we need to know only the ratios of the fusion cross sections.

Preliminary analysis of the ratios of the decay cross sections of ^{60}Zn to ^{59}Cu and ^{60}Zn to ^{58}Ni using statistical CASCADE calculations that include the effects of isospin indicates that the wave functions of these compound nuclei have a small admixture of isospin different from that of the entrance channel. Our preliminary analysis at 47 and 63 MeV excitation energy implies isospin-mixing Coulomb spreading widths of $\Gamma^{\downarrow}_{>} = 20 \pm 10$ keV, which in ^{60}Zn corresponds to a isospin impurity in the compound nucleus of $\alpha^2_{>} = 0.087$ $(+0.029, -0.044)$ and 0.048 $(+0.021, -0.024)$ respectively. At 80 MeV excitation energy our data suggests somewhat larger isospin mixing than expected from the lower energy data. Our results are shown in Fig. 2.1, together with results at lower excitation energy from measurements of particle evaporation cross sections in this mass region.[2] All of the data shown appear consistent with the isospin mixing expected for a constant spreading width independent of excitation energy (dashed curve). We are currently in the process of understanding and reducing the systematic errors in the analysis.

*Now at: Department of Physics, Graduate Physics Building, Center Drive, SUNY at Stony Brook, Stony Brook, NY 11794-3800.

[1]M.N. Harakeh, G. Feldman, E.F. Garman, R. Loveman, J.L. Osborne, and K.A. Snover, Phys. Lett. B **176**, 297 (1986).

[2]J. Wiley, J.C. Pacer, C.R. Lux and N.T. Porile, Nucl. Phys. A **212**, 1 (1973).

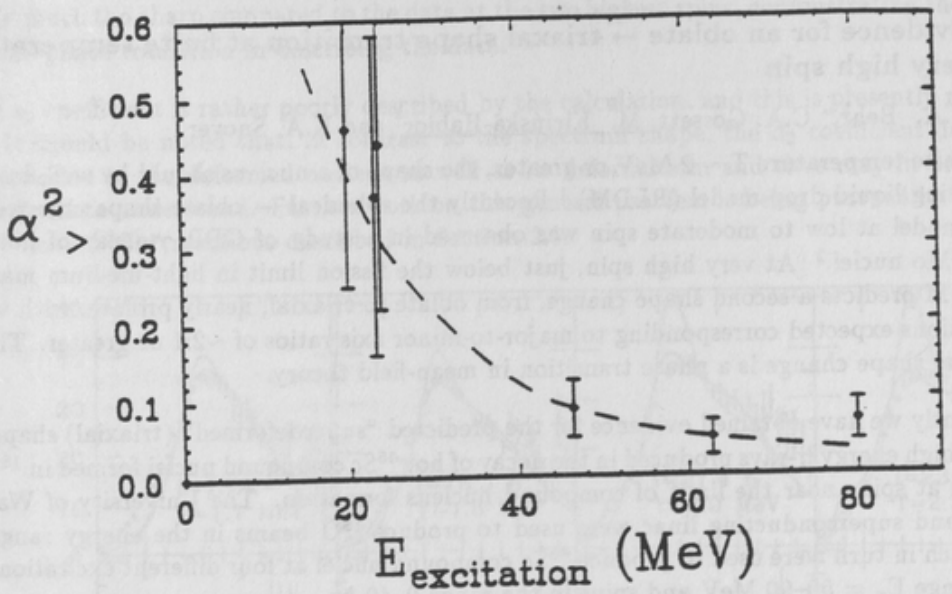

Fig. 2.1. Shown are our preliminary isospin admixtures in ^{60}Zn at excitation energies of approximately 47, 63 and 80 MeV, together with earlier results near $E_{excitation}$ = 20 MeV in this mass region (ref. 2). The curve is a CASCADE calculation assuming $\Gamma^{\downarrow}_{>} = 20keV$, independent of excitation energy.

2.2 Evidence for an oblate → triaxal shape transition at finite temperature and very high spin

J.A. Behr,* C.A. Gossett, M. Kicińska-Habior† and K.A. Snover

At finite temperature T ~ 2 MeV or greater, the shape of a nucleus should be well-described by the rotating liquid drop model (RLDM).[1] Recently the spherical → oblate shape change expected in this model at low to moderate spin was observed in a study of GDR γ-decay of hot rotating ^{90}Zr - ^{92}Mo nuclei.[2] At very high spin, just below the fission limit in light-medium mass nuclei, the RLDM predicts a second shape change, from oblate to triaxial, nearly prolate, with very large deformations expected corresponding to major-to-minor axis ratios of ~2:1 or greater. This oblate → triaxial shape change is a phase transition in mean-field theory.

Recently we have obtained evidence for the predicted "superdeformed" (triaxial) shapes from a study of high energy γ-rays produced in the decay of hot ^{45}Sc compound nuclei formed in $^{18}O + ^{27}Al$ reactions at spins near the limit of compound nucleus formation. The University of Washington tandem and superconducting linac were used to produce ^{18}O beams in the energy range 45–110 MeV which in turn were used to produce ^{45}Sc compound nuclei at four different excitation energies in the range E_x = 50–90 MeV and spins in the range 0–40 $\hbar$.

The measured γ-ray spectral shapes, due primarily to the decay of the giant dipole resonance (GDR) built on excited states, have been analyzed using the Cascade statistical model code to extract the average cross section $\sigma_{abs}(E_\gamma)$ for the inverse process of photoabsorption by the hot nucleus. The results are shown in Fig. 2.2 (top row) as the points with errors for each of the four studied reactions, labelled by the average spin and temperature appropriate to each case. The a_2 angular distribution coefficient in the center-of-mass is shown in the bottom row.

The main feature of interest is the appearance of a second peak or shoulder at $E_\gamma \sim 25$ MeV, on the high energy side of the main GDR peak, for the two higher spin cases. This indicates the presence of large spin-induced deformations $\beta \gtrsim 0.45$ in the ensemble of decaying states.

A quantitative interpretation of the data is greatly aided by comparison with the results of thermal shape fluctuation calculations by Alhassid and Whelan. In these calculations, the nuclear potential energy is found to have an oblate minimum for spins less than 29$\hbar$, the critical value. For higher spins the minimum is triaxial, nearly prolate, with a saddlepoint on the oblate axis at a deformation corresponding to the continuation of the oblate minimum found at lower spin. The result, for spins near and above the critical value, is a very soft potential energy surface with a large equilibrium deformation. The results of thermal shape fluctuation calculations with these surfaces is shown as the heavy solid line in Fig. 2.2, and are in reasonable agreement with the experimental cross sections.

The light solid curves in Fig. 2.2 were obtained using surfaces in which the triaxial shape (phase) transition has been removed. In these surfaces the minimum remains on the oblate axis for all spins, and the curvatures are similar to those found at zero spin. The calculated absorption cross section

*Now at: Department of Physics, Graduate Physics Building, Center Drive, SUNY at Stony Brook, Stony Brook, NY 11794-3800.

†Present address: Institute of Experimental Physics, University of Warsaw, Poland.

[1] S. Cohen, F. Plasil, W.J. Swiatecki, Ann. of Phys. **82** 557 (1974).

[2] J.H. Gundlach, K.A. Snover, J.A. Behr, C.A. Gossett, M. Kicińska-Habior and K.T. Lesko, Phys. Rev. Lett. **65** 2523 (1990).

is clearly much too sharp compared to the data at the two highest spins, demonstrating the essential role of the phase transition in describing the data.

The a_2 coefficient is rather poorly described by the calculation, and this is presently not understood. It should be noted that, in contrast to the spectrum shape, the a_2 coefficient depends on the *orientation* of the deformed nucleus as well as its deformation, and thus may in principle be more difficult to understand. Further work on this general problem is being pursued in a study of $^{18}O + {}^{45}Sc \rightarrow {}^{63}Cu^*$ reactions described in Section 2.6.

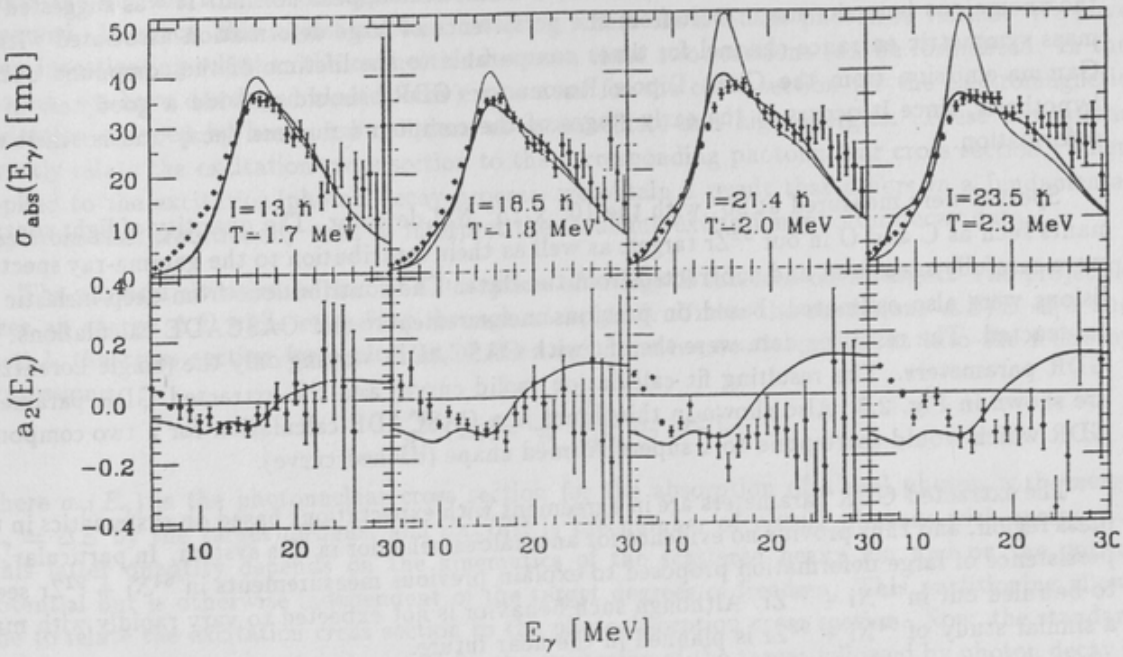

Fig. 2.2. Data points: top row, absorption cross section $\sigma_{abs}^{exp}(E_\gamma)$ determined from the cascade fits to the spectra shape: bottom row, angular distribution coefficient $a_2(E_\gamma)$. Heavy solid curves: fluctuation calculations with the RLDM: light solid curves: fluctuation calculations ($\sigma_{abs}(E_\gamma)$ have been scaled by factors 0.8, 0.8, 1.0 and 1.0 for the four cases respectively, in order to match the experimental magnitudes.

2.3 High energy gamma-ray emission following fusion of ^{58}Ni and ^{92}Zr

Z.M. Drebi, M.S. Kaplan, K.A. Snover and D.P. Wells

We have measured inclusive high energy γ-ray spectra from the decay of ^{150}Er with initial excitation energy $E^* = 57$ MeV formed in the nearly mass symmetric reaction ^{58}Ni + ^{92}Zr at E_{lab} = 241 MeV. Previous studies[1,2] of particle and low energy γ-ray emission in ^{64}Ni + ^{92}Zr — ^{156}Er* indicate anomalous behavior, including the suppression of neutron emission compared to statistical model calculations, whereas ^{12}C + ^{144}Sm induced reactions appear normal. It was suggested that the anomalous behavior may result from the persistence of large deformation associated with the mass symmetric entrance channel for times comparable to the lifetime of the compound nucleus. Gamma-emission from the Giant Dipole Resonance (GDR) should provide a good test of this hypothesis, since it occurs in the early stages of the compound nucleus decay and is sensitive to deformation.

Spectra were measured at 90° with the 10" x 15" NaI detector. The quantity of light contaminants such as C and O in our ^{92}Zr target, as well as their contribution to the gamma-ray spectrum were carefully measured and subtracted from the data. The contributions from deep-inelastic collisions were also estimated, based on previous measurements[3] and CASCADE calculations, and subtracted. The resulting data were then fit with CASCADE, varying only the (single Lorentzian) GDR parameters. The resulting fit calculation (solid curve) and the extracted GDR parameters are shown in Fig. 2.3. Also shown in this figure is a CASCADE calculation for a two component GDR which would correspond to a superdeformed shape (dashed curve).

The extracted GDR parameters are in agreement with expectations based on systematics in this mass region, and thus provide no evidence for anomalous behavior in this system. In particular, the persistence of large deformation proposed to explain previous measurements in ^{64}Ni + ^{92}Zr seems to be ruled out in ^{58}Ni + ^{92}Zr. Although such behavior is not expected to vary rapidly with mass, a similar study of ^{64}Ni + ^{92}Zr is planned in the near future.

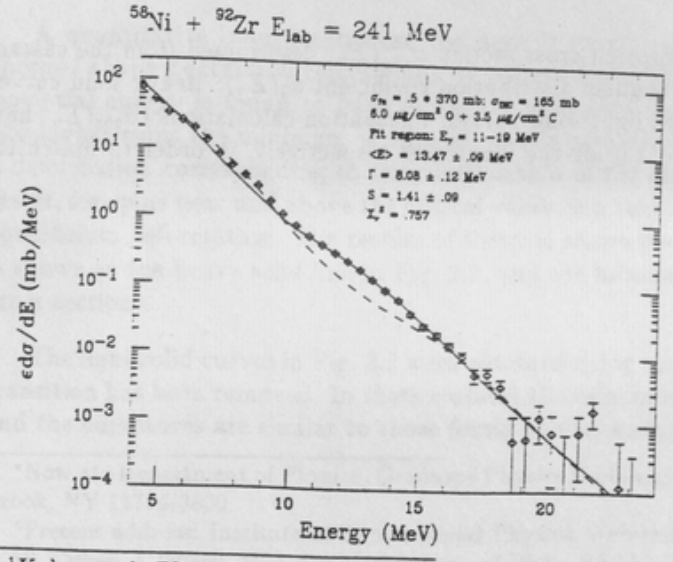

Fig. 2.3. Spectrum obtained after subtraction of target contamination and deep-inelastic contributions, with CASCADE fit (solid) and superdeformation-split GDR (dashed).

[1] Kuhn *et al.*, Phys. Rev. Lett. **51**, 1858 (1983).
[2] Ruckelshausen *et al.*, Phys. Rev. Lett. **56**, 2356 (1986).
[3] F.L.H. Wolfs, Phys. Rev. C **36**, 1379 (1987).

2.4 A formalism for Coulomb excitation/photon decay of the giant dipole resonance

C.A. Bertulani* and A.M. Nathan†

There has been interest in recent years in the study of photon decays of the Giant Dipole Resonance (GDR). Until recently, these studies have utilized the photon scattering reaction. An alternate method has now emerged in which heavy ion collisions are used to electromagnetically excite the nucleus to the GDR (via Coulomb excitation) and the subsequent decay photons are observed. In effect, this is just photon scattering where the incident photon is virtual. We have been investigating whether the connection between these two reactions can be formalized. In the process, we have developed closed-form expressions for the cross section for the electromagnetic excitation induced by heavy ion collisions at intermediate and high energies. These expressions directly relate the excitation cross section to the corresponding photonuclear cross section. When applied to the excitation/photon decay process, we obtain a result that differs in a fundamental way from that traditionally used to interpret the Coulomb excitation/photon decay data.

The physical situation is that of a heavy ion of energy E incident on a target. The projectile loses an energy ΔE while scattering through an angle θ. Under the conditions $\Delta E/E \ll 1$ and $\theta \ll 1$, the cross section for excitation of the target nucleus neatly partitions into the following expression:

$$\frac{d\sigma_C}{d\Omega}\,(E_\gamma) = \frac{1}{E_\gamma}\,\frac{dn_\gamma}{d\Omega}\,\sigma_\gamma\,(E_\gamma),$$

where $\sigma_\gamma(E_\gamma)$ is the photonuclear cross section for the absorption of a real photon with energy $E_\gamma = \Delta E$ by the target nucleus, and $dn_\gamma/d\Omega$ is the number of virtual photons with energy E_γ. This latter quantity depends on the kinematics of the scattered heavy ion and on the optical potential but is otherwise independent of the target degrees of freedom. This partitioning allows one to relate the excitation cross section to the photoabsorption cross section. Now, the standard way to write the cross section $d\sigma_{C\gamma}/d\Omega$ for the excitation of the target followed by photon decay is simply to multiply the above expression by a branching ratio R_γ, which represents the probability that the nucleus excited to an energy E_γ will emit a photon leaving it in the ground state:

$$\frac{d\sigma_{C\gamma}}{d\Omega}\,(E_\gamma) = \frac{1}{E_\gamma}\,\frac{dn_\gamma}{d\Omega}\,\sigma_\gamma\,(E_\gamma)\,R_\gamma\,(E_\gamma).$$

Instead, we propose the following expression:

$$\frac{d\sigma_{C\gamma}}{d\Omega}\,(E_\gamma) = \frac{1}{E_\gamma}\,\frac{dn_\gamma}{d\Omega}\,\sigma_{\gamma\gamma}\,(E_\gamma),$$

where $\sigma_{\gamma\gamma}(E_\gamma)$ is the cross section for photon scattering at energy E_γ. These expressions would be equivalent to each other if it were true that the photon scattering cross section is just the photoabsorption cross section times a branching ratio. In fact, it is not true. In particular, it is not correct to think of photon scattering as a two-step process of excitation to a definite energy followed by photon decay. We are in the process of exploring the implications of using our new expression for the analysis and interpretation of Coulomb excitation/photon decay data.

*Michigan State University, National Superconducting Cyclotron Laboratory, East Lansing, MI 48824.
†Permanent address: University of Illinois at Urbana-Champaign, Nuclear Physics Lab, Champaign, IL 61820.

2.5 Statistical and nonstatistical photon emission from giant resonances

A.M. Nathan*

In view of the recent interest in the study of the photon decay modes of "cold" giant multipole resonances, we have undertaken a project to investigate the effect of the underlying compound nuclear (CN) levels on the interpretation of the experimental data. If one characterizes these CN levels by an average total decay width Γ and by an average spacing D, then the parameter Γ/D characterizes the degree to which the levels overlap. In one extreme regime where the CN levels are non-overlapping ($\Gamma/D \ll 1$), the giant resonance would have an underlying fine structure that one could measure, in principle, with a probe having sufficiently good energy resolution. Averaging over the fine structure, one would expect that the properties of the giant resonances are determined entirely by the average properties of the CN levels. In the opposite regime, where the CN levels are strongly overlapping ($\Gamma/D \gg 1$), the giant resonance would have no resolvable underlying fine structure and so it seems reasonable that one can treat it as though it were a single nuclear level. Between those two extremes, the situation can be quite complicated.

We have developed a formalism that allows one to interpret photon-decay data, taking full account of the underlying CN levels for arbitrary Γ/D. We specifically apply this formalism to reactions we refer to as "generalized photon scattering", which includes the scattering of real as well as virtual photons. The distinguishing feature of these reactions is that the matrix element for excitation of the giant resonance is proportional to the matrix element for photon decay back to the ground state. Our results can be summarized in the following formula, which relates the energy-averaged scattering cross section $\overline{\sigma}_{sc}$ to the energy-averaged photoabsorption cross section $\overline{\sigma}_T$:

$$\overline{\sigma}_{sc} = \frac{8\pi}{3}\left[\left|\frac{E\overline{\sigma}_T(E)}{4\pi\hbar c}\right|^2 \mathcal{E} + \left|\frac{E^2}{2\pi^2\hbar c} P\int_0^\infty \frac{\sigma_T(E')dE'}{E'^2 - E^2}\right|^2\right],$$

This expression would be identical to the "usual" expression relating the scattering to the photoabsorption cross section if the enhancement factor $\mathcal{E}$ were equal to one. The dependence of the scattering cross section on the statistical properties of the CN levels is contained entirely in $\mathcal{E}$, which depends on the distribution of ground-state and total decay widths about their mean value, the distribution of level spacings about the mean value D, and the degree to which the CN levels overlap (Γ/D). In general $\mathcal{E} \geq 1$; in the limit of strongly overlapping levels ($\Gamma/D \gg 1$), $\mathcal{E}$=1. In that limit the resulting expression for the scattering cross section is precisely that expected in the absence of underlying fine structure. Physically this makes sense: for strongly overlapping levels, the fine structure "melts" into the continuum and all the effects of such fine structure on the scattering cross section disappear. In the GDR region, photon scattering data have traditionally been analyzed by implicitly assuming this limiting case, even though it is not always valid. In general the scattering is *enhanced* over that expected in the continuum case. Stated differently, the average elastic scattering cross section is greater than that predicted from the average photoabsorption cross section if the actual photoabsorption cross section varies more rapidly with energy than the average. That enhancement is contained in the factor $\mathcal{E}$.

We have used this formalism to reanalyze photon scattering data in the low-energy tail of the GDR of ^{208}Pb, where the continuum approximation is not expected to be valid. Photoneutron cross sections from Saclay were used to predict the scattering cross section from the above formula.

*Permanent address: University of Illinois at Urbana-Champaign, Nuclear Physics Lab, Champaign, IL 61820.

The enhancement factor was calculated using the "picket fence" assumption for the distribution of level spacings and a Porter-Thomas distribution for the distribution of partial widths. A standard Hauser-Feshbach calculation was used in conjunction with transmission coefficients from an optical model calculation in order to calculate Γ/D for 1^- states in ^{208}Pb as a function of excitation energy. The calculation is compared to data Fig. 2.5. The dashed curve shows the calculated cross section with the enhancement factor set equal to one, while the solid curve shows the full calculation. There are no adjustable parameters in the calculation. It is quite clear that the enhancement factor removes most of the discrepancy between the scattering and photoabsorption data in that energy region. It is interesting to compare this situation to that of ^{206}Pb. While one expects the gross properties of GDR to be similar in the two lead isotopes, one expects the scattering in the low-energy tail to be considerably less enhanced in ^{206}Pb than in ^{208}Pb, since Γ/D is perhaps 5 times larger in ^{206}Pb. Scattering data from Illinois seem to be consistent with an enhancement factor of one. Calculations are under way to see if that conclusion is consistent with the statistical properties of the CN levels in ^{206}Pb.

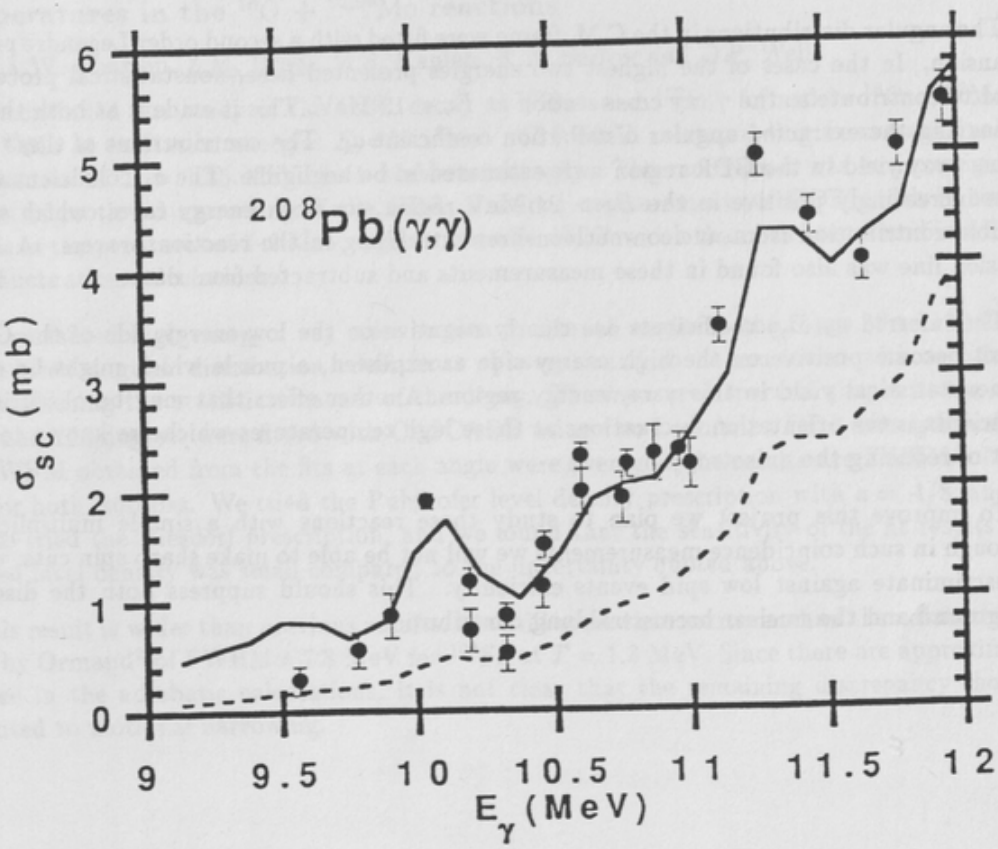

Fig. 2.5. Photon scattering on the low-energy side of the GDR of ^{208}Pb. The solid curve is the full calculation and the dashed curve is the calculation with the enhancement factor equal to one.

2.6 Giant dipole resonance decays of ^{63}Cu formed at high spins and temperatures in the ^{18}O + ^{45}Sc reaction

A.W. Charlop, Z.M. Drebi, M.S. Kaplan, M. Kicińska-Habior,* K.A. Snover and D.P. Wells

In the rotating liquid drop model (RLDM)[1] a transition from oblate noncollective to triaxial prolate-like shapes with very large deformation is predicted in medium mass nuclei for spins just below the fission limit. The prediction of these equilibrium superdeformations motivated us to study giant dipole resonance decays from nuclei around mass 60.[2] The GDR spectrum shape and angular distribution should be sensitive to large nuclear deformations. We have studied the ^{18}O + ^{45}Sc entrance channel forming ^{63}Cu nucleus with initial excitation energies $E^* = 61.1$, 73.9, 99.0, 113.0, and 130.1 MeV, and with average spins $\overline{I}$=15$\hbar$, 21$\hbar$, 30$\hbar$, 33$\hbar$, and 33$\hbar$, respectively. This asymmetric entrance channel should allow the detection of possible nuclear bremsstrahlung at high bombarding energies. Inclusive γ ray cross sections were measured at five lab angles: θ_{lab} =40, 55, 90, 125, and 140 degrees. Results of the first three energy cases were presented earlier.[3] The measured spectral shapes at 90 degrees were fitted with CASCADE using two-Lorentzian GDR strength functions and the Reisdorf level density approach.[4]

The angular distributions in the C.M. frame were fitted with a second order Legendre polynomial expansion. In the cases of the highest two energies presented here, nonstatistical processes were found to contribute to the γ ray cross section at $E_\gamma < 12$ MeV. This is evident at both the spectral shapes and the extracted angular distribution coefficient a_1. The contributions of these processes to the γ ray yield in the GDR region were estimated to be negligible. The a_1 coefficient was found to be increasingly positive in the $E_\gamma > 24$ MeV region, for both energy cases, which suggests a possible contribution from nucleon-nucleon bremsstrahlung in the reaction process. A 15.1 MeV emission line was also found in these measurements and subtracted from data.

The inferred $a_2(E_\gamma)$ coefficients are clearly negative on the low-energy side of the GDR, and do not become positive on the high energy side as expected, a puzzle which might be related to the nonstatistical yield in this γ ray energy region. Another effect that may be obscuring the a_2 coefficients is the orientation fluctuations at these high temperatures which are known to have the effect of reducing the anisotropy.

To improve this project we plan to study these reactions with a simple multiplicity filter. Although in such coincidence measurements we will not be able to make sharp spin cuts, we expect to discriminate against low spin events efficiently. This should suppress both the discrete line background and the nuclear bremsstrahlung contribution.

---

*Present address: Institute of Experimental Physics, University of Warsaw, Poland.

[1] S. Cohen, F. Plasil and W.J. Swiatecki, Ann. Phys. 82, 557 (1974).

[2] See section 2.4.

[3] Nuclear Physics Laboratory Annual Report, University of Washington (1991) p. 5.

[4] M. Kicińska-Habior *et al.*, Phys. Rev. C41 2075 (1990).

Fig. 2.6. Angular distribution coefficients for ^{18}O + ^{45}Sc forming ^{63}Cu at E^* =113 and 130 MeV.

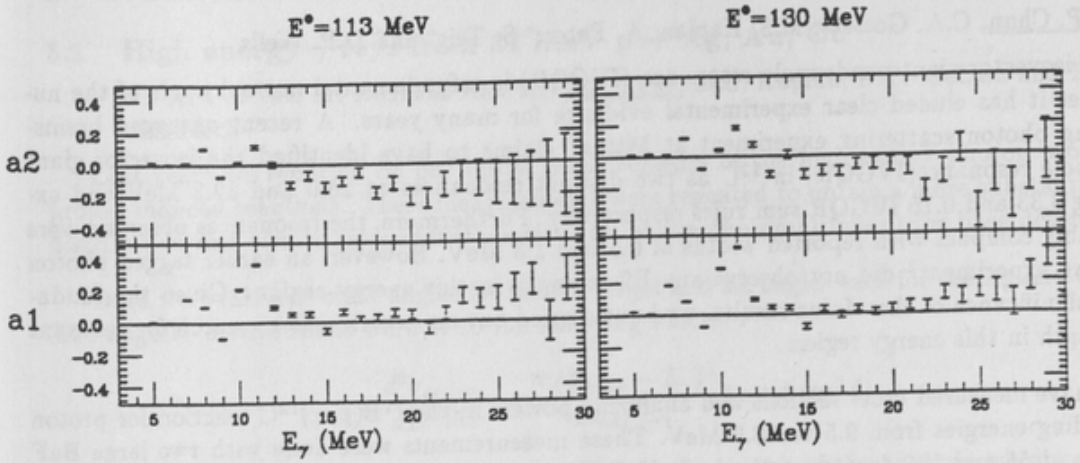

2.7 Giant dipole resonance decays of $^{108,112}Sn$ isotopes formed at moderate temperatures in the ^{16}O + $^{92,96}Mo$ reactions

A.W. Charlop, Z.M. Drebi, M.S. Kaplan, K.A. Snover and D.P. Wells

We continued our study of the GDR decay of $^{108}Sn^*$ and $^{112}Sn^*$ formed in ^{16}O + ^{92}Mo, and ^{16}O + ^{96}Mo at excitation energies E_x=50.8 MeV, 55.8 MeV, corresponding to average final-state temperatures of T = 1.35 MeV, 1.41 MeV respectively. The motivation was to investigate the question of motional narrowing of the GDR. Previous measurements of GDR width in some Sn isotopes at temperatures of 1–2 MeV suggest a smaller GDR width than has been found in adiabatic shape fluctuation calculations.[1]

We measured high energy γ ray cross section at five lab angles in the range 40 to 140 degrees. The deduced angular distribution coefficients a_1 were found to be consistent with zero in both cases confirming the statistical nature of the decay. The measured spectral shapes at the angles: 55 ,90 and 125 degrees were fitted with CASCADE using two Lorentzian GDR strength functions. The FWHM obtained from the fits at each angle were averaged; the results are FWHM= 7.0 ± .3 MeV for both isotopes. We tried the Puhlhofer level density prescription with $a = A/8$, and $A/9$. We also tried the Riesdorf prescription, and we found that the sensitivity of the fit results to the assumed level density was small compared to the uncertainty quoted above.

This result is wider than previous results, but still somewhat narrower than the adiabatic calculation by Ormand[2] of FWHM= 7.8 MeV for ^{108}Sn at T = 1.3 MeV. Since there are approximations involved in the adiabatic calculations, it is not clear that the remaining discrepancy should be attributed to motional narrowing.

[1] Nuclear Physics Laboratory Annual Report, University of Washington (1991) p. 7, and references therein.
[2] W.E.Ormand *et al.* Phys. Rev. Lett. **64**, 2254 (1990). See also Alhassid and Bush Phys. Rev. Lett. **63**, 2452 (1989).

2.8 Polarized radiative capture in $^{11}B(\vec{p},\gamma)^{12}C$

P. Chan, C.A. Gossett, M.S. Kaplan, A. Peter,* S. Teis* and D.P. Wells

The isovector giant quadrupole resonance (IVGQR) is a fundamental normal mode of the nucleus, yet it has eluded clear experimental evidence for many years. A recent untagged bremsstrahlung photon scattering experiment at Mainz[1] claims to have identified the isovector giant quadrupole resonance(IVGQR) in ^{12}C as two distinct resonances at 26.0 and 32.3 MeV and exhausting 0.33 and 0.75 IVGQR sum rules respectively. Furthermore, the resonances observed were remarkably compact with reported widths of 0.5 and 1.3 MeV. However, an earlier tagged photon scattering experiment[2] did not observe any E2 strength in this energy region. Given the fundamental significance of the Mainz results, we have carried out an experiment to search for resonant E2 strength in this energy region.

We have measured cross sections and analyzing powers in the $^{11}B(\vec{p},\gamma)^{12}C$ reaction for proton bombarding energies from 9.5 to 18.9 MeV. These measurements were done with two large BaF detectors at 55 and 125 degrees. and a large NaI detector at 90 degrees. The signature of resonant E2 strength is a large fore-aft cross section asymmetry or large analyzing power due to interference between the dominant E1 giant dipole resonance (GDR) tail and any E2 amplitudes. We used polarized proton beams of $\approx$ 35 to 60 nA on target, which resulted in a counting rate of 10 to 30 kHz. The absolute beam polarization was measured using a ^4He gas target in a separate chamber. The beam polarization was monitored throughout the experiment by elastic scattering into two particle monitor detectors located symmetrically about the beam axis.

A preliminary analysis of the 90 degree data has been done and the analyzing power as a function of excitation energy (γ-ray energy) is shown in Fig. 2.8. These preliminary results show no evidence for compact resonant E2 strength. The monotonic increase of the 90 degree analyzing power with excitation energy arises from the interference of nonresonant, "direct" E2 strength with the GDR tail. The data at 55 and 125 degrees are currently being analyzed. The γ-ray spectra of the 90 degree data were fitted using the lineshape given by P.B. Fernández,[3] and the areas of the photopeaks were extracted.

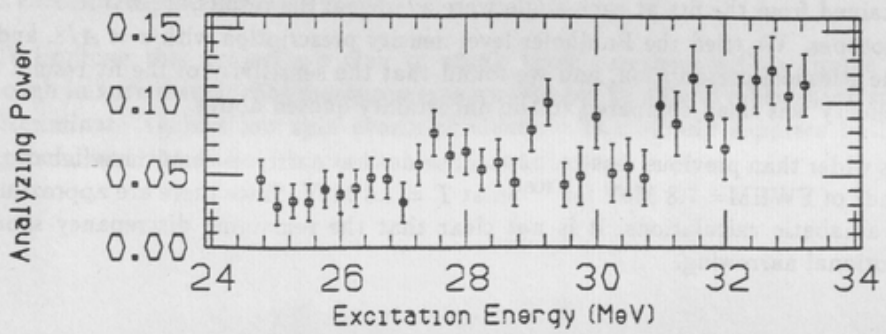

Fig. 2.8. Analyzing power vs. excitation energy at 90 degrees.

*Permanent address: Justus Liebig University, Germany.

[1]K.P. Schelhaas *et al.*, Nucl. Phys. **A506**, 307 (1990).
[2]D.H. Wright *et al.*, Phys. Rev. C **32**. 1174 (1985).
[3]Nuclear Physics Laboratory Annual Report. University of Washington (1985) p. 65.

3 Nucleus-Nucleus Reactions

3.1 High energy γ rays from 34 MeV p + Ag, Au, Cu

C. A. Gossett, M. Kicinska-Habior,* S.J. Luke, M.S. Kaplan, B.T. McLain and R. Vandenbosch

Last year[1] we reported on our initial measurements of the high energy photon production in proton induced reactions. These measurements were repeated to obtain a more substantial angular distribution and also to take advantage of a new active photomultiplier tube base design.[2]

Data were taken at eight angles for the Au target and six angles each for the Ag and Cu targets. The angular distributions were fit to the following function[3]

$$\frac{d^2\sigma_{source}}{dE \cdot d\Omega} = \frac{N\,(E_{max} - E_\gamma)^\lambda}{E_{max}\,E_\gamma}\,(a + b\cos^2\theta),$$

simultaneously for all of the angular data. During the course of the analysis we discovered that the value of E_{max} had to be modified for each angle because the effective Fermi energy changes as a function of angle in the laboratory frame. The modification of the Fermi energy was obtained, self-consistently, by assuming a local Fermi momentum as a function of detection angle in the laboratory. This local Fermi momentum arises from the transformation of the Fermi sphere in the source frame to a Fermi ellipse, whose eccentricity is a function of the velocity of the source in the laboratory frame.

There seems to be some enhancement of the γ ray yield near 35 MeV for all three targets compared to the above function. We think these γ rays might be produced via a direct/semi-direct mechanism. Calculations are being performed to ascertain the magnitude of the yield from such a mechanism. These data are being compared to the bremsstrahlung predictions of the model of Randrup and Vandenbosch[4] to serve as a zeroth order calibration for γ rays produced in heavy ion collisions.

---

*Insitute of Experimental Physics, University of Warsaw, Poland.

[1] Nuclear Physics Laboratory Annual Report, University of Washington (1991) p. 14.

[2] Nuclear Physics Laboratory Annual Report, University of Washington (1991) p. 72.

[3] K. Nakayama and G. F. Bertsch, Phys. Rev. C **34**, 2190 (1986).

[4] Nucl. Phys. A **490**, 418 (1988).

3.2 High energy γ rays from ^{14}N + Ag at 35 MeV/A – revisited

W. Benenson,* J. Clayton,† K. Joh,* D. Krofcheck,‡ S.J. Luke, T.K. Murakami,§ J. Stevenson† and R. Vandenbosch

Several years ago [1] we described measurements of the emission of high energy γ rays in the the reaction ^{14}N + Ag at 35 MeV/A. During the course of the re-analysis[2] an interesting feature of the angular distributions was discovered.

It has been generally thought that most of the hard photon production in heavy ion collisions is the result of bremsstrahlung arising from nucleon-nucleon collisions[3], specifically *pn* collisions because *pp* collisions would be less important by two orders of magnitude on the basis of multipole arguments. The resulting angular distribution would be predominately dipole in nature. This angular distribution would, however, be smeared to yield a more isotropic angular distribution because of the Fermi motion of the nucleons in the nuclei.

The data were fit to all of the angles simultaneously, using the function

$$\frac{d^2\sigma_{source}}{dE \cdot d\Omega} \propto e^{-E_\gamma/E_o} \sum_{\ell=0}^{2} \alpha_{\ell 0} \, |\chi_{\ell 0}(\cos\theta, \phi)|^2 \, .$$

The functions $\chi_{\ell 0}(\cos\theta, \phi)$ in the above expression are the vector spherical harmonics and $\alpha_{\ell 0}$ are the multipole expansion coefficients. The *best* fits to the data seem to indicate the presence of a quadrupole (α_{20}) term. The ratio of the quadrupole to the dipole contribution is 1:2. Nifenecker and Pinston[4] have suggested that the angular distribution for γ rays produced in heavy ion collisions which is

$$2\beta^2 \sin^2\theta[1 + 10\beta^2 \cos^2\theta].$$

The quantity β in the above expression is the velocity of the source in the laboratory frame. This, for our system, leads to a quadrupole/dipole ratio of only 1:6 and therefore cannot be the explanation for the quadrupole contribution in our data.

We are not able to ascertain from the present data whether or not the quadrupole component arises from a nucleon-nucleon mechanism or a nucleus-nucleus mechanism. It is not at all clear whether the "quadrupole" component in the angular distribution is real or an aberration; but, if real, it is unexpected and not at all easily understood.

*National Superconducting Cyclotron Laboratory, Michigan State University, East Lansing, MI.
†Science Applications International Corp., Santa Clara, CA.
‡Lawerence Livermore Laboratory, Livermore, CA.
§Tokyo Institute of Technology, Tokyo, Japan.

[1] Nuclear Physics Laboratory Annual Report, University of Washington (1989), pp. 10–11.
[2] S.J. Luke *et al.*, submitted to Phys. Rev. C.
[3] W. Cassing, V. Metag, U. Mosel and K. Niita, Phys. Rep. **188**, 363 (1990).
[4] Prog. Part. Nucl. Phys. **23**, 271 (1989).

3.3 Modeling cluster emission in heavy ion reactions

C. Hyde-Wright and R. Vandenbosch

The transport model of Randrup and Vandenbosch[1] describes the emission of energetic nucleons and γ-rays in heavy ion fusion reactions. The model is particularly relevant for collisions in which the relative motion of the two ions is comparable with the fermi velocity of nucleons in each nucleus. The projectile and target are each treated as an ideal fermi gas with a time dependent temperature. As the nuclei collide, there is a flux of nucleons across the neck formed between the two nuclei. Once across the neck, a nucleon which was bound in the donor nucleus may be unbound in the receptor. When this nucleon reaches the nuclear surface, a quantal transmission coefficient is calculated to determine the probability of transmission or reflection. Reflected nucleons are assumed to be equilibrated, thereby transferring momentum and heat to the receptor nucleus. Prior to reaching the nuclear surface, the nucleon may suffer one or more NN collisions, in which case each of the nucleons is followed to the surface.

This model is a semiclassical implementation of the expansion of nuclear dynamics in terms of independent nucleons in a mean field, plus two body correlations, plus higher order correlations. We are now developing an extension of this model in which we treat the emissions of deuterons on the same level as the emission of nucleons.

Following a np collision, the relative momentum state of the pair will have a significant overlap with the deuteron momentum space wave-function. However, the np pair cannot form a deuteron without exchanging energy or momentum with the rest of the nucleus, *i.e.* the nuclear mean field. In this model, the natural mechanism for exchanging momentum with the mean field is the refraction of a particle at the nuclear surface.

Consider first a nucleon of momentum $\mathbf{p}$ inside the nucleus, and incident on the nuclear surface (assumed to be plane) at an angle θ. The nucleon will be refracted to momentum $\mathbf{p}'$ at an angle θ' governed by energy conservation and a generalized Snell's law:

$$\frac{\mathbf{p}^2}{2M} + U_N = \frac{\mathbf{p}'^2}{2M} \qquad \frac{Mc}{|\mathbf{p}|}\sin\theta = \frac{Mc}{|\mathbf{p}'|}\sin\theta', \tag{1}$$

where U_N is the potential energy. The momentum transfered to the nucleus is $\mathbf{p} - \mathbf{p}'$. Now consider a np pair of total momentum $\mathbf{P} = \mathbf{p}_1 + \mathbf{p}_2$ and relative momentum $\mathbf{q} = (\mathbf{p}_1 - \mathbf{p}_2)/2$. The energy conservation equation for the refraction of this pair at the nuclear surface into a deuteron state is:

$$\frac{\mathbf{P}^2}{4M} + \frac{\mathbf{q}^2}{M} + U_n + U_p = \frac{\mathbf{P}'^2}{2M_D} + (M_D - 2M) \tag{2}$$

Thus the momentum transfer to the nuclear mean field: $\mathbf{P} - \mathbf{P}'$, places the np pair on the deuteron energy shell.

In our model, if an np pair scatters in the nucleus (with final np relative momentum q) and if the np center-of-mass reaches the nuclear surface without either nucleon rescattering on a third nucleon, we will calculate the probability to form a deuteron as the product of the wave-function overlap squared $|\psi_D(q)|^2$ times the square of the transmission coefficient satisfying the energy conservation condition of Eq. 2. Reflected pairs will be equilibrated.

[1] J. Randrup and R. Vandenbosch, Nucl Phys **A490** 418 (1988).

3.4 Scattering of 87 Mev ^{6,7}Li on ^{12}C

W.J. Braithwaite,* J.G. Cramer, S.J. Luke, B.T. McLain, D.J. Prindle and D.P. Rosenzweig

We are finishing our investigation of the scattering of ^{6,7}Li at 10–15 MeV/nucleon and have done two booster experiments this year to complete our angular distributions. We now have elastic and inelastic cross sections for 87 MeV ^{6}Li + ^{12}C from 4° to 100° in the center of mass and for 87 MeV ^{7}Li + ^{12}C from 4° to 85°. The energy resolution of the booster allowed us to separate the first excited state of ^{7}Li by using narrow acceptance angles and a position sensitive detector.

Fig. 3.4 shows our ^{6}Li cross sections and an optical model fit using Woods-Saxon potentials. The last 20° or so of our data determine a unique potential from a few discrete potentials that fit the data out to 80°. The near-far decomposition shows the dominance of the far side scattering amplitude at large angles and a small airy minimum prior to a nuclear rainbow. The deeper potentials that fit the data inward of 80° show that the ambiguity arises from a shift of the airy minimum of the rainbow and that the minimum is due to interference between the low L and high L partial waves. The weak absorption of ^{6}Li allows the low L waves to pass through the interior region and makes the large angle data sensitive to the potential at small radii.

Our ^{7}Li data show that the first excited state is still significant even at large angles and needs to be resolved to get the correct elastic cross section. Our data also show a sharp fall off at large angles compared to the ^{6}Li data and we plan to use folding model potentials to investigate the density distributions in both cases. Electron scattering experiments have shown a large tail in the charge distribution of ^{6}Li compared to ^{7}Li which should give visible differences in the scattering data. Finally, our inelastic cross sections should provide tests of breakup model analyses which have had success at higher energies.

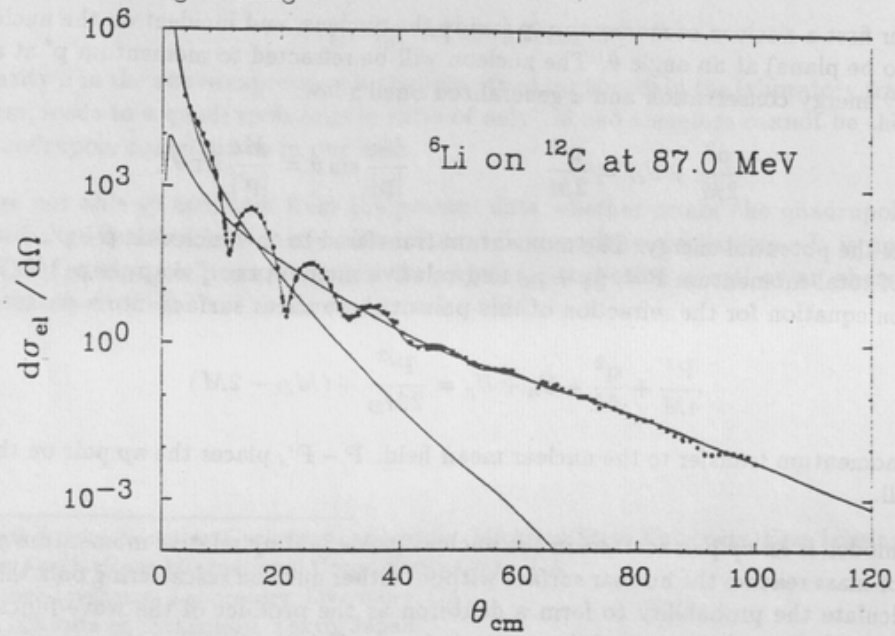

Fig. 3.4. Elastic scattering angular distributions for 87.0 MeV ^{6}Li + ^{12}C with an optical model fit and near-far decomposition.

*Department of Physics and Astronomy, University of Arkansas at Little Rock, Little Rock, AK 72204.

3.5 Entrance channel effects in sub-barrier fusion

J.D. Bierman, A.W. Charlop, Z. Drebi, A. García,* S. Gil,† D.J. Prindle and R. Vandenbosch

We have completed gamma-ray multiplicity measurements for three systems (^{28}Si + ^{142}Ce, ^{32}S + ^{138}Ba, and ^{48}Ti + ^{122}Sn) in our studies of the sub-barrier fusion process. As mentioned previously[1] all three systems lead to the same compound nucleus at approximately the same excitation energies. Our measurements cover an energy range from well above to nearly 10 percent below the interaction barrier of each system. The multiplicities that we obtained are shown in Fig. 3.5 as a function of energy relative to the interaction barrier in the compound nuclear system. We have resolved the inconsistencies that were present in our two ^{28}Si data sets which were caused by inconsistent background subtraction. As can be seen, all three systems produce multiplicities which are consistent with the expectation that the average multiplicity will increase with projectile size. Work on the ^{82}Se + ^{88}Sr system has been postponed due to difficulties in obtaining a ^{82}Se beam through our LINAC booster.[2]

Further analysis of these results is awaiting fusion cross sections from our collaborators at TANDAR in Buenos Aires, Argentina. These cross sections were measured by a delayed x-ray method spanning the same energy range as our multiplicity experiments. The absolute fusion cross sections derived by this method have proven sensitive to input parameters of the complicated decay schemes involved, and we have been working closely with our collaborators to establish these parameters from tabulated data.

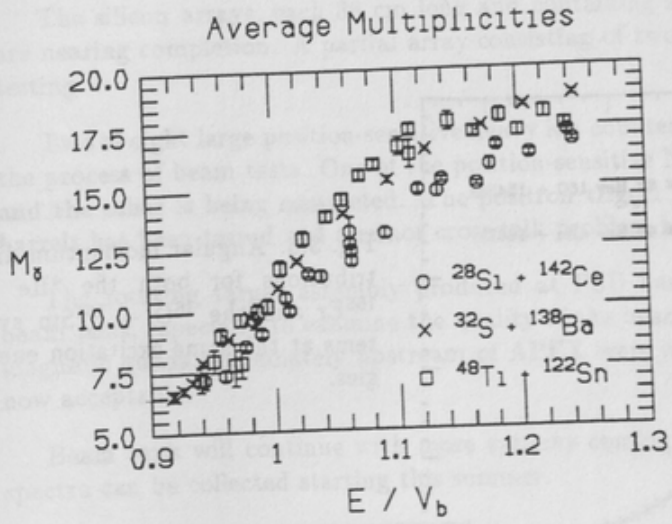

Fig. 3.5. Gamma multiplicities as a function of energy relative to the barrier for ^{28}Si + ^{142}Ce (open circles), ^{32}S + ^{138}Ba (crosses), and ^{48}Ti + ^{122}Sn (open squares).

*Lawrence Berkeley Laboratory (LBL), Berkeley, CA 94720.
†Dept. of Physics, University of British Columbia, Vancouver, British Columbia, Canada V6T 1W5.

[1] Nuclear Physics Laboratory Annual Report, University of Washington (1991) p. 18.
[2] Nuclear Physics Laboratory Annual Report, University of Washington (1992) sec. 11.6.

3.6 Rotational state populations in near-barrier fusion

J.D. Bierman, A.W. Charlop, D.J. Prindle and R. Vandenbosch

The unexpected enhancement of fusion cross section in near barrier reactions has led to several experimental probes of the angular momentum distribution in the compound nuclei of these reactions. Many of these methods have been discussed in a recent review article.[1] This experiment is one such probe. Last year we reported[2] that we had began studies on the $^{16}O + {}^{154}Sm - {}^{170}Yb$ system by determining the rotational state populations for the 4n decay channel of the compound nucleus produced with 68 MeV ^{16}O. This was done using two Compton-suppressed intrinsic Ge detectors and a GeLi detector to tag on certain peaks in the rotational band. Since the last report we have repeated the experiment with 48 MeV $^{4}He + {}^{166}Er - {}^{170}Yb$. The 48 MeV bombarding energy was chosen to match excitation energies in the same compound nucleus as the previous experiment. We use the alpha run to calibrate or check the statistical decay model parameters so that we can extract the angular momentum distribution using the model. Since for very asymmetric systems at well above barrier energies we can accurately predict the spin distribution for the compound nucleus, we can check that the statistical decay model yields the correct spin distribution when the rotational state populations which were experimentally determined are matched. Fig. 3.6 shows the spin population used for the $^{4}He + {}^{166}Er$ system and the resulting distribution for the $^{16}O + {}^{154}Sm$ system. The distribution is much broader for the $^{16}O + {}^{154}Sm$ system as has been seen in other experiments. The average spin, $\langle \ell \rangle = 13.66$, which we determined also agrees with other methods.[3] Since these runs we have received our third Compton-suppressed intrinsic Ge detector which we added to the experimental setup in January when we repeated the experiment with 65 Mev $^{16}O + {}^{154}Sm$. These data are currently being analyzed.

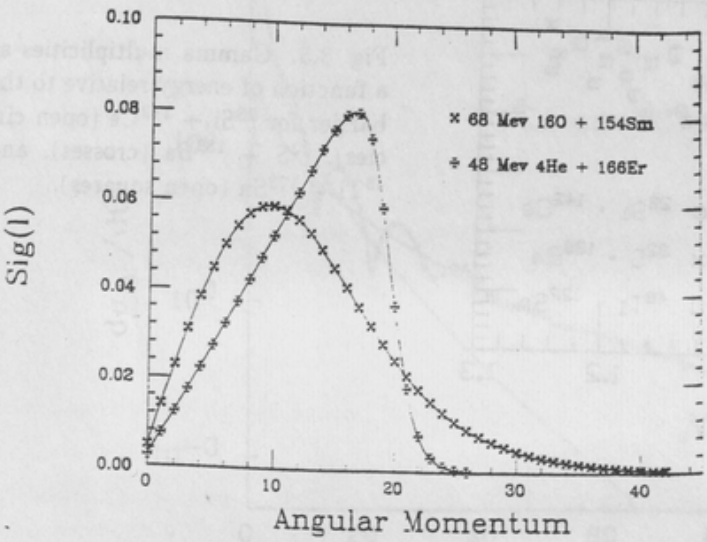

Fig. 3.6. Angular momentum distributions for both the $^{4}He + {}^{166}Er$ and the $^{16}O + {}^{154}Sm$ systems at the same excitation energies.

[1] R. Vandenbosch, Annual Review of Nuclear Science, to be published.

[2] Nuclear Physics Laboratory Annual Report, University of Washington, (1991) p. 22.

[3] S. Gil, A.W. Charlop, A. García, D.D. Leach, S.J. Luke, S. Kailas, and R. Vandenbosch, Phys. Rev. Lett. C **43** 701, (1991).

3.7 APEX progress report

T.A. Trainor and the APEX Collaboration: I. Ahmad,* S. Austin,† R. Betts,* F.P. Calaprice,‡ P. Chowdhury,§ R. Dunford,* J.D. Fox,¶ S. Freedman,* S. Gazes,‖ B. Glagola,* J.S. Greenberg,§ A.L. Hallin,‡ T. Happ,* E. Kashy,† W. Kutschera,* J. Last,* C.J. Lister,§ M. Maier,† J.P. Schiffer,* J. Winfield,† P. Wilt,* A. Wuosmaa,* F. Wolfs‖ and J. Yurkon†

The vacuum vessel, solenoid and many of the subsystems for the APEX spectrometer have been installed in the past year and are undergoing tests. The magnetic field has been scanned with a Hall probe. We found that the field quality was within specifications contained in an earlier analysis of measurement systematics related to field imperfections.[1] The field is equivalent to that generated by the isolated solenoid plus the earth's field plus an image solenoid resulting from reinforcement steel in a vertical wall. Correction for residual nonuniformities will be by adjustment of the silicon array positions to coincide with the true field axis as planned.

Ion chamber monitor detectors produced at the UW Nuclear Physics Laboratory[2] have been installed and await beam tests. One of the cold nitrogen cooling systems[3] for the silicon arrays has been delivered and the other is in the final stages of preparation. Separate regulation systems were tested during the past summer. Aluminized kapton shrouds that surround the silicon arrays and contain the nitrogen cooling gas have also been produced and delivered. These shrouds are 39 cm long and 5 cm diameter and are supported at the end by spring loading. The kapton is 8 microns thick.

The silicon arrays, each 36 cm long and containing 213 active, 1 mm thick silicon segments, are nearing completion. A partial array consisting of two rings of detectors has been installed for testing.

Two of eight large position-sensitive heavy ion counters have been delivered by MSU and are in the process of beam tests. One of the position-sensitive NaI barrels assembled at Yale is complete and the other is being completed. The positron trigger system operating on input from the NaI barrels has been tested and a minor cross talk problem has been solved.

The rotating target assembly produced at FSU has been used in the past few months for beam tests, especially to examine the quality of the beam spot. To improve the initial results two magnetic quads immediately upstream of APEX were replaced, and the spot size and shape are now acceptable.

Beam tests will continue with more systems coming on line. It is hoped that initial electron spectra can be collected starting this summer.

---

*Argonne National Laboratory, Argonne, IL 60439.
†Michigan State University, East Lansing, MI 48824.
‡Princeton University, Princeton, NJ 08543.
§Yale University, New Haven, CT 06520.
¶Florida State University, Tallahassee, FL 32306.
‖University of Rochester, Rochester, NY 14627.

[1] APEX Note (unpublished), T.A. Trainor.
[2] Nuclear Physics Laboratory Annual Report, University of Washington (1991) p. 19.
[3] *ibid.*

4 Fundamental Symmetries

4.1 Charge symmetry in ^{4}He

D.S. Dale,* R.A. Eisenstein,† F.J. Federspiel,‡ M.A. Lucas,† K.E. Mellendorf,† A.M. Nathan,§ A.E. O'Neill¶ and D.P. Wells

The concept of charge symmetry, in which the Coulomb-corrected $p-p$ and $n-n$ interactions are equal to each other, is widely believed to be approximately obeyed in nuclei. In the energy region of the GDR it has long been recognized that ^{4}He is an ideal system to study charge symmetry due to the extreme sensitivity of the ratio of cross sections: $R = \sigma(^4\mathrm{He}(\gamma,\mathrm{p}))/\sigma(^4\mathrm{He}(\gamma,\mathrm{n}))$, to isospin mixing. Any ratio larger than ≈ 1.1 would be a strong indication of a violation of charge symmetry. The individual cross sections have been measured many times, with recent results ranging from $R = 1.7$[1] to $R = 1.1$.[2] A reliable measure of the total photoabsorption in the region of the GDR, which is dominated by these two channels, would allow one to eliminate various combinations of cross sections inconsistent with the sum.

We have measured ^{4}He(γ,γ) cross sections at the University of Illinois tagged photon facility. Photon scattering cross sections can be directly related to total photoabsorption through model-independent relations, and our use of the tagged photon technique allows excellent control of systematic errors. Thus these data place stringent constraints on the *sum* of the $^4\mathrm{He}(\gamma,p)$ and $^4\mathrm{He}(\gamma,n)$ cross sections. Our essential result is that the peak photoabsorption in the region of the GDR is 2.86 ± 0.12 mb. This result is consistent with the charge symmetry breaking results of ref. 1 (2.90 ± 0.16 mb), and inconsistent with the charge symmetry conserving results of ref. 2 (2.37 ± 0.13 mb). While we make no claim about charge symmetry, our result implies that the only reliable way to answer this question is a simultaneous measurement of these two cross sections.

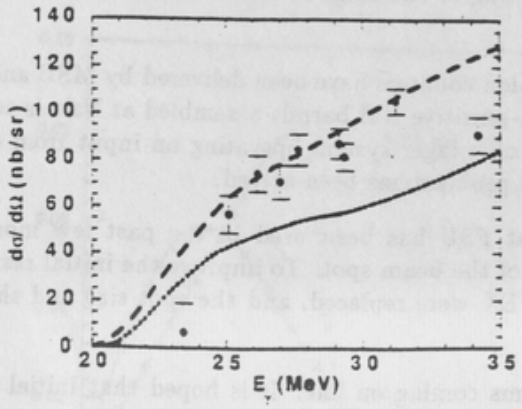

Fig. 4.1. The measured $^4He(\gamma,\gamma)$ cross sections are shown, along with the expected scattering assuming the charge symmetry breaking cross sections of ref. 1 (long dashes), and the charge symmetry conserving cross sections of ref. 2 (dots).

*Department of Physics, Massachusetts Institute of Technology, Cambridge, MA 02139.
†Department of Physics, University of Illinois, Champaign, IL 61820.
‡Los Alamos National Laboratory, H846, Los Alamos, NM 87545.
§Permanent address: University of Illinois at Urbana-Champaign, Nuclear Physics Lab, Champaign, IL 61820.
¶Department of Physics, Wellesley College, Wellesley, MA 02181.

[1] J.R. Calarco, B.L. Berman and T.W. Donnelly, Phys. Rev. C **27**, 1866 (1983).
[2] G. Feldman, M.J. Balbes, L.H. Kramer, J.Z. Williams, H.R. Weller, and D.R. Tilley, Phys. Rev. C **42**, R1167 (1990).

4.2 Development of an apparatus to measure the PNC spin rotation of transmitted cold neutrons in a liquid helium target

E.G. Adelberger, B.R. Heckel, S.K. Lamoreaux* and D.M. Markoff

The motivation of our experiment to measure the parity non-conserving (PNC) spin-rotation of transversely polarized neutrons through a liquid helium target— improving the experimental limits of the isovector pion exchange amplitude in the meson exchange potential that describes the weak interaction between hadrons—has been discussed in recent annual report articles.[1]

Because of technical difficulties at the ILL reactor in France, we now plan to run our experiment at the cold neutron beamline at the NIST reactor in Gaithersburg, Maryland. The technique for determining the PNC spin rotation using two target positions and a π-coil spin precessor was perfected[2] for solid targets. Our cryogenic liquid targets pose severe requirements on the instrument and necessitated new design. The 6 cm square, symmetric beam size at NIST enables us to construct a 4-chamber target system in a symmetric configuration with two sets of two target regions side-by-side as opposed to the previous design for ILL of vertically stacked targets. This will reduce possible systematics that could arise from differences in filling and emptying the two chamber areas with liquid helium.

To isolate the desired parity-violating signal from false signals that mimic this rotation, previous experiments had two target positions separated by a single π-coil. The π-coil rotated the neutron spin vector around an axis transverse to the beam, and parallel to the original polarization vector of the neutrons. The π-coil, however, rotates neutron spins by 180 degrees only for one velocity. This effectively partially depolarizes the beam. To minimize this depolarization, we intend to use a system of 3 π-coils[3] arranged so that the first and third have their rotation axes at 60 degrees from vertical and the middle coil axis is at -60 degrees. Calculations show that a 180 degree rotation can be achieved for the range of velocities between $.8v$ and $1.2v$, where v is the optimum velocity for a single π-coil. By adding a second set of three π-coils in front of the first target position, we create a spread in polarization vectors which is undone by the second set of coils. Calculations indicate for an expected beam velocity spectrum, the effective neutron polarization of two sets of a single π-coil would be 71% and that for the three π-coil system would be 93%. This decreases the running time needed to achieve a given statistical accuracy by a factor of nearly 2.

We have taken advantage of the cryogenic temperatures to make the π coils superconducting, and incorporated a set of superconducting coils to reduce and stabilize any stray axial magnetic fields. One set of coils, wrapped around the liquid helium dewar, cancels residual axial fields. Once the axial magnetic fields are reduced, a second set of superconducting coils, wrapped on the target chamber, will be turned on to lock these fields, and to stabilize them by countering any fluctuations. With this system, we hope to achieve axial magnetic fields of less than 0.1 mGauss with fluctuations less than 1 μGauss.

*Department of Physics, University of Washington, Seattle, WA 98195.

[1] Nuclear Physics Laboratory Annual Report, University of Washington (1987) p. 27 and (1989) p. 18.

[2] B.R. Heckel *et al.*, J. Phys. (Paris) 45, C3 (1984).

[3] Dubbers *et al.*, Nucl. Inst. Methods A270, 95 (1988).

4.3 A new test of the weak equivalence principle

E.G. Adelberger, B.R. Heckel and Y. Su

We are continuing our test[1] of the weak equivalence principle using a rotating torsion balance. The whole apparatus was fully rebuilt in the last summer. While the main design remains the same, quite a few details were modified. The major improvements include:

1. Installation of a new set of ball bearings on our turntable. This removed a tilt variation that occurred once every two cycles.

2. Installation of a new, more solid base for the turntable. This base also serves as the bottom of a improved hermetic heat shield. This change has reduced the noise due to seismic vibration.

3. Replacement of the old fiber by a new (superpolished) 0.8 mil W fiber. The new fiber is attached via. crimping instead of soldering as our previous work.

4. Installation of a magnetic damper to damp out the swing modes of the pendulum. Two fiber monitors were installed to monitor the fiber swing.

5. A detailed examination of the optics system. We found there are several closely spaced light spots on the detector due to extra reflections from the beam splitter. We rotated the autocollimator by 90° to line the spots along the insensitive axis of the detector.

6. Replacement of the vertical Helmholtz coils by larger ones. This has given us larger space to work in as well as a more uniform cancelation of the earth's magnetic field.

7. Cancellation of the $l = 2, m = 2$ gravity gradient using a pair of compensators each of which covers 90° of azimuth.

Data taken since these changes were made are more stable and have smaller error bars than before. With our new level of precision, we need to consider the effect of octapole gravity gradients, namely, the coupling between the residual q_{31} of the pendulum and the Q_{31} of the hillside (see ref. 1 for notation). The gradient of the hillside was measured using special test bodies that created a large, known q_{31} moment of the pendulum. The systematic effect due to the gravity octapole moment turned out to be small compared to our statistical error. Currently we correct for this effect. In the near future, we will install a new pendulum which we expect will have zero q_{30} (and thus no residual q_{31}) to eliminate this problem.

These improvements, together with the feedback control loop on the rotation rate installed earlier,[2] has allowed us to improve our results from ref 1. Our new 1-σ limit on the absolute differential horizontal acceleration of Be/Al test body pairs is $(2.2 \pm 5.7) \times 10^{-12}\mathrm{cm/s^2}$. In terms of the weak equivalence principle, this limit corresponds to $m_i/m_g(\mathrm{Be}) - m_i/m_g(\mathrm{Al}) = (1.0 \pm 3.4) \times 10^{-12}$. Our data also set stringent new limit on composition-dependent interactions with ranges greater than 1 m. For range longer than the radius of the earth, the 2-σ constraint on the coupling constant of a vector interaction coupled to baryon number α_5 is $(0.3 \pm 3.2) \times 10^{-9}$.

[1] E.G. Adelberger *et al.*, Phys. Rev. **D42**, 3267 (1990).

[2] Nuclear Physics Laboratory Annual Report, University of Washington (1990), p. 30.

4.4 Limits on differential acceleration towards the sun from the rotating torsion balance data

E.G. Adelberger, B.R. Heckel and G.L. Smith

Our rotating torsion balance was designed to search for a composition-dependent interaction between our test bodies and a source fixed in the earth's frame. We have now developed a method of analyzing our data to search for interactions coupled to astronomical sources as well. Because our usual data analysis procedure averages over time periods long compared to one day, it would have 'washed out' such signals. We have recently analyzed our data to constrain the differential acceleration towards the sun.

To obtain the astronomical signal we analyze the data in short segments of two rotational periods (about 3 hours) and extract the lab-fixed 1ω signal. The raw data includes the time and date of each point, as recorded by the computer's clock; we use this to find the position of the sun (in this case) at the middle of the data segment. We then search for a modulation of the 1ω lab-fixed signal, correlated to the position of the sun. Specifically we fit the lab-fixed $\sin(\omega t)$ and $\cos(\omega t)$ coefficients in terms of a signal proportional to the sun's horizontal acceleration, a quadrature term, and constant offsets. The constant offsets account for effects fixed in the laboratory — such as temperature gradients, turntable imperfections and local gravity gradients. These offsets may change between different experimental configurations, so each configuration (lasting about 2 weeks) must be fitted separately. The extracted signals are summed, weighted by the inverse error squared.

For data taken between 11/91 and 1/92 our preliminary differential acceleration towards the sun is $a(Be) - a(Al) = (2.3 \pm 8.3) \times 10^{-12}$ cm/sec^2. This is to be compared with 5.93×10^{-1} cm/sec^2, the earth's acceleration towards the sun.

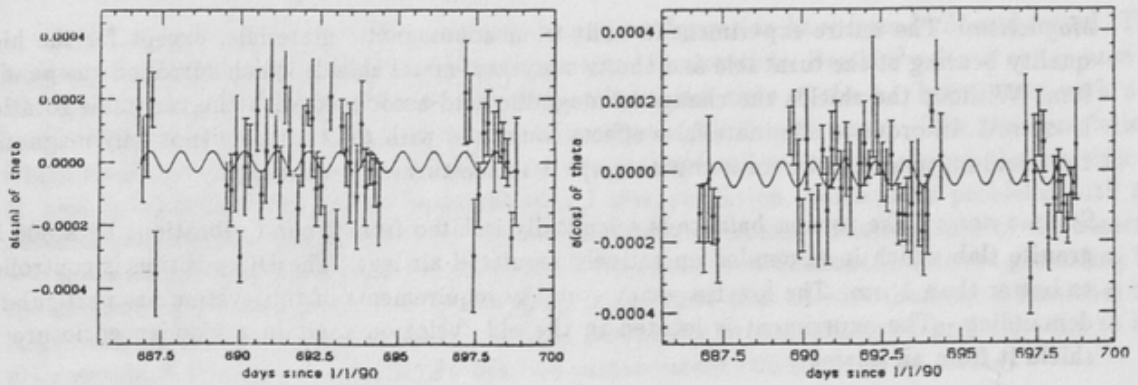

Fig. 4.4. Results of one configuration. The points are the coefficients of the lab-fixed $\sin(\omega t)$ and $\cos(\omega t)$. The curve is the best fit sine wave with the sun's orbital frequency.

4.5 Development of a new rotating-source torsion-balance instrument

E.G. Adelberger, J.H. Gundlach, M.G. Harris, B.R. Heckel, D.W. Sesko, G.L. Smith and H.E. Swanson

We have built and are now testing an apparatus to search for new feeble fundamental interactions with macroscopic ranges down to 2cm (this corresponds to an exchange boson mass of 10^{-5}eV). The experiment consists of 3.0 tonnes of a semiannular depleted uranium attractor mass which slowly rotates around a torsion pendulum. The torsion pendulum carries test-masses which can vary in their composition or other properties. Several measures were taken to isolate the torsion signal from known systematic effects:

Gravity: The Uranium is shaped to minimize gravity gradients at the centre of the torsion pendulum which is only 10 cm from the uranium. Nominally the first non-vanishing multipole moment is l=5. The most significant parasitic multipole moment arising from imperfections in the uranium is Q_{21}. This was reduced by two orders of magnitude by placing Pb compensator masses, using pendulum test bodies that are particularly sensitive to this multipole moment. The expected torsion amplitude is < 2 nrad (<1 mil pendulum tolerances).

The torsion pendulum itself employs a high degree of symmetry so that the first nonvanishing multipole moment is nominally q_{71}.

Tilt: Torsion balances are typically very sensitive to the change in tilts of the fiber suspension point. We eliminated floor tilts from the rotation of the uranium by counterbalancing with 1 tonne Pb mass at a three times larger larger radius. The measured tilt correlated with the source rotation is < 12 nrad.

Thermal control: The vacuum chamber is surrounded by an actively regulated copper shield and several layers of passive shields. On the opposite side of the uranium hollow Al dummy masses rotate on the turntable. Temperature changes at the signal frequency are < 0.1 mK.

Magnetism: The entire experiment is built from nonmagnetic materials, except for the high quality bearing of the turntable and the two layers μ-metal shields which surround the pendulum. Without the shields the change in magnetic field associated with the turntable rotation is <1 mG. In order to eliminate false effects connected with the turntable (not only magnetic) the uranium mass can be rotated with respect to the turntable structure.

Seismic noise: The torsion balance is seismically isolated from ground vibrations by a 800 kg granite slab which is suspended on actively regulated air legs. The DC position is controlled to better than 1 μm. The low frequency stability requirements of this system are particularly demanding. The experiment is located in the old cyclotron vault in a wooden enclosure to shield it from air currents.

We are currently measuring the differential acceleration of Cu and Pb test masses. Ultimately we hope to reach a sensitivity limit of $\alpha_5 = 10^{-6}$ for vector interactions coupled to $I_3 = (N - Z)/2$ for $\lambda > 10cm$.

4.6 Development of the mass-8 β-decay apparatus

E.G. Adelberger, L. De Braeckeleer, P.V. Magnus, W. Schief, K.A. Snover and K.B. Swartz

We are developing an experiment to make a precision test of fundamental symmetries in the $A = 8$ nuclei: the conservation of vector current, the absence of second class currents and time reversal invariance. A description of the experiment is given in previous annual reports.[1,2] In short, the experiment requires the complete kinematic reconstruction of ^{8}Li and ^{8}B β decays from measurements of the β and two α momenta. In the last year the construction of the major mechanical parts of the apparatus consisting of vacuum chamber and rotating arm was completed. Tests of beam transport and ^{8}Li production have been completed and the first two α counters have been constructed.

A test run of ^{8}Li production was very successful. The ^{8}Li is produced by the reaction ^{7}Li(d,p). A deuterium beam of 3 μamps at 1 MeV was focused to a 2 mm spot on a 10 cm diameter rotating target wheel which consisted of 100 μg/cm^2 of LiF evaporated on to 200 μg/cm^2 Ni backing. The beam passed first through the Ni then LiF after which it passed through a catcher of 20 μg carbon, 2 mm behind the target wheel. Some of the ^{8}Li produced in the target was stopped in the carbon catcher. The measured ^{8}Li decays must take place in a thin catcher so that multiple scattering of the α's is kept to a minimum. The catcher, attached to the end of 75 cm arm, is rotated by 180 degrees in 0.3 seconds every 2 seconds placing the catcher foil in the center of the counting chamber. In the counting chamber a silicon detector with approximately the same solid angle as one of the final gas alpha detectors measured the α's. The ^{8}Li production was studied as function of beam energy, a broad maximum is seen at 1 MeV deuterium energy. Studies of target and backing thickness were not done since the only effect of changing target and backing thickness is that the beam energy at which maximum production takes place changes, not the production rate. Approximately 500,000 events in 2 minutes were detected in the alpha detector. In a four hour run, no degradation of the LiF was observed.

Alpha particle detectors of the required size and configuration have been built and tested. The α detector is a low pressure gas detector of the type developed by Breskin[3] with a active area of 20 cm x 20 cm. Each detector measures the position and time of the α. Intial tests with a α source were encouraging. The detector has a position resolution of 1 mm. The time resolution, which could not be measured with only a α source, is expected to be 1 nsec since the rise time of 10 nsec is comparable to similar detectors with 1 nsec resolution. Some early problems with the detector construction and performance have been largely overcome. The response of the detector was not uniform over the area of the detector. With minor modifications (improved grounding for the position planes and techniques for stringing the wires so that all wires had equal tensions) the large nonuniformities were eliminated. A slight periodicity in nonuniformity probably due to the discreetness of the delay lines used for position measurement still needs to be solved.

In the near future a measurement with two α detectors and one β detector is planned. In this measurement all the critical elements (production, alpha and beta detectors), needed for a successful experiment will be tested. It will also test our ability to reconstruct neutrino momenta for electron neutrino angular correlations.

---

[1] Nuclear Physics Annual Report, University of Washington (1990) p. 31.

[2] Nuclear Physics Annual Report, University of Washington (1991) p. 31.

[3] A. Breskin *et al.*, Nucl. Instrum. & Meth., **221**, 363 (1984).

4.7 Isovector radiative decays of the 16.6 and 16.9 MeV doublet in ^{8}Be

L. De Braeckeleer, E.G. Adelberger, J.H. Gundlach, M.S. Kaplan, D.M. Markoff, A.M. Nathan, W.R. Schief, K.A. Snover and D.W. Storm

In order to test the conservation of the vector current in mass 8 nuclei with improved precision, the width of the analog isovector M1 transition and the E2/M1 ratio have to be remeasured with better accuracy. The measurement of the angular correlation of the photon emitted in the reaction ^{4}He(α,γ) at the energy of the 16.9 MeV state determines the E2/M1 ratio for this level. Previous measurements[1,2] of this angular correlation have been done with a long gas cell. Therefore, it was possible to shield the detector from the background generated by the windows, but the shape of these collimators had to be different for each angle. The calculation of the correct solid angle for each angle is a difficult task.

Our approach to this problem is quite different. We use a short cell and detect the photons coming from the windows as well as those from ^{4}He(α,γ). However, a measurement of the photons generated by the same gas cell filled with hydrogen in place of helium ensures a good subtraction of the background. Preliminary data indicate an angular correlation almost characteristic of a pure M1, in disagreement with previous results.[2] We plan to improve our measurement (statistic and systematic) of this correlation until we understand the E2 piece of this transition well enough to investigate C.V.C. at the level of 3% for the M1 transition. Eventually, the 16.6 MeV state angular correlation will be remeasured, as will the total radiative capture cross section across the two resonances.

[1] A.M. Nathan *et al.*, Phys. Rev. Lett. **35**, 1137 (1975).
[2] T.J. Bowles and G.T. Garvey, Phys. Rev. C **18**, 1447 (1978).

4.8 The anomaly in near-threshold pair production

E.G. Adelberger, L. De Braeckeleer and A. García*

We investigated a reported anomaly in near-threshold pair production, using radioactive sources to measure the $\gamma + \mathrm{Ge} \rightarrow e^+ + e^- + \mathrm{Ge}$ cross-section at E_γ=1063, 1086, 1112, 1173, 1332, 1408, 1770, and 1836 keV. Although the standard theory agrees with the data at the higher energies, the theory falls below the data at 1112, 1086 and 1063 keV. (See figure below.) The discrepancy is reduced by including the Coulomb interaction between the e^+ and e^- in the final state. We estimate the effect of the e^+-e^- final-state interaction using an expression, derived by Sakharov for pairs produced in a different kinematic regime (high photon energy but low-relative velocity of the pair). This leads to a multiplicative correction factor

$$F = \frac{2\pi\alpha/v}{1 - \exp(-2\pi\alpha/v)} \ ,$$

where v is the relative velocity of the final leptons.

Our data were corrected for the following effects:

1. Attenuation of the photon flux inside the counter.
2. Multiple photon interactions inside the counter.
3. Escape of the leptons from the active volume of the detector.

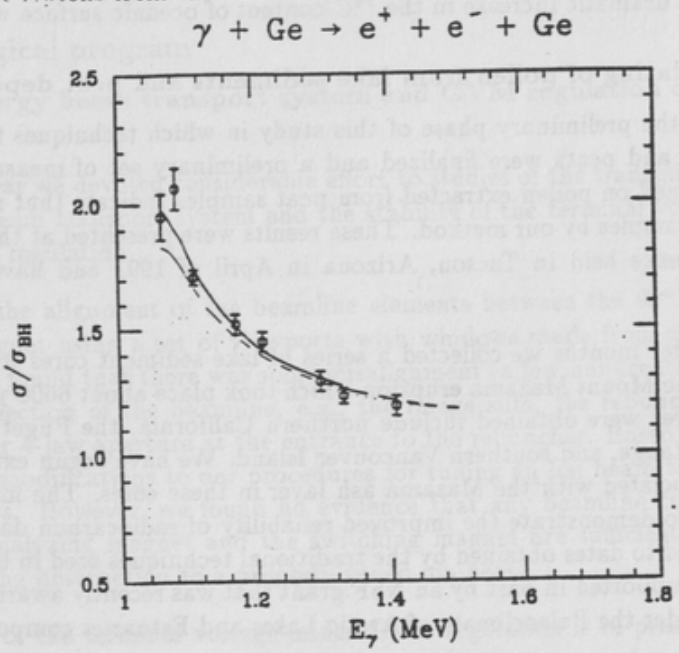

Fig. 4.8. Pair production cross section in units of the Bethe-Heitler cross section. Dotted line: Dirac coulomb wave functions for a point nucleus. Dot-dashed line: Hartree-Fock coulomb wave functions for a nucleus surrounded by its electrons. Solid line: Hartree-Fock calculation enhanced by the Sakarov factor.

*Now at: Lawrence Berkeley Laboratory, B-88, 1 Cyclotron Road, Berkeley, CA 94720.

5 Accelerator Mass Spectrometry

T.A. Brown, G.W. Farwell and P.M. Grootes

5.1 Scientific program

5.1.1 Intra-annual variations of the radiocarbon content of coral from the Galápagos Islands

The ^{14}C content results we have obtained on coral from the Galápagos Islands show pronounced intra-annual variations during the period studied (1970–1973) and an unambiguous signal during the El Niño/Southern Oscillation year 1972. Strikingly similar variations are evident in the sea surface temperature (SST) record for this time period obtained from Academy Bay, Santa Cruz Island. After minor adjustments to the length of time each sample represents to account for variations in coral growth rate due to changes in water temperature, the two data sets have a correlation coefficient of $r = 0.89, n = 16, P < 0.001$. The intra-annual variations reflect the alternation of the source of the Galápagos surface waters between the relatively warm, "^{14}C enriched" waters from the Panama Current and the colder "^{14}C depleted" waters of the Peru Current. These intra-annual variations in the ^{14}C content of the corals have not been observed previously. They are of significance in attempts to determine the source body of the water upwelling into the Peru Current and the Equatorial region and elucidate the subsurface current structure of the South Pacific Ocean. These initial results have been submitted for publication[1] and we now intend to expand our measurements to cover in detail the 1960–1970 period during which ^{14}C from the atmospheric bomb tests caused a dramatic increase in the ^{14}C content of oceanic surface waters.

5.1.2 AMS ^{14}C dating of pollen from lake sediments and peat deposits

We have completed the preliminary phase of this study in which techniques for extracting pollen from lake sediments and peats were finalized and a preliminary set of measurements was made. The results we obtained on pollen extracted from peat samples indicate that reliable dates can be obtained from peat samples by our method. These results were presented at the 14th International Radiocarbon Conference held in Tucson, Arizona in April of 1991 and have been accepted for publication.[2]

During the summer months we collected a series of lake sediment cores from locations within the ash fall area of the Mount Mazama eruption which took place about 6600 years ago. The areas from which these cores were obtained include northern California, the Puget Lowlands, the east side of the Cascade Range, and southern Vancouver Island. We have begun extracting pollen from samples that are associated with the Mazama ash layer in these cores. The measurement of these samples is intended to demonstrate the improved reliability of radiocarbon dates obtained by our technique as compared to dates obtained by the traditional techniques used in beta-decay counting. This project will be supported in part by an NSF grant that was recently awarded to P.M. Grootes and G.W. Farwell under the Paleoclimate of Arctic Lakes and Estuaries component of the ARCSS Program.

[1] T.A. Brown, G.W. Farwell, P.M. Grootes, F.H. Schmidt, and M. Stuiver, submitted to Radiocarbon.
[2] T.A. Brown, G.W. Farwell, P.M. Grootes and F.H. Schmidt, Radiocarbon (1991), in press.

5.1.3 Atmospheric methane

We have continued our collaboration with P.D. Quay, School of Oceanography, University of Washington, in measuring the ^{14}C concentration of atmospheric methane. This project is supported in part by a NASA grant to Dr. Quay and includes measurements on methane from air collected at clean air sites on Washington's coast and Mauna Loa, Hawaii, as well as air collected during oceanographic cruises on the Pacific Ocean.

Our latest results on samples from the clean air site at Cheeka Peak on the coast of the Olympic Peninsula suggest that the concentration of $^{14}CH_4$ in atmospheric methane is no longer increasing at the 1.5±0.4 pM/yr rate found in our 1987–1989 measurements.[3] Our recent results show that the $^{14}CH_4$ concentration has been essentially constant throughout the period from 1989 to 1991 (pM expresses the sample ^{14}C concentration as a percentage of that of the modern standard). The rate of increase (or lack thereof) in the $^{14}CH_4$ concentration of atmospheric methane, when coupled with other data on atmospheric $^{13}CH_4$, allows information to be derived on the strengths of the major sources of atmospheric CH_4. The apparent disappearance of the annual increase in the $^{14}CH_4$ concentration of atmospheric methane indicates that a significant shift may have taken place in the balance among the major sources of atmospheric $^{14}CH_4$, which include fossil fuel releases, biomass burning, and nuclear power plant emissions.

We intend to continue our collaboration with Dr. Quay to elucidate the nature of this $^{14}CH_4$ shift and to attain a better understanding of the causes of the recent rapid increase in the overall concentration of this important greenhouse gas.

5.2 Technological program

5.2.1 High-energy beam transport system and GVM regulation of the terminal voltage

During the last year we devoted considerable effort to studies of the transmission characteristics of the high-energy beam transport system and the stability of the terminal voltage under generating voltmeter (GVM) regulation.

We surveyed the alignment of the beamline elements between the 90° analyzing magnet and the switching magnet using a set of viewports with windows made from glass with very flat and parallel sides. We found that there was some misalignment (a few hundredths of an inch) of several elements in this section of the beamline, e.g., the image slits, the rebuncher resonator, and the 0.70 inch diameter 4-jaw aperture at the entrance to the rebuncher. Based on this information we have made small modifications to our procedures for tuning an ion beam through the high-energy beamline elements. However, we found no evidence that any beamline components between the exit of the 90° analyzing magnet and the switching magnet are sufficiently misaligned to be an unintended limiting obstruction to a properly-tuned ion beam.

The stability of the terminal voltage under GVM regulation is of primary importance to our AMS ^{14}C measurement system as we make all our measurements using this regulation system. In order to study the performance of the GVM system we had the Electronics Shop construct a very stable circuit which allowed us to offset the DC component of the GVM signal (about 7 V

[3] P.D. Quay, S.L. King, J. Stutsman, D.O. Wilbur, L.P. Steele, I. Fung, R.H. Gammon, T.A. Brown, G.W. Farwell, P.M. Grootes, and F.H. Schmidt, Global Biogeochemical Cycles **5**, 25 (1991).

at a terminal voltage of 7 MV) and examine the millivolt variations in the GVM signal which correspond to kV changes in the terminal voltage. Under GVM regulation of the terminal voltage, the ion beam showed a pronounced horizontal movement at the image position of the 90° analyzing magnet, equivalent to a variation of several kV in terminal voltage, at a frequency of about 0.1 Hz, as well as faster variations (about 10 Hz) of slightly smaller amplitude. Under slit regulation of the terminal voltage (in which the terminal voltage is regulated to hold the ion beam in a fixed horizontal position at the image position of the 90° analyzing magnet), the GVM signal showed an equivalent pattern of variation even though the terminal voltage was held essentially constant with respect to the 0.1 Hz variations under this mode of terminal regulation. This low-frequency variation appears to be due to an instability in the current GVM and makes it difficult to tune an ion beam through the 0.375 inch diameter aperture at our detector position (one of the first steps in setting up our measurement system); since it was much easier to tune a beam through that aperture during 1990, this 0.1 Hz variation seems to have only become significant during the last year.

During the latter part of 1991 we also studied the transmission profile of a $^{13}C^{4+}$ beam through the high-energy transport system to a Faraday cup located at our detector position as a function of terminal voltage. With the beamline effectively wide open (all movable apertures moved as far out as possible), we could find no evidence of the radiation that would be produced if the beam were striking any of the beamline elements between the image slits and the detector. We also looked at the image of the $^{13}C^{4+}$ beam produced on a thin quartz slide at the detector position. The movement of the beam image produced on the quartz slide at the detector position was consistent with the variations in terminal voltage under GVM control discussed above, ie, the beam showed a slow drift of about 0.5 in corresponding to the 0.1 Hz variations. By varying the GVM setpoint we determined that the transmission profile for 35 MeV $^{13}C^{4+}$ ions to the detector position has a width of 16–20 kV and a corresponding position range of about 1.8 in at the detector. This is almost twice the width of the $^{14}C^{4+}$ detector we had been using. From these measurements we realized that a detector with a 2 in width would be able to accommodate the changes in beam position that result from terminal voltage fluctuations over a range of 15 kv or more and would eliminate the sensitivity of our measurement system to the terminal voltage variations under GVM regulation discussed above.

5.2.2 A new wide-aperture detector telescope

To meet the need outlined above, a new wide-aperture detector telescope was constructed and used successfully. It is similar to the old one in having two components, an ionization chamber that measures $\frac{dE}{dx}\Delta x$, or "ΔE", and a solid-state particle detector that measures the remaining energy, "E". The ΔE chamber has a sensitive region 2 1/4 in in diameter and approximately 1 3/4 in deep. An aluminized mylar window ($400\mu g/cm^2$), supported by a rectangular grid (0.30 in spacing) of 3-mil stainless steel wire, accommodates an operating pressure of 200T of Ar/CH_4 gas. In practice, the detector aperture is reduced by a front-mounted baffle to a rectangle approximately 1 in high and 2 in wide.

The residual energy E is measured by a 2000-mm^2 Canberra Series CAM passivated implanted planar silicon (PIPS) detector (effective diameter approximately 2 in).

The detector telescope is contained in an Al cylinder (ID 5 in). The window/detector axis is displaced from the cylinder axis to allow for an electron collection space defined by a ground plate,

a Frisch grid and a collector; the latter two electrodes are curved (radius about 3 in) in order to give a more uniform electric field in the collection region and a shorter average electron drift path.

The detector resolution for 35 MeV carbon ions proved to be very satisfactory: for ΔE, about 3.8% (FWHM); for E, 1.9%. The spread in ΔE pulse height can be attributed in part to the outward bulging of the mylar window under pressure, resulting in ion path differences of up to 1/4 in; this is borne out by the fact that the resolution in total energy ($\Delta E + E$) is better (1.6%) than that for either ΔE or E.

To test the discrimination between ^{14}C ions arriving at the detector and the most prevalent contaminant, ^{13}C, the Wien filter (velocity selector) was detuned toward ^{13}C and a mixture of ions thereby admitted. A perfectly clean separation was easily achieved by setting electronic gates to accept only the ΔE and E pulses appropriate to ^{14}C.

Typical transmission curves (beam strength vs. accelerator terminal potential) are shown below for ^{13}C to the image Faraday cup and ^{14}C to the detector, for the old 1-in detector and the new 2-in detector (Fig. 5.). The new detector allows for much wider apertures in the high-energy beamline; the dramatically reduced sensitivity to terminal voltage fluctuations is immediately evident through the broadening of the effective terminal voltage transmission plateau for ^{14}C from 3–4 kV (old system) to 16–20 kV (new system).

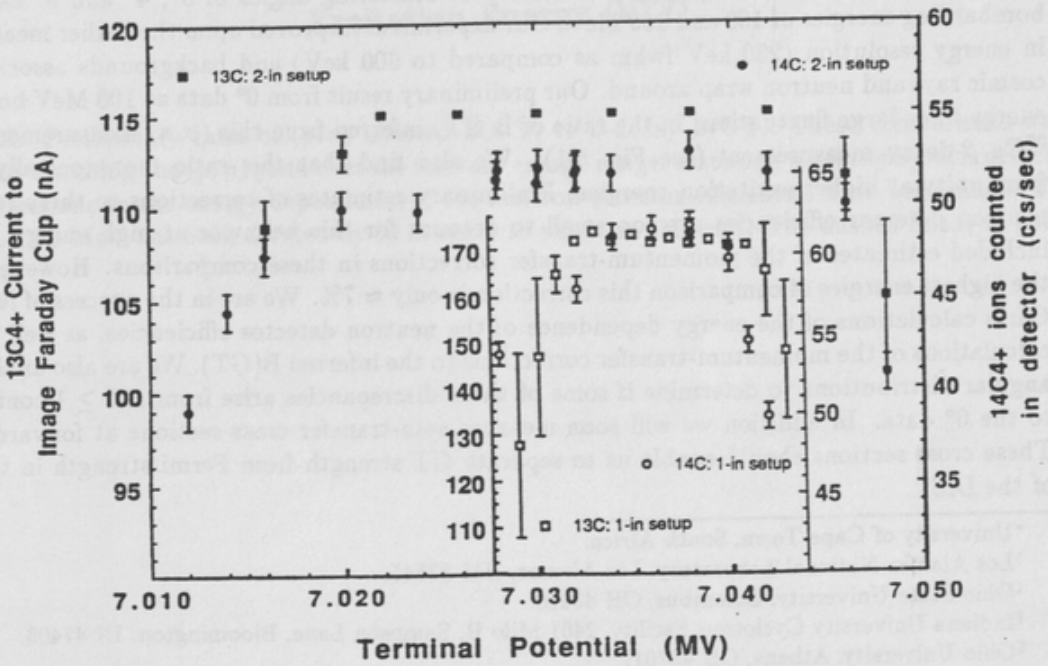

Fig. 5. Typical transmission curves (^{13}C and ^{14}C vs. tandem terminal potential). Lower data set: old beamline parameters and 1-inch detector: ^{13}C to image Faraday cup (open squares), ^{14}C to detector (open circles). Upper data set: new beamline parameters and 2-inch detector: ^{13}C to image Faraday cup (closed squares), ^{14}C to detector (closed circles). See text for discussion.

6 Medium Energy

6.1 A comparison of ^{37}Cl(p,n) cross sections to ^{37}Ca β-decay

E.G. Adelberger, D. Aschman,* R. Byrd,† S. de Lucia,‡ C.D. Goodman,§ B. Luther,‡ P.V. Magnus, D. Marchelenski,‡ B.K. Park,¶ J. Rapaport,¶ L.J. Rybarcyk,† A. Smith,§ E.R. Sugarbaker,‡ T.N. Taddeucci,† L. Wang,¶ X. Wang,¶ Y. Wang§ and D.P. Wells

The measurement of Gamow-Teller (GT) transition strength at high excitation energy has fundamental significance to nuclear physics. For example, the calibration of radiochemical neutrino detectors requires knowledge of GT strength at high excitation energy, and the sum of nuclear GT strength is sensitive to nucleon internal degrees of freedom. In general, β-decay studies of Gamow-Teller transition strength are limited by the low excitation energies accessibility to β-decay. It is believed that forward angle (p,n) cross sections at bombarding energies of $\approx$ 100–300 MeV are accurately proportional to GT strength.[1] If true this would allow measurement of GT strength up to excitation energies substantially higher than can be measured in β-decay. However no detailed comparison of high resolution (p,n) cross sections to high excitation energy β-decay data has ever been done. A recent ^{37}Ca β-decay measurement,[2] which is the isospin mirror reaction to neutrino capture on ^{37}Cl, found that the measured *distribution* of GT strength, as well as the integrated GT strength, disagreed strongly with results from a forward angle ^{37}Cl(p,n) measurement,[3] casting doubt on the claim that forward angle (p,n) cross sections are strictly proportional to B(GT).

We have measured ^{37}Cl(p,n) cross sections at scattering angles of 0°, 4° and 9° degrees and bombarding energies of 100 and 160 MeV. Our experiment improved upon the earlier measurement[3] in energy resolution (230 keV fwhm as compared to 600 keV) and backgrounds associated with cosmic rays and neutron wrap around. Our preliminary result from 0° data at 100 MeV bombarding energy finds large fluctuations in the ratio of B(GT) inferred from this (p,n) measurement and the ^{37}Ca β-decay measurement (see Fig. 6.1). We also find that this ratio monotonically diverges from unity at higher excitation energies. Preliminary estimates of corrections to these ratios from neutron detector efficiencies are too small to account for this behavior at high energy. We have included estimates of the momentum-transfer corrections in these comparisons. However, even at the highest energies of comparison this correction is only $\approx$ 7%. We are in the process of full Monte-Carlo calculations of the energy dependence of the neutron detector efficiencies, as well as DWIA calculations of the momentum-transfer corrections to the inferred B(GT). We are also analyzing the angular distributions to determine if some of these discrepancies arise from $\Delta L \geq 1$ contributions to the 0° data. In addition we will soon measure spin-transfer cross sections at forward degrees. These cross sections should enable us to separate GT strength from Fermi strength in the region of the IAS.

*University of Cape Town, South Africa.
†Los Alamos National Laboratory, Los Alamos, NM 87545.
‡Ohio State University, Columbus, OH 43210.
§Indiana University Cyclotron Facility, 2401 Milo B. Sampson Lane, Bloomington, IN 47408.
¶Ohio University, Athens, OH 45701.

[1] T.N. Taddeucci *et al.*, Nucl. Phys. **A469**, 125 (1987).
[2] A. García, E.G. Adelberger, P.V. Magnus, H.E. Swanson, O. Tengblad and D.M. Moltz, Phys. Rev. Lett. **67** 3654 (1991).
[3] J. Rapaport *et al.*, Phys. Rev. Lett. **47**, 1518 (1981).

We have also measured ^{23}Na(p,n) and ^{40}Ca(p,n) cross sections at 0, 4 and 9 degrees and bombarding energies of 100 and 160 MeV. The degree to which these cross sections can be used to infer B(GT) depends upon the final results of the detailed comparison of the ^{37}Cl(p,n) results to ^{37}Ca β-decay.

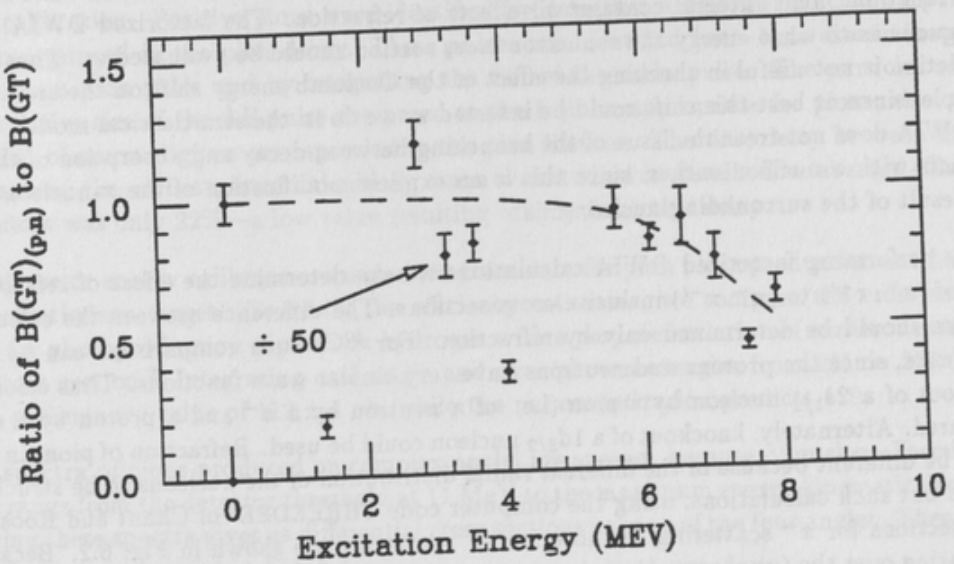

Fig. 6.1. Preliminary ratio of (p,n)-inferred B(GT) to β-decay B(GT). These comparisons were made by summing the (p,n) yield over the relevant energy range, assuming *no background* is present. No corrections to the energy dependence of the neutron detector efficiencies have been made. The point at 3.2 MeV has been divided by 50 in order to put it on this plot. The dashed line is to guide the eye.

6.2 DWIA calculations of refraction in inclusive inelastic pion scattering

D.W. Storm

Certain aspects of the semiclassical modeling of the inclusive inelastic scattering of pions (see section 6.4) can be checked with a distorted wave impulse approximation (DWIA) calculation. Available computer codes use the *factorized* DWIA, in which the π-nucleon t-matrix is factored out of the integral, leaving in the integrand the product of distorted waves and a bound state nucleon wave function. This integral contains all effects of refraction. The factorized DWIA, however, is ambiguous as to what energy the π-nucleon cross section should be evaluated at. Thus this type of calculation is not useful in checking the effect of the Coulomb energy shift on the cross section, for example, since at best this shift could be inserted as we do in the semiclassical model. In principle the DWIA does not treat the issue of the branching between decay and absorption of the pion as it interacts with a nucleon, either, since this is an explicit modification of the π-nucleon interaction as a result of the surrounding nucleons.

By performing factorized DWIA calculations we can determine the effect of refraction on the ratio of $(\pi^+, \pi^{+\prime})$ to $(\pi^-, \pi^{-\prime})$ inclusive cross sections. The difference between the calculated cross sections should be determined only by refraction. For ^{40}Ca such comparisons can be made with confidence, since the protons and neutrons have very similar wave functions. Thus calculations for knockout of a $2s_{1/2}$ nucleon by a pion (i.e. of a neutron by a π^- and a proton by a π^+) can be compared. Alternately, knockout of a $1d_{3/2}$ nucleon could be used. Refraction of pions in these cases might be different because of the different radial distribution of the nucleons to be struck. We have carried out such calculations, using the computer code THREEDEE[1] of Chant and Roos. Ratios of cross sections for π^- scattering to those for π^+ scattering are shown in Fig. 6.2. Because we are integrating over the (unobserved) nucleon, we set the imaginary part of the nucleon-nucleus optical potential to zero. Then, however, we have unrealistic results for the very low nucleon energies, where there appear to be resonances in the nucleon optical potential. For a ratio comparison it is reasonable to ignore the nucleon optical potential.

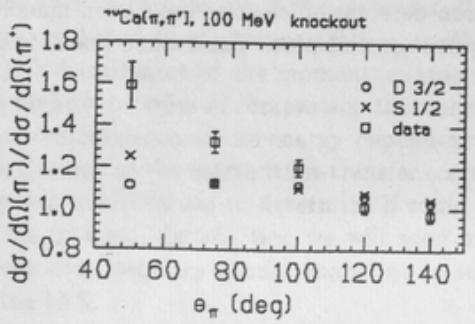

Fig. 6.2. Ratios of π^- to π^+ inclusive inelastic cross sections for ^{40}Ca as calculated in the DWIA (with plane waves for nucleons) and as measured.

The data show a much stronger angular dependence than the calculations. Integrating over angle and then taking the ratio of π^- to π^+ cross sections, we find the DWIA predicts 1.10, as compared to the measured value of 1.13 ± 0.02.

[1] N.S. Chant and P.G. Roos, Phys. Rev. **C15**, 57 (1983).

6.3 Inclusive pion photoproduction on several nuclei

K.G. Fissum*, M. Frodyma,† K. Garrow*, I. Halpern, D.P. Rosenzweig, D.W. Storm and J. Vogt*

The data analysis for the pion photoproduction experiment is nearly completed. In this experiment[1] four detectors were used and a tagged photon beam, covering the energy range 179 to 217 MeV, impinged on targets of carbon, calcium, tin, or lead, as well as on a polyethylene target used for calibration. Positive pions were identified by detecting a delayed coincidence pulse from the muon produced in the pion decay. These pulses are identified both by a discriminator firing after the main pion pulse and by integrating the tail of the main pulse. The particles so chosen had the relative size of the ΔE pulse compared to the E pulse appropriate for pions; also, the time distribution of muon triggers corresponded to the pion lifetime. The time delay between the initial pion pulse and the earliest detectable decay muon was studied in detail. The average efficiency of the detectors was only 22%—a low value resulting mainly from this delay.

The detector energy calibration was derived from data for pion photoproduction on the protons in the polyethylene target. To verify the efficiency estimates, we compare the cross section we measure for photoproduction of pions on hydrogen with a parameterization of earlier measurements of this cross section.[2] Integrating over angle and over photon energies from 211 to 217 MeV, we obtain a preliminary value of 112 ± 4 μb, while the parameterization predicts 129.

The spectra of pions produced on complex nuclei are spread, because of nucleon Fermi motion, over the range from the detector threshold at 11 MeV to the maximum energy kinematically allowed. Integrating these spectra gives us differential cross sections at each of the four angles. These angular distributions are presented in Fig. 6.3.

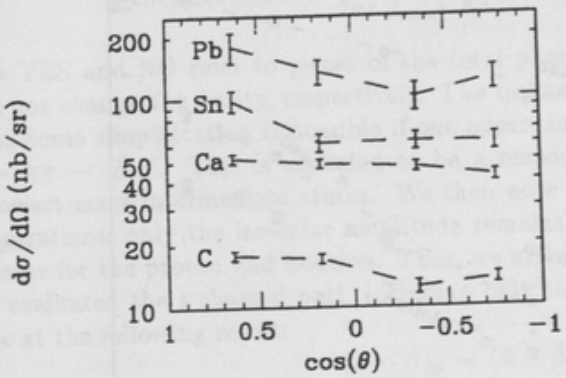

Fig. 6.3. Preliminary differential cross sections for photoproduction of π^+ on four nuclei at four angles. These results are for an 8 MeV band of photon energies centered at 214 MeV. Statistical uncertainties are shown. The curves are to guide the eye.

Although there are about 14 times as many protons in lead as in carbon, the cross section for photoproduction is only about 10 times greater, reflecting increased pion attenuation in the larger nucleus.

*University of Saskatchewan, Saskatoon, S7N 0W0, Canada.
†SLAC, Bin 44, PO Box 4349, Stanford, CA 94309.

[1] Nuclear Physics Laboratory Annual Report, University of Washington, p. 50 (1991).

[2] I. Bloomquist and J.M. Laget, Nucl. Phys. **A280**, 405 (1977).

6.4 Spectra and angular distribution in the inclusive inelastic scattering of pions at 100 MeV

I. Halpern, D.P. Rosenzweig and D.W. Storm

We have measured inclusive spectra of inelastic scattering from a number of nuclei for both plus and minus pions at 100 MeV and are preparing for publication a manuscript which deals with one aspect of these measurements.[1] In this paper we show that the ratio of the total $\pi^- \rightarrow \pi^+$ inelastic cross sections can be accounted for by a model where the scattering involves only a single nucleon. The same model also reproduces the ratios of normal to charge exchange scattering at this energy.[2]

A number of the more differential features of our measurements can also be understood in terms of the same picture. The fall off of the angular distributions at forward directions (Fig. 6.4) reflects the angular pattern for pion scattering from free nucleons, but the fact that this fall off is noticeably steeper for π^+ than for π^- scattering is largely due to the distortion of the basic pattern by the Coulomb deflections of the pions. These deflections also play a role in the comparison of spectral shapes. At back angles the π^- and π^+ spectra look rather similar except that the peak in the π^- spectrum is about 15 MeV below that in the π^+ spectrum in a heavy target. (The spectra are nearly identical in light targets.) The observed shift is partly due to the Coulomb shift of the incident pion's energy and partly to its Coulomb deflection.

Our goal is to see how well the single-scatter picture can account for the observed inclusive scattering spectra at different angles when reasonable assumptions are made about the nucleon momentum distribution, Pauli blocking and pion-nucleon cross sections.

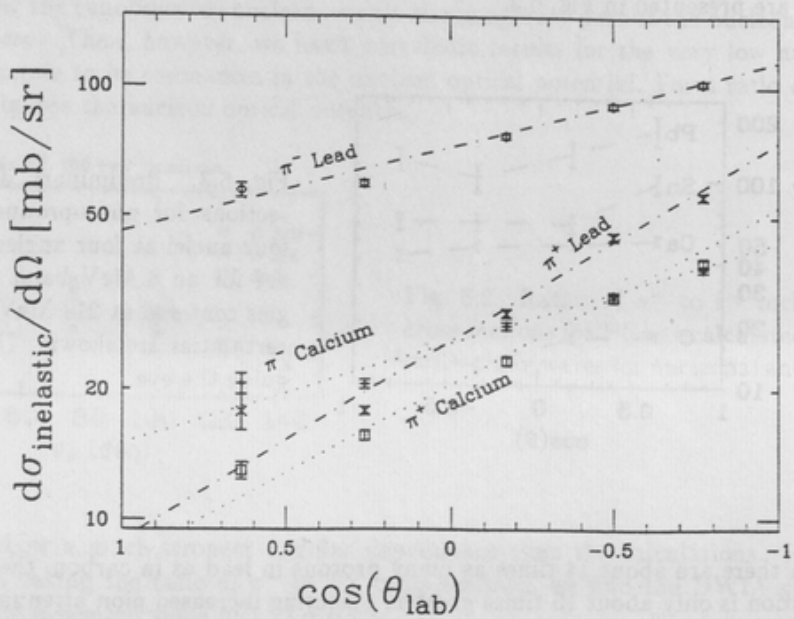

Fig. 6.4. The angular distributions for total inelastic scattering of π^+ and π^- pions from Ca and Pb at 100 MeV.

[1] D.P. Rosenzweig, I. Halpern. D.W. Storm and our collaborators from LANL, M.I.T. and University of Saskatchewan (to be published).

[2] T.J. Bowles *et al.*, Phys. Rev. C. **23**. 439 (1981).

6.5 Dispersion relation sum rules for the nucleon polarizabilities

B.R. Holstein* and A.M. Nathan†

In the past year, new measurements have been reported for the electric and magnetic polarizabilities of the nucleon, $\bar{\alpha}$ and $\bar{\beta}$, respectively.[1, 2] This has revived interest in model-independent sum rules that relate these quantities to other measurable quantities. These sum rules are based on causality and unitarity, which allows one to write a dispersion relation for the photon scattering amplitude. The best known of these sum rules is the one based on the dispersion relation relating the forward photon scattering amplitude to the total photoabsorption cross section:

$$\bar{\alpha} + \bar{\beta} = \frac{\hbar c}{2\pi^2} \int_{m_\pi c^2}^{\infty} \frac{dE}{E^2} \sigma_T(E).$$

For the nucleon, the right-hand-side of this relation has been measured, yielding

$$\bar{\alpha} + \bar{\beta} = 14.2 \pm 0.3 \times 10^{-4}\,\mathrm{fm}^3[\text{proton}]$$

$$\bar{\alpha} + \bar{\beta} = 15.8 \pm 0.5 \times 10^{-4}\,\mathrm{fm}^3[\text{ neutron}].$$

Various attempts have been made to derive sum rules for $\bar{\alpha}$ and $\bar{\beta}$ separately. One possibility is to write a backward (i.e., $\theta = \pi$) dispersion relation for the photon scattering amplitude, yielding the following expression:[3]

$$\bar{\alpha} - \bar{\beta} = \text{s-channel piece} + \text{t-channel piece},$$

where the s-channel piece refers to the process $\gamma N \to \gamma N$ and the t-channel piece refers to the process $\gamma\gamma \to \bar{N}N$. Now, it has been shown that the s-channel piece is given by

$$\text{s-channel piece} = \frac{\hbar c}{2\pi^2} \int_{m_\pi c^2}^{\infty} \frac{dE}{E^2} (1 + \frac{2E}{Mc^2})^{1/2} (\sigma_T^{YES}(E) - \sigma_T^{NO}(E)),$$

where YES and NO refer to pieces of the total photoabsorption arising from multipoles that do or do not change the parity, respectively. The t-channel piece is much more complicated to write down. Some simplification is possible if one approximates the reaction by intermediate $\pi\pi$ states: $\gamma\gamma \to \pi\pi \to \bar{N}N$. This is expected to be a reasonable approximation since the $\pi\pi$ states are the lowest mass intermediate states. We then note that since one must sum over all $\pi\pi$ charge configurations, only the isoscalar amplitude remains, implying that the t-channel part should be the same for the proton and neutron. Thus, we arrive at a sum rule for $(\bar{\alpha} - \bar{\beta})_p - (\bar{\alpha} - \bar{\beta})_n$. We have evaluated the s-channel part, including only the one-pion photoproduction amplitudes. We arrive at the following result:

$$(\bar{\alpha} - \bar{\beta})_p - (\bar{\alpha} - \bar{\beta})_n = -0.1,$$

in excellent agreement with the experimental value -1.2 ± 3.1, in units of 10^{-4} fm^3. Work is under way to take into account the two pion photoproduction amplitudes as well as to evaluate the t-channel contribution.

*Institute of Nuclear Theory, University of Washington, Seattle, WA 98195.
†Permanent address: University of Illinois at Urbana-Champaign, Nuclear Physics Lab, Champaign, IL 61820.

[1] J. Schmiedmayer *et al.*, Phys. Rev. Lett. **66**, 1015 (1991).
[2] F.J. Federspiel *et al.*, Phys. Rev. Lett. **67**, 1511 (1991).
[3] J. Bernabéu and B. Tarrach, Phys. Lett. **69B**, 484 (1977).

6.6 A search for narrow resonant-like structures in proton-nucleus interactions at TRIUMF

I. Chapman,* W.G. Weitkamp and the Dubna-Seattle-Tashkent-TRIUMF Collaboration

The possible existence of dibaryon resonances has been investigated both experimentally and theoretically for a number of years. A dibaryon resonance in this context means an object with baryon number B=2 and a well defined mass, total decay width and spin-parity assignment. Although the existence of dibaryon resonances continues to be controversial, a recent review[1] cited strong evidence for several dibaryon resonances at masses several hundred MeV above the two nucleon mass; a theoretical study recently concluded that a non-strange dibaryon called the d^* is "inevitable"[2] in this mass region. Various experiments suggest that other narrow resonances may exist and various theoretical models predict that whole families of dibaryon resonances may yet remain to be found. Experimental studies of these resonances continue to be an important activity on the interface between nuclear and particle physics.

The Dubna-Seattle-Tashkent-TRIUMF Collaboration[3] is using a double-arm spectrometer to study two-proton mass spectra for protons produced in semi-inclusive reactions $p+ A \rightarrow pp + X$. Each arm of the spectrometer consists of 2 planes of thin plastic scintillators, 2 multiwire proportional chambers and a bank of NaI scintillators, permitting identification of secondary π, p and d particles with better energy resolution than in previous experiments. In addition, this experiment yields information on polarization effects in $(\vec{p}, pp)$ reactions on nuclei. The first data run for this experiment has been run with 500 MeV polarized protons from the TRIUMF cyclotron incident on targets of C, Al, Cu and Pb.

The apparatus for this experiment has been developed and tested in Dubna, Russia and Tashkent, Uzbekestan. The political situation in the states formerly comprising the Soviet Union has complicated preparations, but the apparatus was shipped, installed, tested and completed an initial data run at TRIUMF in March, 1992.

---

*Currently with the U.S. Air Force.

[1] 1. M.G. Huber in *7th International Conference on Polarization Phenomena in Nuclear Physics* Paris, 1990, p. C6-355.

[2] 2. G.J. Stephenson, W.R. Gibbs, T. Goldmans and K. Maltman, Bul. Am. Phys. Soc. **36**, 2172 (1991).

[3] "A Search for Narrow Resonant-Like Structures in the Reaction A$(p, 2p)$ with a Polarized Proton Beam," V.A. Nikitin, Dubna and B.S. Yuldashev, Institute of Nuclear Physics, Tashkent, spokesmen, TRIUMF experiment E627. Collaborators in addition to those mentioned include V.V. Avdeichikov, R. Kutev, P.V. Nomokonov, and A.V. Pavlik, Dubna; V. Chaloupka, W. Dougherty, Z.H. Feng, H.J. Lubatti and T. Zhao, University of Washington Department of Physics; A. Gafarov, A. Kadishnov, Y. Koblik, S. Kan, A. Khaneles, D. Mirkarimov, A. Pak, E. Surin and K. Turdaliev, Tashkent; and S. Yen, TRIUMF.

6.7 Kaon photo-production on the neutron

C.E. Hyde-Wright

Data for the $p(\gamma, K^+)\Lambda$ reaction have been parameterized by the t-, s-, and u- channel exchanges depicted in Fig. 6.7-1.[1] In order to calculate the (γ, K^0) cross section on nuclei for future experiments at CEBAF,[2] I had generalized the model of Hsiao to the $n(\gamma, K^0)\Lambda$ amplitude.

Each diagram in Fig. 6.7-1 has an electromagnetic vertex and a hadronic vertex. In the model cited above, the hadronic couplings $g_{K\Lambda N}$, $g_{K\Sigma N}$, and $g^{V,T}_{K^*\Lambda N}$ (for vector and tensor coupling of the K^*) are adjusted to fit the $p(\gamma, K^+)\Lambda$ data. In the present calculation, I apply isospin symmetry to these four couplings. Since the Λ is an isoscalar, the $N\Lambda K$ vertex is the same for either neutron or proton: $g_{p\Lambda K^+} = g_{n\Lambda K^0}$. Similarly for the vector meson vertices: $g^{V,T}_{K^{*+}\Lambda p} = g^{V,T}_{K^{*0}\Lambda n}$. However, the $N\Sigma K$ vertices are related by $g_{n\Sigma^0 K^0} = -g_{p\Sigma^0 K^+}$. The electromagnetic couplings in Fig. 6.7-1 are not constrained by isospin. For the neutron case, the proton charge and magnetic moment, e and μ_p are replaced by the neutron charge and magnetic moment, 0 and μ_n, respectively. The K^0 charge is 0, so the K^0 exchange diagram b) vanishes. The Λ and $\Sigma \to \Lambda$ magnetic moments μ_Λ and μ_T are unchanged. For the vector K^* exchange, the transition moment $g_{K^*K\gamma}$ must be replaced by the neutral kaon transition moment. The transition moment is related to the decay width by:[3] $\Gamma_{K^*\to K\gamma} = 9.8 MeV |g_{K^*K\gamma}|^2/4\pi$. From the measured decay widths,[4] $|g_{K^{*0}\to K^0\gamma}/g_{K^{*+}\to K^+\gamma}| = 1.53 \pm 0.22$. This determines the magnitude but not the sign of this ratio. For the phase of the neutral decay mode, I use the cloudy bag model of Singer and Miller.[5] The quark and pion cloud terms contribute in-phase to the K^* photon-decay, with the K^{*0} amplitude of opposite sign as the K^{*+} amplitude. Remarkably, the calculations agree with the K^* photon decay widths within the 10% experimental uncertainty.

Following Thom, Hsiao defined the Λ magnetic moment as $\mu_\Lambda = \kappa_\Lambda e/2M_\Lambda$, with $\kappa_\Lambda = -1.0$, instead of the experimental value of $\kappa_\Lambda = -0.729$. This choice is defended for the $p(\gamma, K^+)\Lambda$ case, since the Λ and Σ exchange diagrams are kinematically almost identical, and any error in μ_Λ is absorbed by the phenomenological fit to $G_\Sigma = \kappa_T g_{K\Sigma N}$, where κ_T is the $\Sigma \to \Lambda + \gamma$ transition magnetic moment. However, the $n(\gamma, K^0)\Lambda$ amplitude depends on the difference of the the Λ and Σ exchanges whereas the proton amplitude depends on the sum, as a result of the isospin structure discussed above. I use $\kappa_\Lambda = -0.729$ and adjust the value of G_Σ, keeping $\kappa_\Lambda g_{K\Lambda N} + G_\Sigma$ constant. This adjustment has negligible impact on the $p(\gamma, K^+)\Lambda$ amplitude. The final coupling constants are listed in Table 6.7.

Sample differential cross sections are plotted in Fig. 6.7-2. The neutron result is significantly different from the proton case it is derived from. Backward peaking Λ and Σ exchanges interfere (partially) destructively for the proton and constructively for the neutron. The forward peaking K-exchange is suppressed for the neutron.

Additional models of kaon photo-production include s-channel exchange of nucleon resonances[6] and u-channel exchange of hyperon resonances.[7] These models can also be generalized to the

[1] S.S. Hsiao and S.R. Cotanch, Phys Rev **C28**, 1668 (1983).
[2] CEBAF Exp 91-014, C.E. Hyde-Wright, Spokesman
[3] H. Thom, Phys Rev **151**, 1322 (1966).
[4] Particle Data Group, Phys Lett **B204** 1 (1988)
[5] Paul Singer and Gerald A. Miller, Phys Rev **D33** 141 (1986).
[6] R.A. Williams, C.R. Ji, and S.R. Cotanch, Phys Rev **C43**, 452 (1991).
[7] R.A. Adelseck, C. Bennhold, and L.E. Wright, Phys Rev **C32** 1681 (1985).

neutron case, provided there are constraints on the $\gamma + n \rightarrow N^*$ vertices. In the absence of adequate data, these electromagnetic couplings can be constrained by quark models.[8]

Table 6.7-1. Effective coupling constants derived from set-1 of Hsiao.

	$\frac{g_\Lambda}{(4\pi)^{1/2}}$	$\frac{G_\pi}{(4\pi)^{1/2}}$	$\frac{G_V}{(4\pi)}$	$\frac{G_T}{(4\pi)}$
$p(\gamma, K^+)\Lambda$	2.57	0.824	0.105	0.064
$n(\gamma, K^0)\Lambda$	2.57	-0.824	-0.159	-0.097

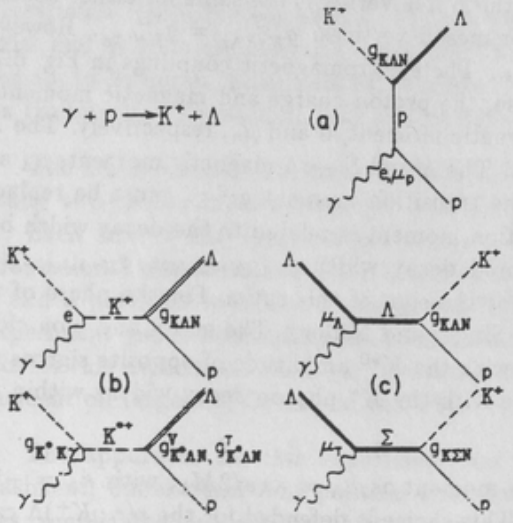

Fig. 6.7-1. Feynman diagrams for the elementary reaction $\gamma + p \rightarrow K^+ + \Lambda$. The five graphs represent the lowest order, nonresonant contributions for (a) direct, (b) scalar and vector kaon exchange, and (c) Λ and Σ exchange.

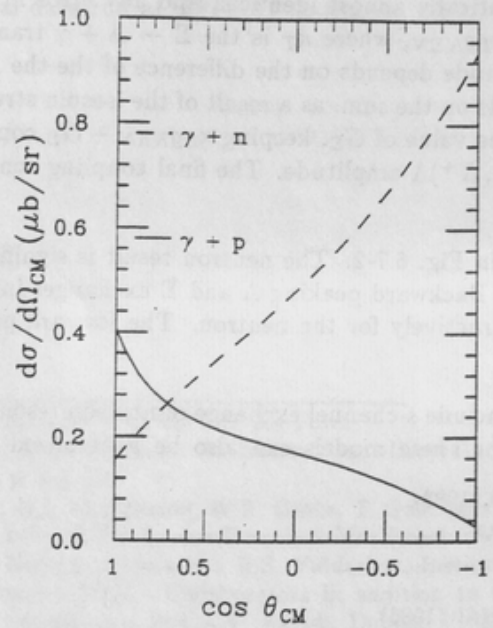

Fig. 6.7-2. Theoretical $N(\gamma, K)\Lambda$ cross section, for $k = 1.2$ Gev.

[8] R. Koniuk and N. Isgur, Phys Rev **D21** 1868 (1980).

6.8 Inelastic and deep-inelastic electron scattering from H, D, and ^{9}Be

R.G. Arnold,* A. Bodek,† P.E. Bosted,* L. Clogher,* S. Dasu,† P. de Barbaro,† F.S. Dietrich‡ M. Frodyma,§ R.A. Gearhart,¶ K.A. Giffioen,‖ R. Hicks,** C.E. Hyde-Wright, C. Keppel,* S.E. Kuhn,†† A. Lung,* R. Miskimen,** G. Peterson,** G.G. Petratos,¶ S.E. Rock,* S.H. Rokni,¶ Z. Szalata,* Y.Tau* and K. van Bibber‡

In experiment E140X at SLAC, new data were taken this year on deep inelastic scattering from H, D and ^{9}Be. The purpose of this experiment is to extend the deep inelastic measurements of $R = \sigma_L/\sigma_T$ to both higher and lower regions of $x = Q^2/(2M\nu)$. By helicity conservation, this ratio vanishes in the limit of massless quarks. For Q^2 not too large compared with M_N^2, R is a measure of effect of nucleon binding on the quark mass and transverse momentum (relative to the photon momentum). Data were taken with the 8 GeV spectrometer on H and D for $0.1 < x < 0.5$, with emphasis on the low x region. In order to obtain adequate counting rates at high x, data were taken on ^{9}Be for $x = 0.6$ and 0.7.

Additional data were taken with the 1.6 GeV and 8 GeV spectrometers on H and D in the first and second resonance region. These data will permit the separation of the longitudinal and transverse cross sections at high Q^2. These data will complement the NE-11 data on the elastic from factors.[1] These measurements were inspired in part by the analysis of (unseparated) data on the resonances.[2] Above $Q^2 = 5$ (Gev/c)^2 the inelastic form factor for the S_{11} resonance is consistent with the $1/Q^4$ behavior predicted by perturbative QCD. However, the data on the P_{33} (Δ) resonance decrease as $1/Q^6$. This behavior of the Δ supports the pQCD prediction that at high Q^2 the Δ resonance will be dominantly longitudinal.

The first stage of analysis of the raw E140X data is complete. This analysis includes the calibration and alignment check of all detectors and the purging of events recorded during "bad beam-spills" as measured by various beam monitors. Presently, the reduction of data to physics variables is in progress.

*The American University, Washington DC 20016.
†University of Rochester, Rochester, N.Y. 14627.
‡Lawrence Livermore National Laboratory, Livermore, CA 94550.
§Now at: Slac, Bin 44, Stanford, Ca 94305.
¶Stanford Linear Accelerator Center, Stanford, CA 94305.
‖University of Pennsylvania, Philadelphia, PA 19104.
**University of Massachusetts, Amherst MA 01003.
††Stanford University, Stanford CA 94305.

[1] Previous article, this Report.

[2] P. Stoler, Nucl Phys **A532** (1991) 377c.

6.9 Elastic and quasi-elastic electron scattering from the proton and the deuteron

J. Alster,[*] R.G. Arnold,[†] P.E. Bosted,[†] C.C. Chang,[‡] L. Clogher,[†] F.S. Dietrich[§] R.A. Gearhart,[¶] K.A. Giffioen[‖] R. Hicks[**] C.E. Hyde-Wright, S.E. Kuhn,[††] J. Lichtenstadt[*] A. Lung,[†] R. Miskimen[**] G. Peterson[**] G.G. Petratos,[‡‡] S.E. Rock,[†] S.H. Rokni[**] L. Stuart,[§] K. Swartz, Z. Szalata[†] and K. van Bibber[§]

Data analysis is now complete for an extensive set of high Q^2 elastic and H(e,e') data taken during the NE-11 experiment at SLAC. These results extend the region of separation of the G_{Mp} and G_{Ep} from the previous limit of 4 (GeV/c)^2 to nearly 9 (GeV/c)^2. Of various models examined, the data on G_{Ep} are in best agreement with the dipole fit, whereas G_{Mp} is in best agreement with model of Gari and Krümpelmann,[1] which is a phenomenological fusion of the Vector Dominance Model (VDM) at low Q^2 and the perturbative QCD (pQCD) scaling predictions at high Q^2. For $Q^2 > 3.0$ (GeV/c)^2 the experimental ratio $Q^2F_2(Q^2)/F_1(Q^2)$ of the Pauli and Dirac Form Factors is a constant, as predicted by pQCD. These results have been submitted for publication.[2]

The Gari and Krümpelmann model also predicts that for the neutron form factors for $Q^2 > 4.0$ (GeV/c)^2 G_{En} will dominate over G_{Mn} as a result of the $1/Q^2$ fall off of F_2 relative to F_1. This is in marked contrast to the low Q^2 region, where G_{Mn} dominates. The analysis of the inelastic $D(e,e')$ data below the Δ-resonance is nearly complete. This data should provide new constraints on the form factors of the neutron.

[*]Tel Aviv University, Ramat Aviv 69978 Israel.
[†]The American University, Washington DC 20016.
[‡]University of Maryland, College Park MD 20742.
[§]Lawrence Livermore National Laboratory, Livermore, CA 94550.
[¶]Stanford Linear Accelerator Center, Stanford, CA 94305.
[‖]University of Pennsylvania, Philadelphia, PA 19104.
[**]University of Massachusetts, Amherst MA 01003.
[††]Stanford University, Stanford CA 94305.
[‡‡]University of Rochester, Rochester, NY 14627.

[1]M.F. Gari and W. Krümpelmann, Z. Phys., **322** 689 (1985).
[2]P.E. Bosted *et al.*, Submitted to Phys Rev Lett, March 1992.

6.10 A test of the low-energy theorem for radiative pion capture

C.A. Gossett, D. Hutcheon,* M.S. Kaplan, M. A. Kovash,* A.M. Nathan† and the E643 collaboration

Chiral symmetry, a fundamental albeit broken symmetry of QCD makes a definite prediction for the s-wave part of the threshold pion photoproduction amplitude on the nucleon. This so-called Low Energy Theorem uniquely relates this amplitude to other fundamental constants, such as the pion and nucleon masses, the axial coupling constant, and the pion decay constant. For the $p(\gamma,\pi^0)$ reaction, recent measurements from Mainz and Saclay have suggested that this theorem might be violated, although recent theoretical work has cast doubt on this conclusion. Nevertheless, the fundamental importance of this theorem is such that new investigations of the $p(\gamma,\pi^0)$ reaction are under way at both Saskatoon and Mainz. These will be complemented by new measurements of $p(\gamma,\pi^-)$ at Saskatoon as well as the E643 experiment, $n(\gamma,\pi^-)$, at TRIUMF.

This experiment will be a low-energy investigation of the inverse pion photoproduction reaction $\pi^- p \rightarrow \gamma n$ reaction at pion kinetic energies of 10, 15, and 20 MeV. Absolute cross sections will be determined at four angles ranging from 30° to 135°. At each beam energy, these data will allow a model-independent extraction of the s-wave amplitude to an accuracy of approximately 4%. These data will be the lowest energy cross section measurements of this fundamental process and will provide the most stringent experimental test yet of the Low Energy Theorem for this reaction.

The experiment will utilize a very thin liquid hydrogen target, the low-energy pion beam from the M13 channel at TRIUMF, and a pair of very large NaI crystal spectrometers, provided by the Kentucky and Boston U. groups. Each detector is capable of achieving an energy resolution of around 1.5% FWHM at 130 MeV. This energy resolution is necessary in order to distinguish the photons from in-flight capture of pions from the far more copious photons from the capture of stopped pions. This problem is especially severe for the lowest energy pions. Since the goal of the experiment is to measure the capture cross section as close to threshold as possible, it is crucial to the experiment to have that kind of energy resolution. Preliminary runs have indicated that our goal of getting backward angle measurements at energies as low as 10 MeV can be achieved.

This target, which will be approximately 1-cm thick, is currently under construction by the cryogenics group at TRIUMF. The principal responsibility of the NPL group will be to measure the thickness of the thin liquid hydrogen target to an accuracy of 2%. For this purpose, we will measure the yield of Compton-scattered gamma rays from a low-energy gamma-ray source. Since the Compton scattering cross section is the well-known Klein-Nishina cross section, it should be straightforward to achieve the desired accuracy. The current timetable is for the construction of the target to be completed by early May. We hope to measure the thickness at TRIUMF during the month of May. Beam time for the production run is currently scheduled for July.

*Triumf, 4004 Wesbrook Mall, Vancouver, BC V6T 2A3, Canada. (Co-spokesmen)
†Permanent address: University of Illinois at Urbana-Champaign, Nuclear Physics Lab, Champaign, IL 61820.

6.11 The electric form factor of the neutron from the $D(\vec{e}, e'\vec{n})p$ reaction

B. Anderson,* A. Baldwin,* D. Barkhuff,† K. Beard‡ W. Bertozzi,§ J. Cameron¶ C. Chang‖ G. Dodson,§ K. Dow,§ T. Eden,* M. Farkhondeh,§ J. Finn,‡ B. Flanders** C.E. Hyde-Wright, W. Jiang, D. Keane,* J. Kelly,‖ W. Korsch,§ S. Kowalski,§ R. Lourie,† R. Madey,* D. Manley,* P. Markowitz,‡ J. Mougey,†† B. Ni,¶ T. Payerle‖ P. Pella,‡‡ T. Reichelt,[a] P. Rutt,‡ M. Spraker,¶ D. Tieger,§ W. Turchinetz,§ P. Ulmer,†† S. Van Verst,† J. Watson,* L. Weinstein,§ R. Whitney†† and W. Zhang*

We measured the $D(\vec{e}, e'\vec{n})p$ reaction at the MIT Bates Laboratory. Incident longitudinally polarized electrons of energy 868 MeV were scattered in quasi-elastic kinematics to an angle of 37° and detected in the OHIPS spectrometer. The electron polarization was measured with an upstream Moller polarimeter.[1] The preliminary electron polarization is (0.42 ± 0.02). The neutron is detected in the direction of the momentum transfer $\vec{q}$. The neutron polarization in the electron scattering plane is measured with a double scattering polarimeter.[2]

The spin independent $D(e, e'n)p$ cross section is the incoherent sum of the cross section for longitudinally and transverse polarized virtual photons. The neutron polarization times the unpolarized cross section is proportional to the electron polarization times the interference between the amplitudes for longitudinal and transverse virtual photons. In the kinematics with $\vec{p}_n \simeq \vec{q}$, contributions from the proton and from meson exchange currents (MEC) are calculated to be small, and the cross section is dominated by electron scattering from an initial neutron at rest. In this approximation, the electron helicity dependent neutron polarization measures the ratio G_{En}/G_{Mn} of the neutron form factors.[3] A preliminary analysis of the data for 544 μA-hours of beam is completed.

*Dept. of Physics, Kent State University, Kent OH 44242.
†Dept of Physics, University of Virginia, Charlottesville, VA 22901.
‡Dept. of Physics College of William and Mary, Williamsburg, VA 23185.
§Massachusetts Institute of Technology Bates Laboratory, PO Box 846 Middleton, MA 01949.
¶Indiana University Cyclotron Facility, 2401 Milo B Sampson Ln, Bloomington, IN 47405.
‖Dept of Physics and Astronomy, University of Maryland, College Park, MD 20742.
**Dept. of Physics, American University, Massachusetts Ave NW, Washington DC 20016.
††Continuous Electron Beam Accelerator Facility, 12000 Jefferson Ave, Newport News VA 23603.
‡‡Dept of Physics, Gettysburg College, Gettysburg, PA 17325.
[a]University of Bonn, Germany.

[1] J. Arrinton *et al.*, Nucl. Inst. Meth. **A311**, 39 (1992).
[2] J.W. Watson *et al.*, Nucl. Inst. Meth. **A272**, 750 (1988).
[3] R.G. Arnold *et al.*, Phys. Rev. **C23**, 363 (1981).

7 Ultra-Relativistic Heavy Ion Collisions

7.1 CERN experiment NA35: 200 GeV/nucleon Sulfur on Cu, Ag, and Au

W.J. Braithwaite, P. Chan, J.G. Cramer, D.J. Prindle, T.A. Trainor, X. Zhu and the NA35 Collaboration

Experiment NA35 which uses ultra-relativistic heavy ion beams from the CERN Super Proton Synchrotron, was originally approved in 1983 and has been in operation, in one form or another, since 1985. The experiment has been very successful in using a streamer chamber to record heavy ion collisions in a 1.5 T magnetic field. Many new insights into relativistic heavy ion collisions have been provided by NA35, but the economic and human constraints of scanning streamer chamber photographs have limited the number of events in a given data sample to a few thousand.

In late 1990 a new time projection chamber (TPC) with an active volume of 2.4 x 1.2 x 1.08 m^3 was built by the Munich group and added to the experiment in a position downstream from the magnet, as shown in Fig. 7.1. The University of Washington Ultra-Relativistic Heavy Ion Group joined the NA35 Collaboration just after a 1990 test run of the TPC and has been able to participate in the fall 1991 run (6 weeks) and spring 1992 NA35 run (6 weeks). These are the final runs of the experiment and the first in which the TPC is fully operational. With the successful operation of the TPC it has become possible to increase the number of events in a given data sample to a few hundred thousand. This has had a qualitative effect on the style of data analysis and the quality of the resulting data in NA35.

Significant new results from the NA35 Collaboration have been reported at the recent Quark Matter Conference. Investigations of strange particle production indicate a tendency toward flavor equilibration in nucleus-nucleus collisions which has not been seen in proton-nucleus collisions. Investigations of three dimensional factorial moments in the production of negative pions show non-statistical multiplicity fluctuations that may be explainable in terms of the expected Bose-Einstein correlations between the emitted pions. Analysis of source sizes using HBT interferometry with improved statistics on the pions emitted in central collisions indicates that the emitting source has a characteristic radius of about 5 fm (as compared to estimates of as much as 8 fm from previous reports with poorer statistics).

For the spring 1992 NA35 run the number of readout pad-channels of the TPC will be increased by a factor of 4, and it will be turned with its long axis along the beam to provide an increased sample of dE/dx for improved identification of antiprotons. Seven members of the University of Washington URHI Group will participate in all or part of this run, and we will be active participants in the data analysis when the run is completed later this year.

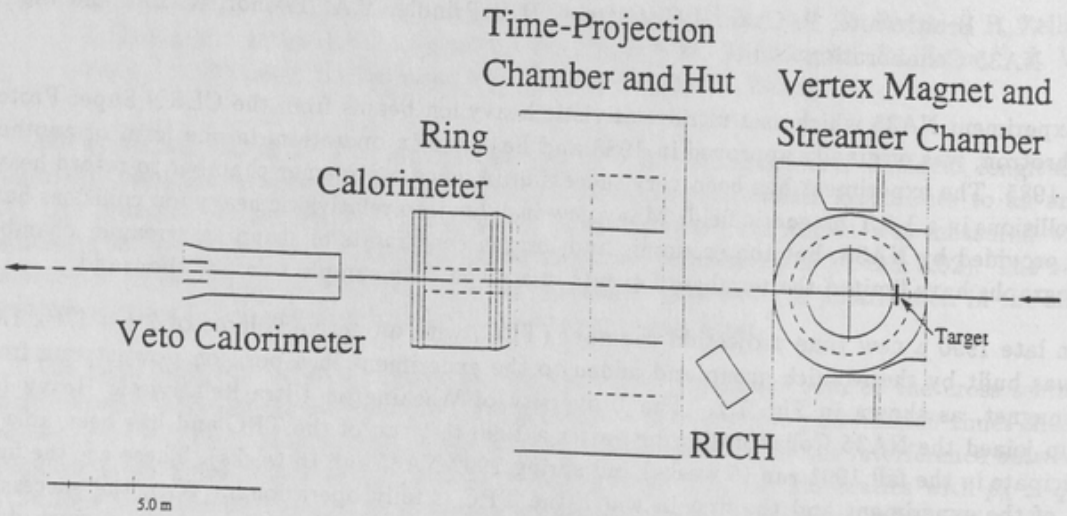

Experiment NA35
A Tracking Spectrometer for Heavy Ion Collisions

Fig. 7.1

7.2 Tests of silicon drift detectors as vertex trackers for STAR

J.G. Cramer, D.J. Prindle, T.A. Trainor and the STAR-SVT Working Group

The silicon vertex tracker (SVT) design for STAR employs the relatively new technology of the *silicon drift detector* (SDD).[1-5] An SDD can be thought of as a miniature two-dimensional time-projection chamber fabricated on a silicon wafer. A standard n-type silicon wafer is lithographed with a set of parallel constant-voltage conducting strips separated by integrated voltage-divider resistors, so that an electric drift field is established in the plane of the wafer. Charge carrier electrons created by ionization from the passage of charged particles through the silicon move down the wafer to the end, where their charge is collected on a set of anodes spaced about 200 microns apart. Each anode is connected to an electronics system which measures the magnitude and the arrival time of the collected charge. Interpolation between adjacent anodes together with determination of the arrival-time centroid can provide position resolutions down to about 10 microns.

The SDD is well suited to the STAR detector because the drift collection times and cell occupancies of the device are well matched to the beam repetition rate and event multiplicity of RHIC events. It also offers the possibility of providing dE/dx information for low-momentum pions for particle identification. Particle identification of relativistic particles is complicated by the high energy tail in the distribution of deposited energy. However, estimates at CERN made by Schukraft predict that combined dE/dx measurements from a three or four layer SVT can provide good particle identification information. We would like to verify these predictions with dE/dx measurements of pions and other particles using our SDD prototypes.

A central Au + Au collision at RHIC is expected to produce several thousand pions in a broad energy distribution which peaks at about 250 MeV/c. From February 27 to 29, 1992 we conducted preliminary tests of an SDD prototype using the M-11 pion beam line at TRIUMF to produce 300 MeV/c negative pions which were passed through a prototype detector with 20 channels of electronics. This allowed us to test our prototype SDD unit in a controlled environment similar to that expected from RHIC collision events.

The data from the first TRIUMF run are now being analyzed to extract the detailed shape of the dE/dx distribution for pions in the selected momentum bite. This is of interest in assessing the usefulness of SDD energy loss information in particle identification at relatively low momenta, to complement or supplement the identification capabilities of the STAR TPC system. We have requested a second run at TRIUMF in September, 1992, to continue these measurements and to extend them to the lower energy M-13 pion beam line where we can investigate the response of the SDD to pions in the momentum range 50 to 150 MeV/c.

[1] P. Rehak and E. Gatti, Nucl. Instrum. Meth. **225**, 608 (1984).
[2] E. Gatti, Nucl. Instrum. Meth. **226**, 129 (1984).
[3] P. Rehak *et al.*, Nucl. Instrum. Meth. **235**, 224 (1984).
[4] E. Gatti *et al.*, Nucl. Instrum. Meth. **A253**, 393 (1987).
[5] E. Gatti *et al.*, Nucl. Instrum. Meth. **A274**, 469 (1989).

7.3 STAR SVT prototype tests at LBL

C. Naudet,* G. Odyniec,* J. Schambach,* T.A. Trainor and the Star Collaboration SVT Group

As part of the LBL-UW collaboration to develop a silicon vertex detector (SVT) for the STAR detector at RHIC we have set up a laboratory to test prototype silicon drift detectors (SDD) at LBL. The essential elements consist of a detector housing, a computer-controlled microscope and stage, a PC-based data acquisition system and a pulsed IR source.

The initial SDD prototype consists of a 300 u x 1 cm x 1.5 cm silicon wafer with an array of 42 anode pads along one short side. An array of cathode strips grades a drift field perpendicular to the pad row. Ionization produced by a fast charged particle passing through the detector drifts toward the anode pads and is collected on some subset of the pads. The time and space distribution of collected charge is used to reconstruct the hit position of the fast particle.

The detector housing serves as a shield against ambient light and EMI. as well as providing temperature stabilization. It contains preamp/shapers and a biasing network for the SDD. The pulsed IR source provides a precise method for creating charge at a well-defined point on the detector for calibration purposes. The computer-driven microscope stage. in combination with the light source. permits measurement of drift-speed distributions. pad responses and two-track resolution.

The data acquisition system is based on a Macintosh PC and CAMAC crate system. Pad outputs are digitized by flash ADCs and displayed as histograms.

This system was also transported to TRIUMF recently for in-beam tests of this prototype SDD with a pion beam (cf. article 7.2).

(a) (b)

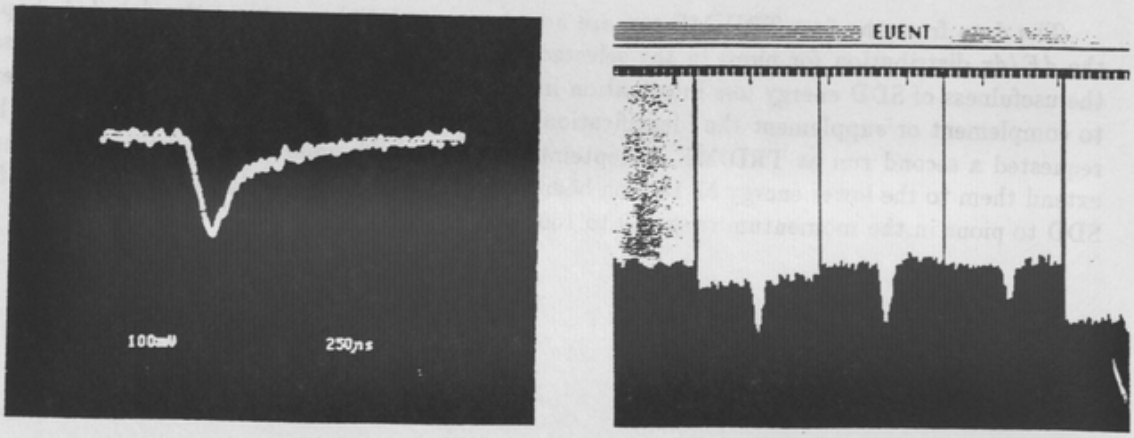

Fig. 7.3. (a) 300 MeV/c pion signal on one anode pad after preamp/shaper: (b) pion signal on three neighboring anode pads digitized by CAMAC flash ADCs.

*Lawrence Berkeley Lab, Berkeley, Ca.

7.4 Analytical relations for pion and kaon source sizes from Hanbury-Brown-Twiss correlation widths

W.J. Braithwaite, J.G. Cramer and J. Nettleton

In experimental determinations of pion source characteristics using Hanbury-Brown-Twiss (HBT) interferometry with pions emitted in ultra-relativistic heavy ion collisions, it is frequently desirable to establish the maximum source radius and/or duration that is accessible with a given instrumental resolution of the two-particle vector momentum-difference $\vec{q} = (q_r, q_t, q_l)$ of the correlated particles.

We have used the symbolic algebra program *Mathematica*[1] to solve the analytic Kolehmainen-Gyulassy[2] correlation formalism for an exact expression for the source radius r_t and an approximate relation for the source duration τ_0 in terms of $\vec{q}$ and the transverse momentum p_t.

The expression for the maximum transverse radius (given below) is for *uncharged* two-particle correlations under the condition that the momentum-width of the uncharged correlation function is equal to 3/2, half way between its peak and background values. The similar expression for maximum τ_0 (not shown) is more complicated and is based on a series expansion. We find that the above criterion provides a value for maximum r_t which is very similar to that obtained in numerical calculations of the peak positions of *charged-particle* HBT correlations.[3]

The values for uncharged pions (kaons) were found to lie consistently between the peak of the charged-particle correlation and its half-peak-value point. Therefore apart from the reduction in peak-value for the charged particle correlation, the expressions derived from the uncharged HBT correlation give conservative estimates of measurable source characteristics.

$$r_t(q_r, q_t, q_l; p_t) = \frac{\hbar}{\sqrt{{q_r}^2 + {q_t}^2}} \sqrt{\frac{1}{2} \log\left(2 \frac{|\mathrm{K}_0(\sqrt{u_{12} + v_{12}})|^2}{\mathrm{K}_0(\frac{m_1}{T})\mathrm{K}_0(\frac{m_2}{T})}\right)}$$

where $m_1 = \sqrt{(p_t + q_r)^2 + \mu^2}$ and $m_2 = \sqrt{(p_t - q_r)^2 + \mu^2}$ are transverse masses of correlated bosons, $u_{12} = [\frac{1}{2T}(m_1 + m_2) + i\frac{\tau_0}{\hbar}(m_1 - m_2)]^2$, and $v_{12} = 2[(\frac{1}{2T})^2 + (\frac{\tau_0}{\hbar})^2]m_1 m_2 \sinh^2[\frac{1}{2}(y_1 - y_2)]$. Here μ is the pion (or kaon) rest mass, K_0 is an irregular modified Bessel functions of order 0 and possibly complex argument, and y_1 and y_2 are the rapidities of the correlated particles.

We are using these results to examine the limits on measurable HBT source size implied by the momentum and two-track resolution of various STAR detector design alternatives.

[1] Steven Wolfram *et al.*, Wolfram Research, Inc.

[2] K. Kolehmanien and M. Gyulassy, Phys. Lett. B **180**, 203 (1986).

[3] J.G. Cramer, Phys. Rev. C **43**, 2798 (1991).

7.5 Gas detector prototype studies

T.A. Trainor and X. Zhu

We have commenced pilot studies for gas multiplicity detector development for STAR and other ultrarelativistic heavy ion detector systems. The general motivation for this program was described last year.[1] Initially we are investigating a single-stage high performance planar avalanche counter with very good rf and electrostatic structures to examine the performance limits to such structures, and particularly the limits to dynamic range of the detected particle primary ionization imposed by detector stability requirements.

An example of the performance of this detector is shown below. The detector active region is 2 cm diam, 1.25 mm thick and operating with isobutane or Argon-CH4 in various ratios. The detector can accommodate both single photoelectrons and ^{241}Am alphas under the same operating conditions with excellent signal-to-noise ratio for either signal. The pulses have passed through a single 10x gain stage of a Philips 776 amplifier. Gas gain is limited only by regenerative field emission from the cathode upon arrival of positive ions from the avalanche.

We have also designed a multigap detector to study planar avalanche structures in combination with ionization/drift regions, gate structures and wire planes, again to examine the dynamic range limits on such structures at high gain. These results will allow us to design a prototype segment of a full-scale large area detector. The goal of this program is to achieve high-gain, versatile detector structures which are capable of high particle fluxes yet stable against discharge initiated by highly ionizing slow knockon particles.

(a) (b)

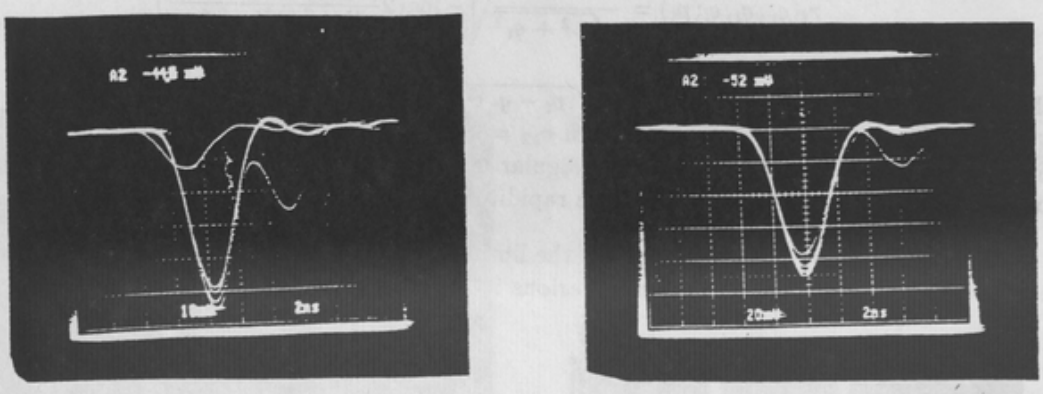

Fig. 7.5. (a) detector response to photo electron, 1240 v bias, 70 Torr; (b) response to 241 Am alpha, 1100 V bias, 70 Torr.

[1] Nuclear Physics Laboratory Annual Report, University of Washington, p. 45 (1991).

7.6 Test of the NA35 readout electronics

R. Jones,* J. Schambach,* X. Zhu and the NA35 collaboration

We have successfully tested 52 readout boards ($\sim$ 6656 channels) for the NA35 Time Projection Chamber (TPC) which is going to be used for the upcoming April run in CERN. The readout boards are printed circuit boards custom designed and built at the Lawrence Berkeley Laboratory. Development of the new TPC electronics is a collaborative effort of the LBL, University of Washington, MPI Munich, the University of Frankfurt and GSI.

Each readout board contains eight Switched Capacitor Arrays (SCAs), two Analog to Digital Converters (ADCs), memory, optical link circuitry and multiplexing and logic chips to handle the data flow between these elements. The SCA, as is apparent from the name, is an array of capacitors which can be selected and controlled by an array of switches. It is used to store analog signals. Each SCA chip contains 16 channels of 512 capacitors. The eight SCAs on one readout board are multiplexed to share the two ADCs. The digital signal from the ADCs is further multiplexed and is sent to the receiver board through a fiber optics link. Preamplifiers and shapers are used before the readout boards to condition the signal from TPC readout pads.

Testing the readout electronics was done in two steps. First a SCA test stand was set up using a Macintosh and a commercial data acquisition software package called KMAX. The pedestal and linearity of the SCA chips were checked as they arrived from the factory. Only those chips with low pedestal and high linearity were selected for use in the readout boards. The yield was about 50%. Then a second test stand was set up to test the completed readout boards.

We obtained 128 channels of preamplifiers and shapers from MPI Munich where they have been constructed. The 128 channels of preamplifiers and shapers are contained on eight small printed circuit boards, and each preamplifier/shaper board is connected to a SCA on the readout board via a 40-pin flat ribbon cable. An EOS[1] quad receiver board resident on a 9U VME card was used to process the fiber optics data from the readout board. The test was controlled by a SunSPARKS station II computer. For the software, we utilized the EOS Test Manager (developed by C. MacParland of LBL) for control of the boards and the NA35 Pad Monitor (developed by J. Schambach of LBL) for display of the data.

The test consisted of a measurement with pedestal only and a measurement with pedestal and a calibration pulse. The calibration pulse was obtained by injecting certain amount of charge into the preamplifiers. Differentiated by the shapers, the signal appeared at the input of the SCAs as a pulse. For a readout board, we examined the pedestal and calibration spectra of all the channels to determine whether the board was functioning properly. For the bad boards we found, among other things, misplaced components, bad SCAs, open soldering, solder bridges and broken traces. Once a board had passed the preliminary test we would leave the power on and test it again 12 hours later. Of the 52 boards tested, only one failed after power on for 12 hours. The test data were saved on computer disk for future use in analyzing the TPC production data.

*Lawrence Berkeley Laboratory, Berkeley, CA.

[1] "Nuclear Equation Of State", a LBL experiment. The NA35 electronics is essentially modified EOS electronics.

7.7 Maximum likelihood analysis of dE/dx sampling at relativistic energies

J.G. Cramer

At relativistic energies the technique of dE/dx particle identification is complicated by presence of the "Landau tail" in the dE/dx probability distribution. When a relativistic charged particle passes through a thin slab of material there is a sizable probability that the particle will have a hard scattering with an electron, resulting in anomalously large energy loss and distortion of the dE/dx distribution. For this reason it is necessary to make a number of independent samples of dE/dx and to analyze them in a way that removes the high energy tail and provides a reliable estimate of the most probable energy loss Δ_p, which can be used in identifying the particle.

In dE/dx measurements with time projection chambers (TPC) or silicon vertex trackers (SVT) the method of the "truncated mean" has become standard. The dE/dx samples are ordered by value, the upper 50–60% of the samples are excluded under the rationale that they are contaminated by the Landau tail, and the remaining samples are averaged to give an estimate of Δ_p. This procedure has been demonstrated to work well in TPC applications and has been shown with Monte Carlo calculations to be applicable also to multi-layer SVT detectors.

The problem with the truncated mean procedure is that it throws away data. This can be a particularly severe problem when there are only a few measured samples available, as in the case of a three or four layer SVT. We have therefore devised an alternative scheme for estimating Δ_p, the *maximum likelihood method*, which uses *all* the measured values of dE/dx and also exploits the known physics of the energy loss process by using a measured or computed dE/dx distribution function.

We assume that the probability distribution of dE/dx for a particular incident particle energy E is given by $P(x, x_0)$ where Pdx is the probability of measuring a pulse height between x and $x + dx$ and x_0 is the most probable energy loss Δ_p. Since it is a probability distribution, $P(x, x_0)$ is normalized so that its integral is unity and its maximum occurs at x_0. We will further assume that the distribution function scales proportional to x_0, i.e., $\frac{1}{\alpha}P(x, \alpha x_0)$ is the appropriate distribution function when the centroid pulse height is αx.

Therefore, if $P(x, x_0)$ is a known function, the problem of extracting the best estimate of x_0 from an ensemble of measurements reduces to extracting α from those measurements. We propose to do this in the following way. For n dE/dx measurements $x_1, x_2, \ldots, x_n$ choose an initial "guess" value of $\alpha = \sum_{i=1}^{n} x_i/nx_0$. Now define $G(\alpha)$, which is the joint probability or *likelihood* of having measured the observed points, given the assumed probability distribution P. It has the value $G(\alpha) = \alpha^{-n} \prod_{i=1}^{n} P(x_i, \alpha x_0)$. Now repeat this procedure over a range of values of α and obtain the α value for which $G(\alpha)$ is maximum. Then the estimate of dE/dx which has maximum likelihood is αx_0.

The statistical properties of this new method of dE/dx analysis have not yet been investigated, but we have been able to show that the procedure gives the expected result for the limiting cases when n=1 or 2 or when n is very large. We are preparing Monte Carlo calculations of the dE/dx resolution obtained with maximum likelihood analysis as compared to more conventional truncated-mean prescriptions.

7.8 STAR trigger system

T.A. Trainor

The RHIC collider is presently intended to provide a beam crossing rate at each detector site of 8.9 MHz. Some fraction of these crossings is expected to contain events of interest to the STAR detector. For p-p the minimum bias trigger rate should be $\sim$ 1 MHz, whereas for Au-Au the rate should be $\sim$ 1000 Hz.

The STAR trigger system is required to sense the occurance of desired events in a time of order one crossing for the lowest order (min bias) trigger, and initiate processing in other detector systems. We have developed a baseline trigger system consisting of an array of fast detectors, a logic system, and a computer manager.

The design trigger detector array at present consists of a scintillator annulus to cover one unit of pseudorapidity (eta) near $|\eta| = 5$, a gas multiplicity annulus to cover the range $2 < |\eta| < 4.5$ and an adaptation of the STAR TPC anode wires to extend multiplicity coverage to $1 < |\eta| < 2$.

The trigger logic is contained in two end cap trigger units at either end of the STAR solenoid and a main trigger unit with computer manager at the midplane.

The detectors are segmented so that mean hit occupancy/segment for a Au-Au event is 10–20%. Hits are ORed to form the min bias trigger, which is combined with timing information from the scintillator annuli to filter out bad events outside the standard RHIC crossing time and space windows.

Higher level triggers which serve to further filter the data on longer time scales include collision centrality determined by total particle multiplicity measured over some eta range and fluctuations in the multiplicity distribution which may signal the onset of unusual QCD thermodynamics such as a phase transition.

These and other trigger functions such as on-line calibration and efficiency checks will be managed by computer driven gates to reduce the event rate to 1–10 Hz, which is the intended bandwidth for mass storage.

7.9 NA35 TPC systematics

T.A. Trainor

The NA35 TPC is a box structure with active volume 1 m x 1.2 m x 2.4 m. The electron drift is vertical with readout plane at the top. The TPC is located 5.36 m downstream from the center of the NA35 vertex magnet, and is used to visualize particle tracks produced in collisions of protons and sulfur nuclei with a variety of targets at the CERN SPS as part of a program of research in ultrarelativistic heavy ion reactions.

In connection with an NA35 run at CERN in September–October, 1991 I carried out an analysis of systematic errors for the newly installed TPC. The figures below represent a small sample of the results. In Fig. 7.9-2 I show the position and angle correlation in the horizontal (bend) plane with the vertex magnet on. The TPC was centered on the beam line. The dark vertical band shows the spectrum of somewhat degraded protons transmitted through a copper target. The index marks unexplained tracks which were charged in the beam transport system, passed undeflected through the vertex magnet and then made tracks in the TPC. The diffuse group of tracks in the upper left quadrant were determined to be mu-minus particles from a production target 0.7 km away. A slight deviation of the degraded protons from vertical on the correlation served to characterize the effective field boundary of the vertex magnet.

In the second figure (Fig. 7.9-2) the prominent hook in the correlation was found to be due to a systematic error in the charge cluster centroid determination near the inner walls of the TPC. Failure to detect this systematic would have resulted in significant distortion of the corresponding P_t spectra.

Other results of this analysis included precise techniques to determine the effective location of the TPC and the realization that with the greater precision capability of the TPC the usual beam defining system must be replaced. For the run scheduled for April–May, 1992 a silicon strip detector hodoscope has replaced the old scintillator system.

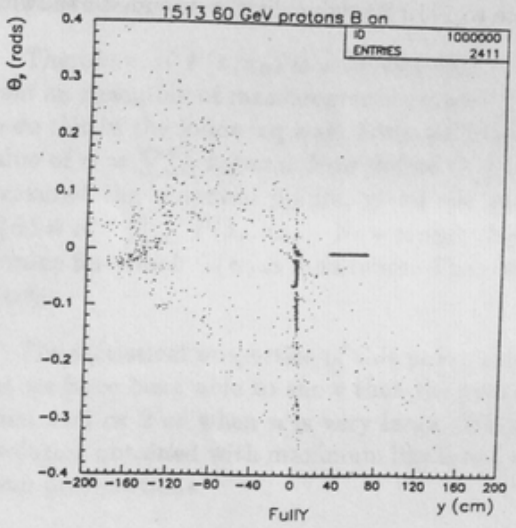

Fig. 7.9-1. (see text)

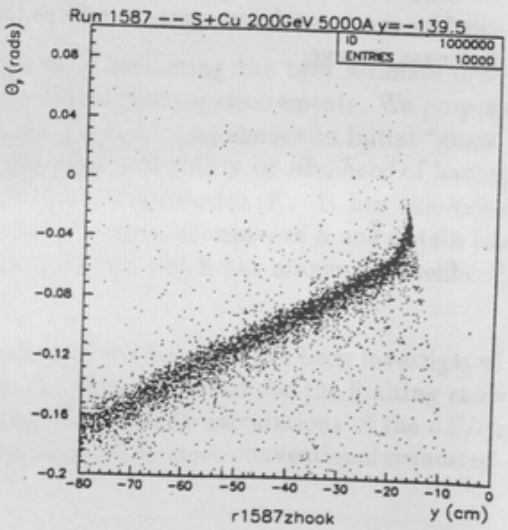

Fig. 7.9-2. (see text)

8 Cluster Fusion

8.1 Cluster and Molecular Impact Nuclear Fusion

J. Neubauer, T.A. Trainor, R. Vandenbosch, D.I. Will and D. Ye

We have continued our study of cluster and molecular $d + d$ fusion described in last year's report.[1] A major thrust during the past year has been the study of the fusion yield for small deuterated water clusters. This was motivated by the surprising results of Bae *et al.*[2] who reported an enhancement for clusters comprised of as few as two water clusters. We have performed a careful study with cluster anions with up to four molecules and have not been able to confirm their results. Our yields are two order of magnitude lower than theirs for four molecules per cluster and can be reproduced by calculations which assume only free deuteron-deuteron fusion. This work has been published.[3]

The recent successful completion of isolation transformers operating up to 300 keV[4] has enabled us to search for molecular impact enhanced fusion with deuterated p-toluene sulfonic acid anions, $C_7D_7SO_3^-$, incident on a deuterated polyethylene target. We have set an upper limit of $1x10^{-13}$ protons per deuteron at an ion energy of 324 keV. This low yield is inconsistent with the typical yields measured by Bae *et al.* One might have expected a larger yield on the basis of the size dependence originally reported by Beuhler *et al.*,[5] but our limit is not inconsistent with their later data[6] with somewhat better mass resolution. The latter data, however, only extends down to clusters with 100 molecules.

Beuhler *et al.*[6] have noticed that one observes cluster impact enhanced fusion even when normal H_2O clusters are accelerated, although at a rate more than an order of magnitude lower than with D_2O clusters. We have also observed this with small H_2O cluster anions, and have initiated an investigation with carbon clusters. The use of a homogeneous projectile should enable less ambiguous interpretation of the results. C_n clusters with n up to about 19 are readily produced in our sputter ion source by bombarding graphite with Cs. We have obtained a sample of C_{60} courtesy of Rainer Beck of the U. W. Chemistry Department and Manfred Kappes of Northwestern University and attempted to produce C_{60} clusters in our ion source. This has been unsuccessful to date, although very small yields of predominantly odd-numbered clusters are seen up to $n \sim 50$. This will be pursued further. In the meantime we have measured the fusion yield for smaller clusters through $n = 19$. These results are shown in Fig. 8.1. These results are plotted versus energy per carbon atom so that cluster enhancement would manifest itself as a discrepancy between the yields for clusters as compared to carbon ions at the same energy per carbon. It can be seen that we have no evidence for cluster enhancement. Furthermore, we have been able to reproduce the observed trend by a variant of the Carraro *et al.*[7] knock-on model with improved energy transfer

[1] Nuclear Physics Laboratory Annual Report, University of Washington (1991) p. 15.
[2] Y.K. Bae, D.C. Lorents and S.E. Young, Phys. Rev. A **44**, 4091 (1991).
[3] R. Vandenbosch, T.A. Trainor, D.I. Will, J. Neubauer and I. Brown, Phys. Rev. **67**, 3567 (1991).
[4] G. Harper, this report, Sec. 12.3.
[5] R.J. Beuhler, G. Friedlander and L. Friedman, Phys. Rev. Lett. **63**, 1291 (1989).
[6] R.J. Beuhler, Y.Y. Chu, G. Friedlander, L. Friedman and W. Kunnmann, J. Phys. Chem. **94**,7665 (1990).
[7] C. Carraro, B.Q. Chen, S. Schramm and S.E. Koonin, Phys. Rev. **A42**, 1379 (1990).

and stopping parameterizations. In this model fusion is induced by target deuterons struck by carbon atoms and colliding with other target deuterons.

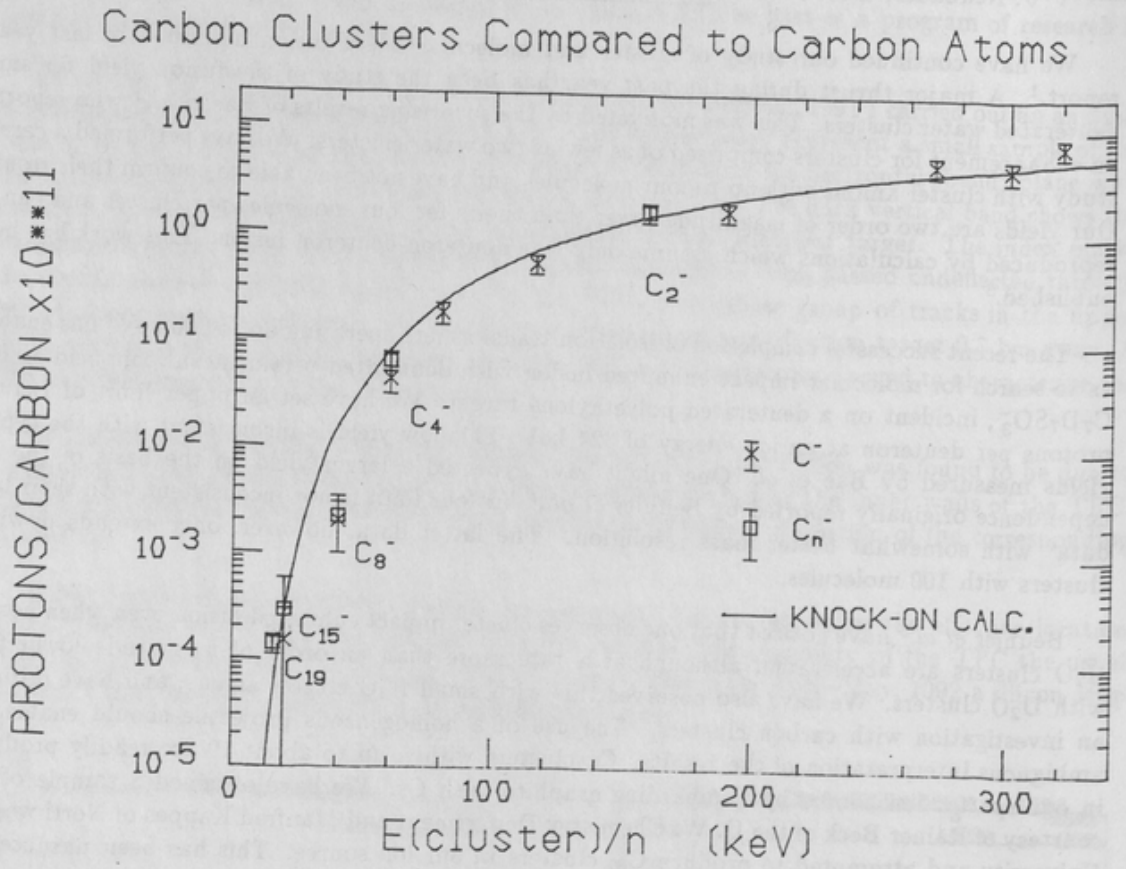

Fig. 8.1. Comparison of fusion yields for carbon clusters with those for single carbon atoms. Collective effects would be revealed on this plot by a larger yield for clusters compared to single atoms at the same energy/atom.

8.2 New Theory of Projectile Stopping at Low Energies

T.A. Trainor

For a variety of applications involving projectile impact on targets at low energies, including ion implantation, sputtering and cluster impact fusion, there is a need to understand in detail the low energy projectile stopping process. Despite decades of effort the description of projectile stopping below 100 keV*A is still fairly uncertain. I have attempted to provide a semiclassical theory which is kinematically consistent and well behaved in various limiting cases.

It is usual to separate projectile stopping into two parts: electronic (scattering from target electrons) and nuclear elastic (scattering from target nuclei). At high energies the electronic stopping power is given by the Bethe formula which assumes a uniform target electron density with binding to an uncharged lattice. The binding energy measure I is the single parameter. In some treatments at low energies the electronic stopping power is assumed to vary as $\sqrt{E}$ (based on an electron gas model). In a typical parameterized fit to data[1] these two descriptions are combined by a splicing prescription to obtain a smooth transition from one energy region to the other.

For the electronic component of my theory I generalize the Bethe formula by recognizing that the charge distributions of the target and projectile at any given projectile energy are critical to the energy loss process, and in particular that the average neutrality of the target must be represented in a more general theory. Starting with a modification to the impact parameter-scattering angle relationship which includes shielding of target electrons by nuclei beyond some characteristic distance b_0, I develop a general expression for stopping which includes this shielding as given in the expression

$$\frac{dE}{dx} = \frac{2\pi n e^4 Z_1^2 Z_2^2}{mv^2}\left\{[1+(\frac{b_1}{2b_0})^2]\,\ln[\frac{1+(\frac{b_1}{2b_0})^2}{(\frac{I}{\Delta E_0})^2+(\frac{b_1}{2b_0})^2}] - (\frac{b_1}{2b_0})^2[\frac{1-(\frac{I}{\Delta E_0})^2}{(\frac{I}{\Delta E_0})^2+(\frac{b_1}{2b_0})^2}]\right\},$$

where $b_1 e^{\frac{b_1}{a}} = \frac{2e^2 Z_1 Z_2}{mv^2}$; $a > 0.75Z^{-\frac{1}{3}}$Å; $b_0 \sim 3$Å; $I \sim 13ZeV$ and $\Delta E_0 = 2mv^2$.

The projectile charge state is represented by a, with the lower limit corresponding to a neutral projectile. As the projectile energy falls the mean projectile charge state decreases with a neutral projectile as the limiting case. This is represented by a reduction in the shielding distance a consistent with a Thomas-Fermi potential for the projectile. This theory gives a consistent description of electronic stopping of light projectiles on light targets over an extended energy range in work to date. In addition it deviates significantly from the $\sqrt{E}$ dependence sometimes assumed at low energies, with a cutoff at low energy corresponding to the consequences of electron binding in target atoms. This behavior is confirmed in studies of very low energy projectiles on dielectric targets.

For the case of nuclear elastic stopping the I parameter in the general stopping expression represents atom binding into the target lattice, important in studies of lattice melting, but for considerations of projectile stopping this parameter may be neglected. The simplified general formula which describes nuclear elastic stopping is given below.

[1] H.H. Anderson and J.F. Ziegler, *Hydrogen Stopping Powers and Ranges in All Elements*, Pergamon, New York (1977).

$$\frac{dE}{dx} = \frac{2\pi n e^4 Z_1^2 Z_2^2}{Mv^2}\left(\frac{b_1}{r_1}\right)^2 \left\{\left[1+\left(\frac{b_1}{2b_0}\right)^2 \ln\left[1+\left(\frac{2b_0}{b_1}\right)^2\right]-1\right\},$$

where $b_1 e^{\frac{b_1}{a}} = \frac{2e^2 Z_1 Z_2}{Mv^2}$; $a = 0.75Z^{-\frac{1}{3}}$ Å; $b_0 = 0.75Z^{\frac{1}{3}}$ and $r_1 = \frac{2e^2 Z_1 Z_2}{Mv^2}$.

In the low energy limit this formula properly goes over to a hard sphere stopping expression. In this expression the shielding (b_0) and closest approach (b_1) parameters must be obtained from the Thomas-Fermi model. The ratio b_1/b_0 gives a measure of the mean scattering angle at a particular projectile energy. When this parameter nears unity the projectile has essentially lost its identity and the remaining projectile energy is shared with nearest neighbors to initiate a diffusion process. Failure to stop the range integration at this point has resulted in unphysically large range values in other treatments.

8.3 Proposed cluster impact fusion mechanism

T.A. Trainor

The report of fusion yields many orders of magnitude above those expected from the simple $d-d$ cross section observed by Beuhler *et al.*[1] in the impact of energetic deuterated water clusters on deuterated targets has caused great interest in the general physics community in the past two years. Proposed explanations have included modification of the $d-d$ cross section at low energies, contamination of the cluster beam by light fragments and a variety of cluster stopping models which seek to augment the initial cluster deuteron energy to a level consistent with the observed yields and an unmodified $d-d$ fusion cross section. Further experiments by Beuhler et al. tend to confirm their initial observations. The result of my analysis indicates that the best general approach to explaining these results involves fusion yield enhancement by thermalization of the cluster kinetic energy during the cluster stopping process, as first suggested by Echenique.[2]

While there have been a number of speculations on the process of thermalization of the cluster energies and calculations of fusion yields based on assumed temperatures, there has been no detailed model to date which relates the stopping and thermalization process to the achieved temperature. To this end I have made a study of low energy projectile stopping (cf. section 8.2) and have developed a kinematically consistent model of the cluster thermalization process which reproduces the general features of the cluster impact fusion yield dependence on cluster size and incident energy.

A key feature of this model is that for cluster sizes near the peak of the experimental yield curve ($n \sim 200$) the cluster size is comparable to the "nuclear scattering" range of oxygen atoms in oxygen or carbon. Under these conditions the cluster oxygens and an equivalent number of target oxygens form a shock (not a plasma) during the initial stages of cluster stopping which is highly thermalized and which has an elevated density. The temperature of the shock is determined by the relative energy of the shock and its "image" in the CM. This temperature is approximately 400 eV for the conditions of the BNL experiments. The thermalized shock still bears the CM energy of the shock and image, and a fraction of this may serve to increase the temperature of the leading surface of the shock (to 500 eV) as it continues to slow down in the target.

With the details of this model it is possible to explain the peak observed in yield vs cluster size as due to a combination of decreasing energy for fixed energy/cluster and increasing cluster size which enhances shock formation by large-scale lattice disruption.

[1] R.J. Beuhler, G. Friedlander and L. Friedman, Phys. Rev Lett. 63, 1292 (1989).
[2] P.M. Echenique, J.R. Manson and R.H. Ritchie, Phys. Rev. Lett. 64, 1413 (1990).

9 External Users

9.1 Radiation effects in electronic and optoelectronic devices

B. Evans,* C.A. Gossett,* B. Hughlock* and A. Johnson*

The Boeing High Technology Center is developing new optoelectronic technologies for space applications. Space contains a harsh radiation environment. This radiation can produce many effects on electronic and optoelectronic devices. Additionally, as new technologies emerge new radiation effects are uncovered. In order to develop space systems capable of operating reliably, the basic mechanisms of radiation effects must be studied and understood.

Next year a space satellite will be placed in orbit containing optoelectronic transceiver parts recently developed at the High Technology Center. This past year we studied the radiation damage mechanisms on laser diodes and LEDs used in these parts. Additionally, we studied single-particle effects in InP heterostructure transistors and basic ion-induced charge collection mechanisms.

The Van de Graaff accelerator was used to provide the ion beams necessary for these studies. The results of these studies are being used to predict the reliability of these parts in space and will be useful in future designs of electronic systems for space applications.

Last year's work resulted in two papers presented at the IEEE Nuclear Science Radiation Effects Conference which have been published in the conference proceedings:

A. Johnston *et al.*, "The Effect of Temperature on Single-Particle Latchup", IEEE Trans. Nuc. Sci., NS-38, 1435, 1991.

B. Hughlock *et al.*, "Ion Induced Charge Collection in GaAs MESFETs and its Effect on SEU Vulnerability", IEEE Trans. Nuc. Sci., NS-38, 1442, 1991.

*High Technology Center, Boeing Space and Defense Group, Seattle, WA 98124.

9.2 Summary of single event upset testing by BPSRC at the UWNPL

D.L. Oberg,* J.L. Wert* and E. Normand*

Boeing Physical Sciences Research Center (BPSRC) personnel, in support of the 777 Aircraft program, conducted Single Event Upset (SEU) characterization testing on selected semiconductor device-types using heavy ion beams generated by the University of Washington Nuclear Physics Laboratory (UWNPL) Tandem Van de Graaff accelerator. The outcome of the testing, for each device-type, was a qualitative determination of device SEU susceptibility and a characteristic curve for SEU cross-section as a function of particle Linear Energy Transfer (LET).

SEU can be experienced in airplane electronic systems as a result of the natural atmospheric radiation environment at high altitudes. This is in contrast to previous SEU testing conducted at UWNPL that supported space applications.[1] The predominant cause of SEU at these altitudes are the neutrons produced by galactic cosmic rays. The 777 Aircraft program recognized the importance of neutron induced SEU to the reliability of their electronic systems and commissioned BPSRC to determine the SEU characteristics of design candidates thought to be particularly sensitive to SEU.

The mechanism for neutron induced SEU is related to the amount of energy deposited by the incident particle within a sensitive volume of a semiconductor device. The objective of the heavy ion beam testing conducted at the UWNPL was to measure the dependency of SEU probability on particle energy deposition (in terms of cross section as a function of particle LET). The characteristic curve for each device indicated the threshold LET and associated cross section for producing SEU. Figure 9.2-1 shows the threshold LET and associated cross section for a SRAM. These characteristics are used in an analytical procedure to determine the upset rate of the given device-type in the atmospheric neutron environment. This procedure involves integrating the product of the differential atmospheric neutron energy spectrum and the Burst Generation Rate (BGR) over energy and multiplying times the sensitive volume. This function BGR, is defined as the probability that a neutron incident on silicon will produce an energetic recoil with energy E_r or greater. It is related to the threshold LET. The sensitive volume is taken as the SEU cross section times the device-type sensitive thickness. The sensitive thickness in silicon is at least 1μm, based on calculations for typical devices[2] and has often been taken as 3–5μm. The assumed value used for this study was confirmed by upset measurements on the same device-type using a beam of neutrons.[3,4] Figure 9.2-1 presents the results of this procedure for the SRAM data presented in Figure 9.2-1.

The heavy ion beam testing involved the following ions/LETs from the Tandem Van de Graaff: Bromine/33 MeV-cm^2/mg, Chlorine/17 MeV-cm^2/mg, Fluorine/5.1MeV-cm^2/mg, Oxygen/3.7 MeV-cm^2/mg, and Carbon/2.2 MeV-cm^2/mg. The electrical state of the device under test was compared with the electrical state of an unexposed reference and an upset was recorded on a scaler when the electrical states differed. The cross section at each LET was calculated as the number of upsets recorded divided by the exposure fluence.

*Boeing Defense and Space Group, P.O. Box 3999, M/S 2T-50, Seattle, WA 98124.

[1] Nuclear Physics Laboratory Annual Report, University of Washington (1987), p. 44.

[2] P.J. McNulty, W.G. Abdel-Kader and J. Lynch, "Modeling Charge Collection and Single Event Upsets in Microelectronics," Nucl. Instr. Meth. **1**, 52 (1991).

[3] J.L. Ziegler and W.A. Lanford, "Effect of Cosmic Rays on Computer Memories," Science, **206**, 776 (1979).

[4] J.R. Letaw and E. Normand, "Guidelines for Predicting Single Event Upset in Neutron Environments," IEE Trans. Nucl. Sci. **NS-38**, 1500 (1991).

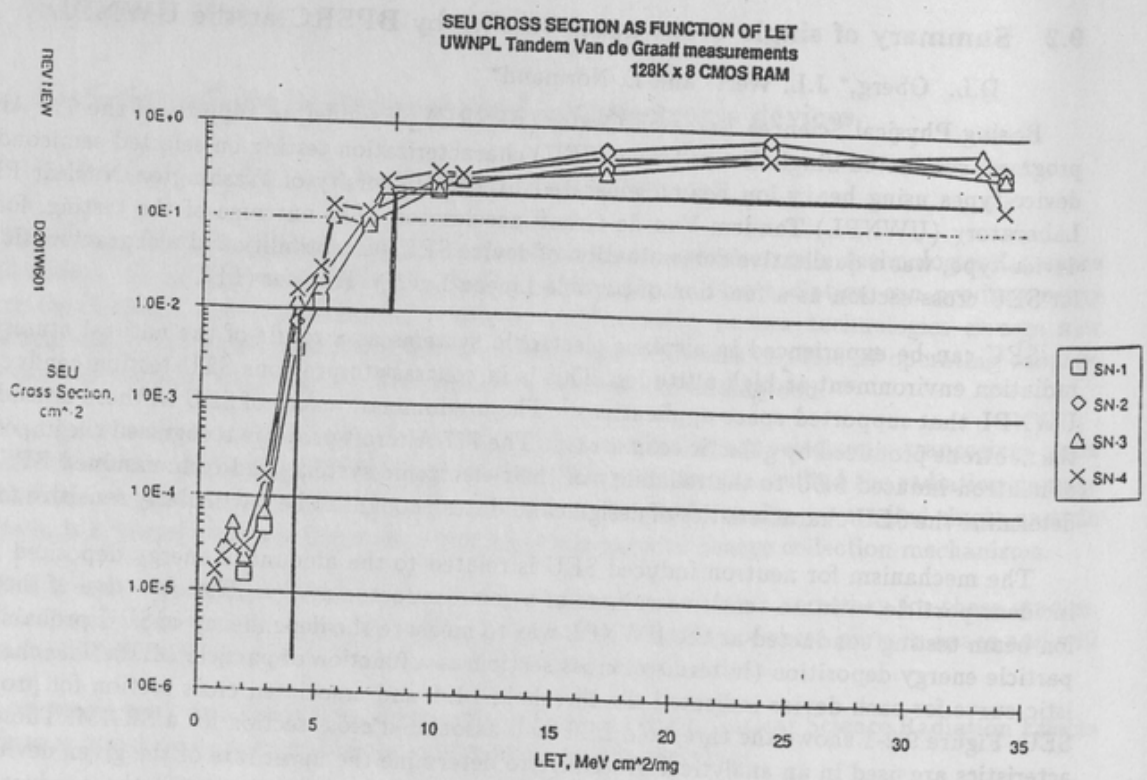

Fig. 9.2-1.

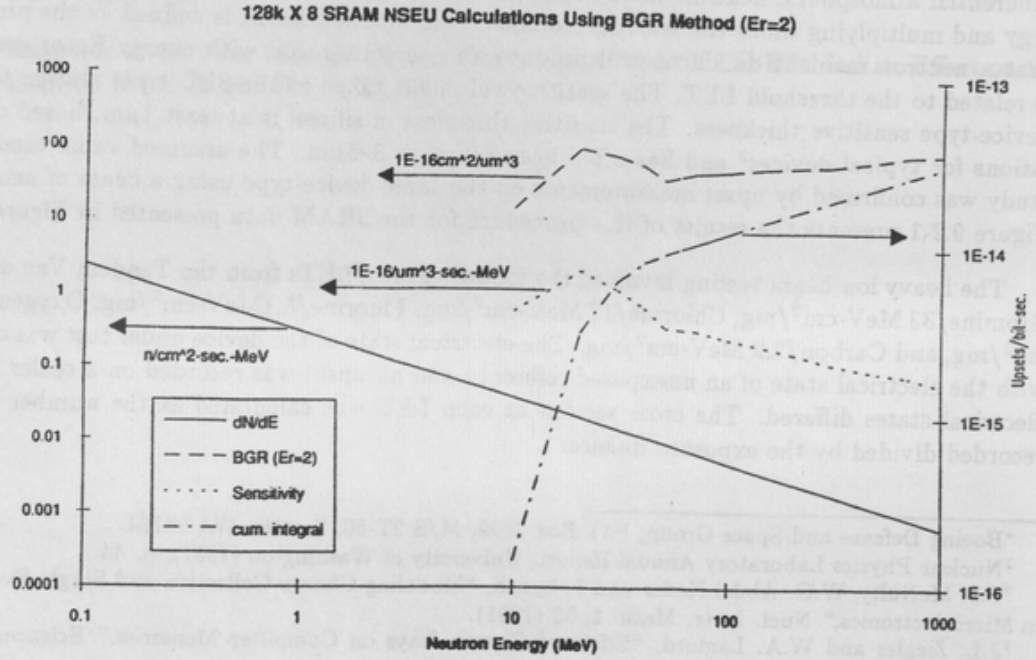

Fig. 9.2-2.

9.3 Targetry for production of radionuclides from ^{3}He irradiation of O and C

J.M. Link,* K.A. Krohn,* W.G. Weitkamp and D.I. Will

New accelerator technology developed by the neutral particle beam program of the Strategic Defense Initiative is being applied to production of radionuclides for positron emission tomography (PET). A cooperative effort between the PET radiochemistry group at the UW and Science Applications International Corp. of San Diego is developing a radionuclide production system that uses a radiofrequency quadrupole (RFQ) accelerator, which provides both advantages and challenges over cyclotrons. The advantages include small size and weight, simple operation/maintenance, minimal shielding and ~80% less power than a cyclotron of equivalent capability. The RFQ produces an 8 MeV, high current (7.5 mA), pulsed beam of He^{++}. The collaborative responsibility of the investigators at the UW is to research and design targetry and chemical systems capable of producing ^{11}C, ^{13}N, ^{15}O, and ^{18}F in sufficient amounts for PET, which are compatible with the energy and power constraints of the RFQ.

The reactions are $^{16}O(^3He,p)^{18}F$, $^{16}O(^3He,\alpha)^{15}O$, $^{12}C(^3He,d)^{13}N$, and $^{12}C(^3He,\alpha)^{11}C$. A ^{3}He beam has some important advantages over low energy H^+ or D^+ for production of C, N, O, and F for PET; readily available oxygen or carbon is used for the targets and nuclear reactions yield fewer neutrons, so require less shielding. Carbon targets only yield neutrons from the $(^3He,n)^{14}O$ and $(^3He,pn)^{13}N$ reactions. All other reactions which produce neutrons have thresholds higher than the beam energy. Oxygen targets only yield neutrons from the $(^3He,n)^{18}Ne$ reaction.

The ^{3}He beam of the tandem van de Graaff accelerator at the Nuclear Physics Laboratory is ideal for testing targets. We have had 9 runs this year to measure radionuclide and neutron yields from C and O and to measure the radiochemical form of the products. Thick target yields for C, N, O, and F radionuclides and the neutron measurements confirmed the feasibility of the PET-RFQ. Our yield for production of ^{11}C from carbon agreed well with the literature. The thick target saturation yields for ^{15}O and ^{18}F from ^{16}O are ~20% greater than calculated from literature cross sections. More neutrons were observed with C than with O targets and the neutrons were predominantly forward scattered, especially with C targets (Fig. 9.3-1).

The nuclides ^{15}O and ^{11}C are produced by $(^3He,\alpha)$ reactions and so are of low specific activity (SA). This is not a practical limitation for labeled H_2O and O_2, but is a severe limitation for $C^{15}O$ and many ^{11}C compounds. We are taking advantage of recoil chemistry to form compounds which are chemically separable from the target material. We have increased SA 1000-fold for $O\text{-}^{15}O$ produced in water and this is sufficient to make safe $C^{15}O$. Similar principles are being used to increase the SA of ^{11}C, yielding a higher SA in the gas products than for ^{11}C retained in the solid carbon. A target of 8 mg/cm^2 is required for the full ^{11}C yield, but several thin foils will give more volatile activity than 1 thick piece of C (Table 9.3). Calculations based on a simple model of the kinematics of the nuclear reaction and electronic stopping of recoil ^{11}C in elemental C (Fig. 9.3-2 below and Sec. 9.4) suggest that as much as 90% of the recoiling ^{11}C escapes from thin (100 μg/cm^2) foils. This loss decreases as foil thickness increases, due to stopping of ^{11}C in the foil. We have tested this by irradiating different thickness of C, both with and without thin Ag wrapping to catch the recoil ^{11}C. Our results are shown in Fig. 9.3-2 and agree qualitatively with the model calculations. The energetic ^{11}C atoms are moderated by He bath gas and react with traces of O_2 to yield $^{11}CO_2$. The target requires optimizing of geometry, gas composition and pressure, but the resulting SA should be sufficient for labeling.

*Department of Radiology, University of Washington, Seattle, WA 98195.

This research program is supported by SDIO-84-89-C-0046, subcontract 13-900224-49.

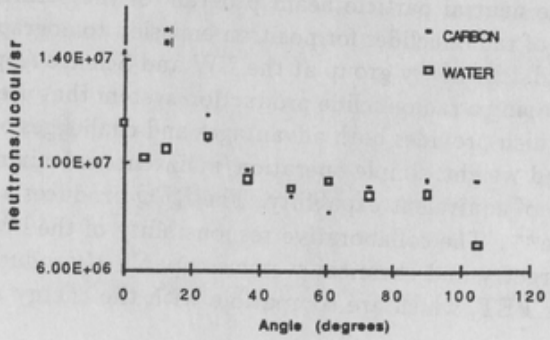

Figure 9.3-1. Angular dependence of neutron yields.

Table 9.3. Experiments to improve the specific activity of ^{11}C.

*Carbon Target** number/thickness	*Separation between foils*	*Percentage of volatile* ^{11}C**
1 foil of 1 mm	0 mm	1%
8 x 0.6 mg/cm^2	9 mm	29%
4 x 0.6 mg/cm^2	15 mm	39%
2 x 0.6 mg/cm^2	35 mm	53%

* The target also contains 2 atm He plus 0.1% O_2.
** The volatile activity was >99% $^{11}CO_2$, the most convenient form for subsequent radiochemical syntheses.

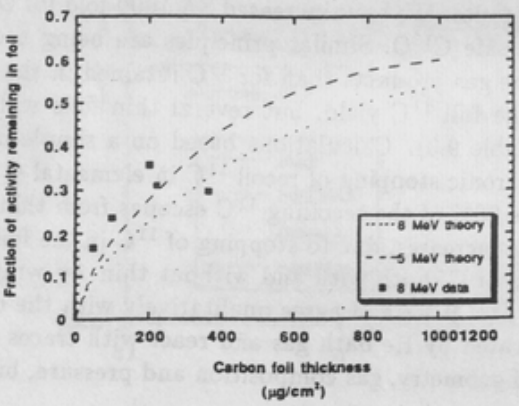

Fig. 9.3-2. Radiochemical form of recoil.

9.4 Yield predictions for PET radionuclide targets

K.A. Krohn,* J.M. Link* and W.G. Weitkamp

The most suitable geometry for the target used to make the PET radionuclides ^{11}C and ^{13}N via the $^{12}C(^3He,\alpha)^{11}C$ and the $^{12}C(^3He,d)^{13}N$ reactions described in Sect 9.3 appears to be a series of thin carbon foils separated by helium gas containing a small percentage of oxygen.. The helium gas can be pumped off to extract the radionuclides. One can maximize the yield of ^{11}C or ^{13}N nuclei in the gas by adjusting the geometry of this target. Using beam time to do this maximization is tedious and expensive so a computer simulation has been performed.

In the simulation each foil is divided into thin laminas. The ^3He energy at the center of the lamina and the cross section for the appropriate reaction is calculated. For each lamina the angular region in which the ^{11}C or ^{13}N nuclei stop in a specific gas space or foil is determined; the yield of ^{11}C or ^{13}N nuclei stopping in gas or in foils is obtained by integrating the cross section over this angular region and summing over all appropriate laminas, foils and gas spaces.

The calculation aims at a 10% precision; irregularities in carbon foils, imprecise alignment of foils, lack of sufficiently precise cross section data and computational complexities make it difficult to do better. It is assumed that the effects of range straggling can ignored and that the ^3He, ^{11}C and ^{13}N particles all travel in straight lines.

In all of the calculations described below, the incident ^3He energy is 7 MeV. The total cross section measurements used for the $^{12}C(^3He,\alpha)^{11}C$ reaction are those of Cirilov *et al.*[1] The measurements for the $^{12}C(^3He,d)^{13}N$ reaction are those of Cochran and Knight.[2] In both cases it is assumed that the cross sections are isotropic in the center of mass frame of reference and that only reactions to the ground states of ^{11}C and ^{13}N need be considered.

The validity of the calculation can be checked by comparing the total thick target saturation yield with a measurement. The yield for the $^{12}C(^3He,\alpha)^{11}C$ reaction given by the calculation is 6.7 mCi/μA, which is in satisfactory agreement with our measured value of 7.1 mCi/μA. The yield for the $^{12}C(^3He,d)^{13}N$ reaction is 0.45 mCi/μA which is a factor of two off from our measured value of 0.22 mCi/μA. The cause of this discrepancy is under investigation.

For both reactions, the simulation gives two maxima for the yield as a function of foil thickness and spacing. One maximum occurs when the foil thickness approaches zero. This is not a useful maximum however because the number of foils is too large to be practical. For the other maximum the optimum geometry at a helium pressure of 1 atmosphere is as follows: for ^{11}C, 0.55 mg/cm^2 thick foils separated by 3.4 cm gives a yield of 1.52 mCi/μA; for ^{13}N, 0.3 mg/cm^2 thick foils separated by 1.8 cm gives a yield of 60 μCi/μA. The maxima are rather broad, decreasing roughly 10% when either the foil thickness or spacing is changed by 40%.

Changing the helium gas pressure for fixed geometry has a very dramatic effect on the yield of radionuclides in the gas. However, if one varies the foil spacing so as to keep the same quantity of gas between foils, the yield remains the same.

A short report giving details of this calculation is available.

*Department of Radiology, University of Washington, Seattle, WA 98195.

[1]S. D. Cirilov, J. O. Newton, and J. P. Schapira, Nucl. Phys. **77** (1966) 472.

[2]D. R. F. Cochran and J. D. Knight, Phys. Rev. **128** (1962) 1281.

10 Instrumentation

10.1 Effect of a poorly coupled PMT on position measurement in liquid scintillator detector

J.F. Amsbaugh, C.E. Hyde-Wright and W. Jiang

We have constructed an array of four time of flight (TOF) scintillation detectors. The detector is liquid scintillator BC-501 in a 5"ϕ by 10" right cylindrical cell[1] with diffuse reflecting walls. Both ends of the cell have 1/4" pyrex windows for coupling photomultiplier tubes (PMT). XP-2041 5" PMTs with voltage bases S563[2], voltage divider B are used. These PMTs have a curved photocathode, and a thin plastic plano concave adapter is used. Our design also uses a conetic magnetic shield[3] which screws into the base. The spring loaded socket of the base keeps the two optical joints in compression. The optical coupling is made with silicone potting compound. Sylgard 184.[4]

The time difference and amplitude ratio of the two PMT pulses from each detector are used to measure the position of conversion along the long axis of the cell. In TOF application better energy resolution is then obtained by correcting the flight path length. Since the axis of the cell points to the target, PMTs are in front and back. In one detector, a skewed distribution of events was observed in one detector, when compared with the others. Reexamination of the gain match, bases, and efficiency with collimated γ sources was inconclusive. The only difference was that one front PMT needed slightly higher voltage for gain matching than would be indicated by the constant gain test data supplied with each PMT. Disassembly of that PMT revealed air gaps in both optical joints of 12 and 14% of the total area. These gaps may have been larger when under compression. All four detectors are now very similar. In the figure the distribution of the front amplitude divided by the sum of front and back amplitudes is displayed. On the left is data from a ^{11}B(d,n) run before fixing the optical coupling. On the right is data from a ^{26}Mg$(^{18}$O$,Xn)$ run after repairs. Data from one of the other detectors is displaced above for comparision, reflecting different experimental conditions.

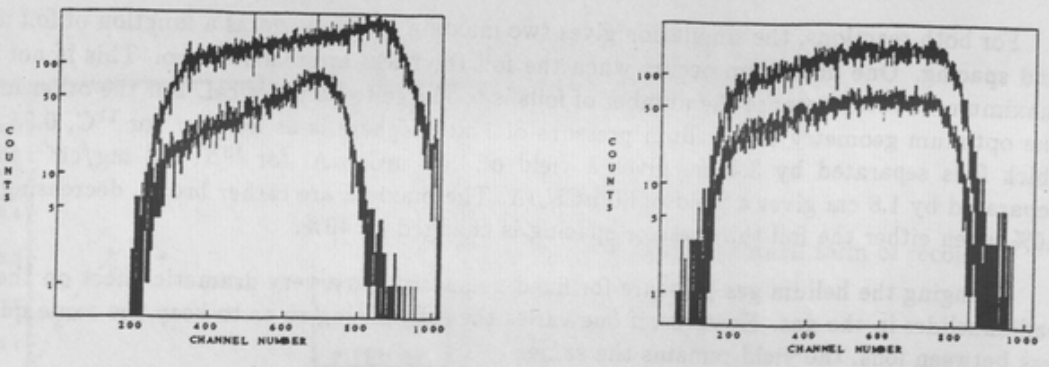

Fig. 10.1.

[1] Bicron Corp.
[2] Phillips
[3] Magnetic Shield Corp.
[4] Dow Corning

10.2 Neutron time-of-flight study

J.F, Amsbaugh, C.E. Hyde-Wright, W. Jiang, P. Magnus and D. Ye

We have constructed an array of four liquid scintillator detectors in order to detect neutron-neutron coincidences from the decay of compound nuclei formed in heavy ion fusion reactions. In the sequential emission of two neutrons of nearly equal energy E_1 and E_2, there is a quantum interference between the amplitude for emission in the order (1,2) or (2,1). This interference results in a suppression of the two neutron yield (relative to the incoherent yield), for n-n relative energies less than the compound nuclear inverse-lifetime Γ.[1] Our goal is to measure neutron-neutron coincidences with sufficient resolution to independently measure the width and depth of this suppression. Our detectors are each 5"ϕ by 10" long BC501A cells with a 5" PMT at each end. The detector axis is mounted along the line of sight from the target 2 meters away.

We measure neutron energy by time of flight. There are two sources of energy resolution, time resolution and position resolution. The time resolution comes from the time spread of the beam and the detector timing response. We define the time of flight from the average of timing from the two ends of the scintillator. For the detector 10" long it's very important to localize the event detected. The amplitude ratio Front/(Front+Rear) is linear in the longitudinal position of conversion. We correct the flight path with this quantity.

We measure the neutron energy resolution with $^{11}B(D.n)^{12}C^*$ reaction. After carefully balancing the gain and correcting the position of conversion, we obtain a curve shown below which is a fit to the observed width of four states in ^{12}C, from which we extract a position resolution of 3.6 cm FWHM and a time resolution of 1.3 ns.

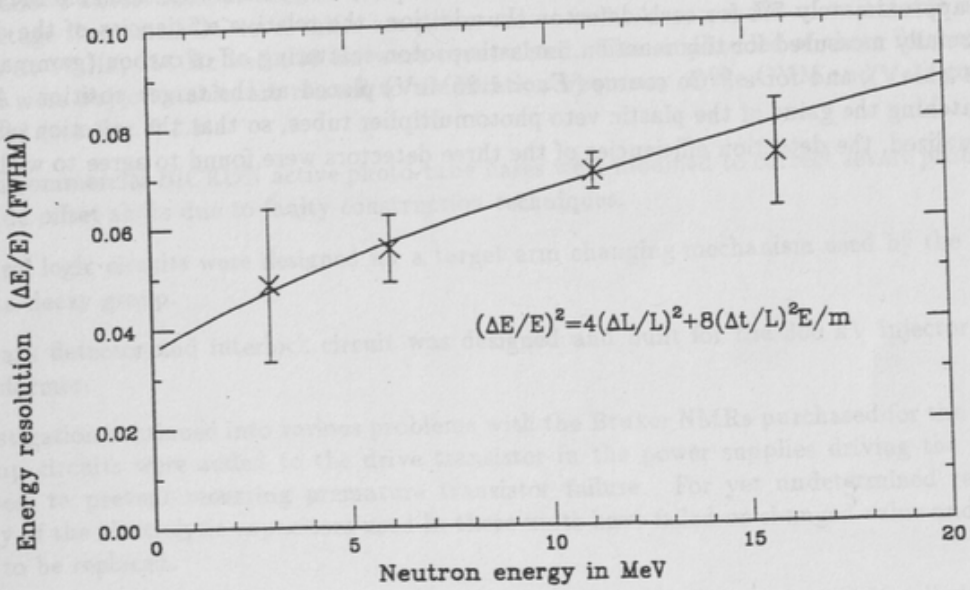

Fig. 10.2. Energy resolution as a function of energy.

[1]S.E. Koonin, W. Bauer, A. Schäfer, Phys Rev Lett. **62** 1247 (1989).

10.3 The barium fluoride array

M.S. Kaplan, D.J. Prindle, K.A. Snover, R. Vandenbosch and D. Ye

Installation of three BaF_2 detector assemblies for high energy gamma decay studies is now complete. Each assembly consists of a 17 cm long by 14.5 cm diameter BaF_2 crystal and a 5 inch Hamamatsu R1251 photomultiplier tube, surrounded by a one inch thick annulus of plastic scintillator and four inches of lead shielding. In front of the BaF_2 crystal is a one inch thick disk of plastic scintillator and a 2.5 inch thick heavymet (90% W) collimator. The plastic scintillator is primarily used to veto cosmic ray events. A LED light pulser system for monitoring the BaF_2 gain is currently being installed in the detectors.

The BaF_2 assemblies are mounted on carts that allow independent positioning in distance from the target and angle from the beam axis. An assembly can be positioned so that the front face of the crystal is between ten inches and 25 inches from the target. Two inserts have been made for each collimator, one tapered for a distance of ten inches and corresponding to a geometrical acceptance of 0.73% of 4π, and the other is tapered for a distance of 20 inches and has an acceptance of 0.29% of 4π.

A table has been built to support the BaF_2 assemblies and carts on the opposite side of the beam from the large NaI detector. A small modification to the NaI cart was required to allow a strong central support post for the BaF_2 table which is required because of the weight of the BaF_2 assemblies. The central post acts as a support for the BaF_2 table, a pivot for the NaI cart and a mount for the scattering chamber.

Recently, several in beam tests of the three BaF detectors were performed. Spectra taken for the $^{11}B(p,\gamma)$ reaction at $E_p = 7.25$ MeV indicate the energy resolution for 22.6 MeV gamma rays is approximately 7% for each detector. In addition, the relative efficiencies of the detectors were carefully measured for this reaction, inelastic proton scattering off of carbon (gamma-ray energy = 4.44 MeV), and for a ^{60}Co source ($E_\gamma = 1.25$MeV) placed at the target position. After carefully matching the gains of the plastic veto photomultiplier tubes, so that the rejection efficiencies were equalized, the detection efficiencies of the three detectors were found to agree to within about 1%.

10.4 Electronic equipment

R.E. Stowell and T.D. Van Wechel

Again this year a large portion of the electronic shop's time was spent on maintenance and repair rather than on design and construction projects. Some projects that were undertaken included:

a A YEASU HF transmitter was extensively modified to allow pulsed keying of the excitation for the weak field cavity on the polarized ion source. An RF leveling loop was added to accurately control the amplitude of the RF excitation of the weak field cavity. This unit replaces an older unreliable vacuum tube unit (see Section 11.11).

b Modifications and improvements were made to the commercial tandem NMR display chassis to correct recurring C.R.T. display problems. Poor original construction techniques eventually led to high voltage breakdown and intermittent loss of the NMR trace.

c Considerable time and effort went into developing chemical safety procedures for the printed circuit photo etch room, including proper disposal procedures and a storage area for used materials.

d Two additional active photo-tube bases using op-amps as the active element were built to supplement the one completed last year.[1] These bases are to be used on the barium fluoride detector array on the gamma ray spectrometer.

e In conjunction with the AMS group, several circuits were built to provide more careful observation of the tandem GVM signal and to perhaps provide improved GVM controlled regulation of the tandem in the future. A DC offset circuit was constructed that subtracts the DC component from the GVM signal and amplifies the resulting difference by a gain of 100. This allows observation of the AC component of the GVM similar to AC coupling with the advantage that small DC level shifts are preserved as well. Also, a series of switchable notch filters at 57 Hz, 114 Hz and 800 Hz were constructed. The amplitudes of these frequencies which were objectionable, are related to the rotation frequency of the GVM and were greatly reduced (see Sec. 5.2.1).

f Seven commercial BICRON active photo-tube bases were modified to correct severe problems with dc offset shifts due to faulty construction techniques.

g Control logic circuits were designed for a target arm changing mechanism used by the Mass 8 beta decay group.

h A spark detector and interlock circuit was designed and built for the 300 kV injector deck transformer.

i Investigation continued into various problems with the Bruker NMRs purchased for the linac. Clamp circuits were added to the drive transistor in the power supplies driving the NMR probes, to prevent recurring premature transistor failure. For yet undetermined reasons many of the electrolytic capacitors used in these units have failed or changed value and have had to be replaced.

j Three high quality cable runs between Cave 2 and Counting Room 4 were installed using Andrews LDF4-50A cable. These will be used for the energy signals from the barium fluoride photo-tube array on the gamma ray spectrometer.

[1] Nuclear Physics Laboratory Annual Report, University of Washington, p.72 (1991).

11 Van de Graaff and Ion Sources

11.1 Van de Graaff accelerator operations and development

C.E. Linder and W.G. Weitkamp

The most prominent difficulty with the tandem during the year was that the charging belt dumped charge onto the HE column, leading to vertical instability in the position of the beam as it exited the tandem. This problem and the current attempt at a solution are discussed in Sect. 11.12.

We have installed two sets of new resistors in the tandem, replacing about half of our 17 year old resistors. Our new resistor assembly design, which was based on extensive in-accelerator testing, consists of 4 Kobra[1] resistors in a PVC tube. Each resistor has a value of 100 MΩ, a tolerance of 1% and a maximum operating voltage of 32 kV. The first set of assemblies was installed in April 1991 and the second set in October 1991. In February 1992, we removed a sample of each set and measured the resistances, comparing them to a standard assembly. The first set, in the accelerator 11 months, decreased in value by 8.8% and the second set, in the accelerator 5 months, decreased by 1%. The larger decrease is unexpected; our test resistors didn't show this much change. Hopefully this is just the result of a "seasoning" process and the resistors will hold this value for the long term. We are currently preparing a third set of 100 resistor assemblies for installation in the machine.

Our beam tubes are beginning to show signs of spark damage to the glass insulators. Beam tubes 1, 3 and 4 now have operated at voltage for 57,000 hours. Tube 3 shows especially severe spark tracking, leading us to install half-value resistors across the first two active insulators in the tube to reduce the voltage stress. To compensate for the resultant change in vertical steering, half-value resistors have also been installed across insulators 13, 14 and 15.

In addition to routine maintenance, we upgraded the tandem water cooling system by installing a sand filter, which is quite effective in keeping the water clean. We also installed a new diffusion pump on the 60 inch scattering chamber and thoroughly leak chased the chamber, removing an accumulation of small leaks.

During the year from March 1, 1991 to February 29, 1992 the tandem operated 4578 hours. Additional statistics of accelerator operations are given in Table 11.1.

[1] K&M Electronics, West Springfield MA 01089.

Table 11.1
Tandem Accelerator Operations
March 1, 1991 to February 29, 1992

Activity	*Days Scheduled*	*Percent*
A. Nuclear Physics Research, Ion Sources Alone	15	4
B. Nuclear Physics Research, Tandem Alone		
Light Ions	24	7
Polarized Ions	17	5
Heavy Ions	34	9
Accelerator Mass Spectrometry	19	5
Subtotal	94	26
C. Nuclear Physics Research, Booster and Tandem Coupled		
Light Ions	16	4
Heavy Ions	56	15
Subtotal	71	19
D. Outside Users		
Boeing Corporation, Tandem	18	5
Boeing Corporation, Tandem and Booster Coupled	2	1
University of Washington Department of Radiology	7	2
Subtotal	27	8
E. Other Operations		
Tandem Development	40	10
Tandem Maintenance	76	21
Unscheduled Time	45	12
Subtotal	161	43
Total	366	100

11.2 Safety improvements in the laboratory

N. Cabot, A. Charlop, D.T. Corcoran, D.W. Storm, H.E. Swanson, R. Vandenbosch, W.G. Weitkamp and D.I. Will

In recent years there has been increasing pressure from Federal, State and University agencies to upgrade the safety environment at laboratories such as ours. Maintaining a safe environment has always been important here,[1] but special emphasis has been placed this year on complying with recent regulations, prioritizing our actions so as to use our limited resources of time and money on those problems most likely to have an impact on actual safety in the laboratory.

To assist in the oversight of our safety program, we have formed a safety committee consisting of a faculty member, the technical director, a graduate student and an employee. This committee has been meeting regularly to monitor safety programs, plan for revisions to Lab safety policy and review new activities for possible hazards.

We have formalized our training program for new students and employees. All new personnel now receive 3 hours of safety training, which includes familiarization with hazards and mitigating procedures for mechanical, chemical, electrical and radiation hazards specific to the Laboratory. This training is in addition to the 4 hours of general laboratory safety training given all entering graduate students at the University.

A great deal of effort has been expended to improve our chemical safety. A thorough clean up of the chemical labs was carried out with about half of our stock, excluding cryogens and solvents, being disposed of as no longer useful for our research. Proper storage facilities were procured for the remaining chemicals, and the chemicals were inventoried. All chemical laboratories were stocked with safety equipment such as spill kits, gloves, aprons, face shields and wall charts describing hazards. Standard procedures have been developed for some of the more common activities involving chemicals; generic procedures available from the University are used to cover other activities.

In the 1960's, a 2000 square foot high bay ceiling in the cyclotron building was sprayed with asbestos as a fire retardant. The recent discovery that some of this material was flaking off led to a full scale abatement project, funded by the University. The entire area was sealed off and contractor personnel scraped off the asbestos while University Environmental Health and Safety personnel monitored the area for possible asbestos contamination. The project affected Laboratory activities not only because the area was inaccessible for three weeks, but because all the apparatus in the area had to be temporarily relocated to accommodate the project.

[1] Nuclear Physics Laboratory Annual Report, University of Washington (1976) p. 20.

11.3 300 kV isolation transformer

G.C. Harper

The injector deck AC power is provided by a 3 phase, 30 kVA transformer designed for 300 kV DC isolation. The primary is delta connected 450 VAC at 20 A, the secondary is wye connected 208 VAC at 83 A, and both windings are electrostatically shielded. A commercially manufactured unit was first put into operation in 1986 and has always been plagued with problems at high isolation voltages. Development of a new isolation transformer for the injector deck AC power which began last year [1] continued and was successfully completed this year.

The tests last year concluded with the failure of a grounded core prototype which used sulphur hexafluoride as the insulating medium. It was believed that using transformer oil instead of an insulating gas might cure the problems experienced with tracking along the surfaces of the polyethylene inter-winding insulation. Oil increased the ultimate track-breakdown voltage from 150 kVDC to over 200 kVDC. It was determined that the core would have to be biased to the mid-potential of the windings in order to increase the effective track length of the insulation wrap.

A rectangular core geometry was adopted to maximize the available volume in the fiberglass tank. The core was biased to the mid-potential with a 15 GΩ resistor string. The primary leads and the secondary leads were enclosed in 2 cm diameter copper conduits integrally connected to the respective shields. One quick attempt was made to use sulphur hexafluoride again, but the prototype could only hold 210 kVDC in the gas. When this unit was submerged in oil it was able to hold 300 kVDC for 24 hours without sparking and withstand 10 rapid charge-discharge cycles.

Two additional units were constructed and tested. Both passed similar tests individually. When the 3 phases were combined in a triangular configuration to form a complete transformer, sparking occurred along the outer tank surfaces in the space between the 3 tanks at 290-300 kVDC. It was determined that the external electrostatic design was such that the electric field increased dramatically at the top and bottom of the tanks when in close proximity. This condition was aggravated by the presence of the steel flange bolts which produced regions of high electric fields outside the tanks at both the top and bottom flange surfaces. The tanks were separated by 6-7 cm and the sparking ceased except in cases where the voltage was increased rapidly without conditioning.

Experience with the repair of internal problems shows that turn around time for repair of one of the units is 2 days with an additional day for conditioning. Repairs and oil conditioning are done in house. The transformer has been run successfully at 300 kVDC for a 4 day long experiment where frequent source changes dictated a need to elevate and de-elevate the injector deck several times. The transformer was conditioned from 240 kVDC to 300 kVDC in about 15 minutes each time the deck was elevated to avoid problems with the external electrostatics caused by the bolts. Plans have been made to eliminate this final problem by replacing the tank flange bolts with insulating threaded rod and nuts.

[1] Nuclear Physics Laboratory Annual Report, University of Washington (1991) p. 80.

11.4 Injector deck and 860i sputter source

G.C. Harper and D.I. Will

Transient suppression has been updated for the high current power supplies for both ion sources. The supplies were originally protected with series elements made from winding the current leads in common mode around ferrite cores and with shunt elements composed of MOV devices or Tranzorbs.[1] The common mode winding was necessitated by the large DC current flowing in the leads. Differential windings would saturate the cores. Large transients from sparks in the sources frequently produced differential spikes energetic enough to reach and damage the supplies. This problem was circumvented by producing large (7.5 cm diameter 7.5 cm long 20T #10 AWG wire) air core inductors as the series elements. The series and shunt elements are mounted on the backs of the power supplies in an isolated high voltage rack. This seems to have eliminated the transient problems.

The software for the computer control of the injector deck, polarized ion source, pre-tandem optics and low energy buncher has been entirely restructured to increase efficiency. Three other additions specific to the injector deck were made. Two sets of XY electrostatic steering plates previously used only in local control have been added to the computer control system. The menus for the portable knob boxes in the tunnel and the console areas have been updated to include hardware changes and to facilitate beam tuning. The power-up sequence for the on-deck beam chopper has been put under remote control, which permits the chopper to be turned on and off with the deck elevated.

The ionizer for the 860i sputter source[2] was modified this past year to speed and ease replacement. The previous design consisted of four helical turns of tantalum coaxial heater surrounded by three loosely attached molybdenum heat shields covering the outer surface and ends of this ionizer coil. Whenever an ionizer failed (usually seen either as an open inner conductor or as a short between the inner conductor and the grounded shell of the coaxial tantalum heater), the whole assembly including the three shields was discarded and a new assembly fabricated. The new design places these three heat shields on the inner surface of the chamber surrounding the ionizer. This modification permits replacing only the tantalum coaxial heater coil itself. The three layer molybdenum shield need only be removed from the ionizer chamber, cleaned, and put back into place each time the tantalum heater coil is replaced with a new one.

[1] Tranzorb is a trademark of General Semiconductor Industries, Inc.

[2] This is a General Ionex Corporation Model 860 Negative Ion Sputter Source modified as described in Nuclear Physics Laboratory Annual Report, University of Washington (1988) p. 52.

11.5 Superconducting booster linac operations

D.T. Corcoran, G.C. Harper, M.A. Howe, D.W. Storm, D.I. Will and J. A. Wootress

During the period March 1, 1991 to Feb 29, 1992, the superconducting booster was operated for 73 days, as compared to 67 days in the calendar year 1990. Beams ranged in mass from protons to ^{58}Ni, with emphasis on ^{4}He, ^{18}O, and ^{32}S. The maximum available fields obtained from the resonators was increased for the low beta resonators. We now are able to obtain average fields of 2.9 MV/m from the low beta resonators, as opposed to 2.8 MV/m obtained last year. We still obtain an average of 2.4 MV/m from the high-β resonators. These fields are the average of all resonators during actual long term operation. The improvement results from replacing some of the low beta resonators with replated ones.

The transmission of beams through the linac has been improved substantially. One of the main sources of poor transmission between the entrance of the linac and the 180° bend was improper buncher tuning. This transmission now is primarily determined by the efficiency of the low energy buncher, and this efficiency is essentially the expected value, that is between 60 and 70%. Transmission to the end of the linac was improved by enlarging some apertures through which the beam must pass. It is now possible to obtain 90% transmission from the 180° bend to the Faraday cup after the rebuncher. All of the beam can be transmitted from that cup to the experimental target through a 3-mm diameter aperture.

After making repairs to stuck couplers and repairing the open power cable mentioned in last years report,[3] we have been able to operate all of our resonators routinely.

We have been using the rebuncher more often, either to achieve good timing or good energy resolution on target. Measurement of these resolutions is limited by the detectors. For alpha particles, for example, 100 keV was measured for a 35-MeV beam using a silicon detector whose resolution was known to be worse than 50 keV. For lithium ions, 100-keV resolution has been obtained for an 87-MeV beam using a detector with an estimated 65-keV resolution. A time resolution of 380 psec was obtained for an ^{18}O beam using a detector with an estimated resolution of 350 psec. Although these figures for FWHM resolution are impressive, there can be tails on the distributions which may have significant impact on a particular measurement.

We have not had to replace any more compressors. The strategy of running the compressors unloaded instead of shutting them down and of starting with the full line voltage seems to be successful in extending their lifetimes significantly. The compressor with the longest running time has run for 49k hours.

[3] Nuclear Physics Laboratory Annual Report, University of Washington (1991) p. 76.

11.6 Efforts towards producing a ^{82}Se beam in the LINAC

A.W. Charlop, D.W. Storm, R. Vandenbosch and D.I. Will

We have made several attempts at producing a 300 MeV ^{82}Se beam as part of an on-going project.[1] We have experienced two problems which, when taken in conjunction, make the production of this beam impractical at this time.

The first problem that we encountered was with the stripper foil lifetime. With a ^{82}Se beam at 9 MV a stripper foil will degrade in approximately 15 min. With a full foil wheel of 180 foils this gives about 2 1/2 days of actual beam time before the tandem must be taken offline for a week for refoiling. We have to use the foil stripper because the lower charge state ions from the gas stripper do not have sufficient velocity for acceleration by the LINAC. These limitations in themselves are not prohibitive. We could do the experiment as several short runs if most of this time was avaliable for data taking. However, when the second problem is considered, the time needed to complete this part of the overall experiment becomes prohibitive.

In order to get the Se beam from the tandem into the LINAC, we need to strip the beam a second time. This is required to put the rigidity of the beam within the operating range of the dogleg magnets and to set the charge state of the beam so that the LINAC can accelerate the beam to the necessary energy. It is accomplished with a stripper foil which is located after the tandem and just before the first dogleg magnet. The fact that this stripper interacts with the full un-analyzed beam coming out of the tandem is the root of our problems. In the current setup, to be able to reach our target energy the Se beam out of the tandem needs to have an energy of 116 MeV and must be stripped to charge state +24 or more. The charge states after the post-tandem stripper range from +18 to +25. Thus charge state +12 out of the tandem second stripped to +24 meets the above requirements. However, the magnetic rigidity of this (+12, +24, 116 MeV) beam is nearly the same as that for the (+11, +23, 107 MeV), (+10, +22, 98 MeV), and (+9, +21, 89 MeV) beams. The magnetic fields needed to select these beams are 9490 gauss, 9511 gauss, 9516 gauss, and 9501 gauss respectively. The momentum resolution of the dogleg is insufficient to select a single one of these beams. Thus it is difficult to get the tandem energy regulation to work. Because the +10 and +11 charge states have higher intensity there are great difficulties in setting up the LINAC.

We could solve this problem by placing the second stripper foil in the high energy column of the tandem midway between the terminal and the high energy end of the acceleration tubes. This would help in two ways. First it would increase the final energy out of the tandem by allowing some acceleration of the second-stripped ions. This would also help acceleration through the LINAC by giving the ions a greater velocity out of the tandem. Secondly, by placing a second stripper in the mid-section of the high energy beam tube, the charge state pair closest in rigidity is about 100 gauss away from the desired pair, which would now be the most intense.

[1] Nuclear Physics Laboratory Annual Report, University of Washington (1991) p. 18.

11.7 Calculation of phases for resonators

D.W. Storm

Until recently, we have been determining the operating phase of each resonator in the linac by first finding its bunching phase (the phase for which there is no energy gain but for which the particles arriving early receive less energy gain than the late particles). This has been done by manually changing the resonator reference phase until the beam was observed on a scanner after the 90-degree bending magnet following the linac section. Provided the beam was centered on the scanner before the resonator was turned on, when the beam is again centered on the scanner there is no energy gain; whether this is the bunching or debunching phase is determined by noting which direction the beam moves with increasing phase. The accelerating phase is 70 degrees away from the bunching phase, and this setting is made with a single touch screen button.

The correct value for the accelerating phase (or the bunching phase) results from a combination of the time of flight of the beam from the beginning of the linac and the arbitrary, but presumably fixed, electronic phase shift for the particular resonator. This is the phase shift resulting from cable lengths and electronic components. We made a calculation of the time of flight assuming uniform acceleration across the resonator gaps and taking into account the locations of the resonators, the gaps, and the energy gain in the resonators. Then we solved for the electronic phase shifts from recorded operating phases. By comparing results for these phase shifts for different runs, we could test the calculation and the assumption of fixed electronic phase shifts. We found similar, but not identical results for these phases for a series of several runs with different ions that occurred over a period of six months. The standard deviation was about 8 degrees.

Even if the calculation of phases were perfect, we would also have to know the resonator fields in advance in order to calculate settings of all the resonator phases for linac tune up. Since there is a small but significant discrepancy between the predicted phases and those obtained in the manual tuning, we decided to incorporate the phase calculation into the automatic tuning program. This program is described in section 11.9. By having an initial estimate of the phase for each resonator, the program can find the correct phase quickly and reliably. Since it adjusts the magnet after setting each resonator, it then checks that resonator's field and has the correct energy gain to use in the phase calculation program for setting the next resonator. Thus, although we cannot calculate all the operating phases from the assumed initial conditions with sufficient accuracy to set the linac, we can use the calculations effectively as initial estimates for an optimization program. In particular, having a good initial estimate prevents the automatic tuning program from finding some spurious beam tail and setting the phase incorrectly.

11.8 Resonator plating development

D.T. Corcoran, M.A. Howe and D. W. Storm

During 1991 we plated and tested a low beta resonator once and a high beta resonator two times. We continued to use the thin plating technique described previously.[1] The low beta resonator plated in this way had a Q factor which decreased with increasing electric field, similar to that observed in the tests reported previously. The resonator required 6.8 W to produce a 3 MV/m field. This value is barely acceptable for the linac.

The high beta resonators exhibited much more electrical discharge during the conditioning period than had the previous ones. Consequently, we were not able to achieve the high field pulse conditioning that we had previously used with the high beta resonators. Low field Q's in the two tests were 2.3×10^8 and 4.5×10^8. The first of these is mediocre and the second quite good. However, associated with the mediocre low field Q was a 3 MV/m field obtained with 17 W, while the resonator with the good low field Q factor required 24 W to reach 3 MV/m. With a high beta resonator, we would like to obtain 3 MV/m with 12 W or less. It is probable that the excessive discharges were related to dust or some other contaminant, and that without the discharges more effective conditioning would provide better high field Q's.

With the thin plating technique, the surface is fairly dull looking, while the resonators which performed successfully for us when we were using the polishing technique were very shiny. Perhaps the combination of oxidation and surface texture leads to the falling Q factor, and if it can be avoided we would be able to obtain better high field Q values. Certainly the electrical discharges are also a significant problem.

We learned that the group at Legnaro had been plating and polishing resonators using a closed system.[2] This technique appears to have the advantage that the lead surface is not exposed to air until after it has been dried, so this oxidation is minimized. Also, they have been using a polishing technique which permits enough control of the amount of polishing that they do not have to plate as thick a lead layer as we had used with our older polishing technique. Keeping the resonator closed should to help keep dust and other contaminants out as well. We have completed the modifications which permit us to polish, rinse, and dry the resonator without exposing it to air. In several tests that we have performed so far, we have found that too much lead is removed at the point where the polish is introduced, and we are trying to rectify this problem.

[1] Nuclear Physics Lab Annual Report, University of Washington (1991) p. 79.
[2] Paulo Busso, LNL, Private Communication.

11.9 Improvements to the linac control systems

G.C. Harper, M.A. Howe, D.W. Storm

In a continuing attempt to automate control of the linac, a program (Autotune) has been written which can find the operating phases of the resonators. It assumes only that the beam is focused and centered on the horizonal slits following the 90 degree dipole after the south row. It then turns on a resonator, calculates the operating phase using the calculation described in section 11.7, changes the reference phase until the beam is found, and then iterates the reference phase until the beam is centered on the slits. Next, now that the bunching phase is known, the actual operating phase is set and the program looks for the beam at the new energy by iterating the dipole current. It then moves on to the next resonator. Using a scanner, the program monitors the tandem beam during this procedure and will pause if the beam is interrupted by a tank spark and resume when the beam returns.

In a recent test of the program, the south row was tuned four times by Autotune with each complete tune taking about 30 minutes. The last four resonators were not included in the test since they are difficult to start. The program will be extended to the north row in the near future.

The injector deck satellite code has suffered from several problems since it was first written several years ago. It was a program originally designed to control just the deck, but then the low energy buncher, and later the polarized ion source were added. As a result communication to the deck satellite was sluggish and the code was a nightmare to maintain. Also the deck Anac boxes would occasionally reset because of voltage transients. The code has been rewritten from scratch in order to address these problems. It now consists of three processes:

- REFRESH. This process rewrites the data base out to the hardware DAC's every few tens of millisecs. This fixes the anac box reset problem.
- SATCMD. This process handles communication from CSX and modifies the data base as needed.
- UPDATE. This process reads the adc's and keeps CSX informed of data base changes.

The new deck satellite code is approximately half the size of the original code and has been designed for easy expansion as new functions are added.

There have been numerous minor additions to the Booster main control program (CSX). They are as follows:

- The tandem terminal voltage and deck elevation are now read by CSX, displayed and used in the dogleg setup calculations.
- The beam current on each Faraday cup is displayed on the cups page, and transmissions are also displayed.
- The list of 24 hour refrigerator trend charts was expanded to show the supply pressure.
- Remote expansion engine controls were implemented and a software closed loop speed controller was added.
- Crew log sheets can now be printed that look like the traditional tandem log sheets but have some values filled in by CSX from the global data base.

11.10 Cryogenic operations

M.A. Howe, D.I. Will and J.A. Wootress

The booster linac is cooled by liquid helium which is thermally shielded by liquid nitrogen. The liquid nitrogen is delivered in lots of ~6000 gallons by semitrailer tanker. In 1991 liquid nitrogen consumption was similar to 1990 at 241,000 gallons.[1] The helium is purchased as high purity bulk gas and liquified by our helium refrigerator. Usage of 115,400 SCF in 1991 was down 25% from that in 1990 (when there were four major power outages.) During 1991 a warm helium supply system, a bed-and-engine vacuum pumping system, and a purge gas recovery system were completed. These facilitate engine and bed deriming by warm-up, evacuation, and purge. The following table summarizes our maintenance for January 1, 1991 to December 31, 1991:

Item	In Use	Major Services	Times Performed
Refrigerator			
Cold Box	100%	warm/pump/purge	0
Main Dewar	100%	warm/pump/purge	0
Top Expander	~7241 Hrs	warm/pump/purge	16
	~100 RPM	main seals	1
		wristpin, crank, and cam follower brngs	1
		valve rod and valve seals	1
		flywheel bearings	1
Middle Expander	~7818 Hrs	warm/pump/purge	16
	~130 RPM	main seals	1
		wristpin, crank, and cam follower brngs	1
		valve rod and valve seals	1
		flywheel bearings	1
Wet Expander	~5118 Hrs	warm/pump/purge	6
	~40 RPM	main seals	1
		wristpin, crank, and cam follower brngs	1
		valve rod and valve seals	1
		flywheel bearings	1
Screw Compressors			
RS-1	49,259 Hrs	total/running	
	8605 Hrs	1991	
		replaced charcoal/oil	0
RS-2	45,726 Hrs	total/running	
	6936 Hrs	1991	
		replaced charcoal/oil	0
RS-3a	15,504 Hrs	total/running	
	8418 Hrs	1991	
		replaced charcoal/oil	0
Distribution System	99%	warm/pump/purge lines	0

[1] Nuclear Physics Laboratory Annual Report, University of Washington (1991) p. 78.

11.11 The crossed-beams polarized ion source

D.T. Corcoran, C.A. Gossett and G.C. Harper

In the past year, the crossed-beams polarized ion source was used in two data taking runs. During May, in a 5 day run, polarized protons were accelerated to 9.0-19.0 MeV. At the end of June, in a 6 day run, polarized deuterons were accelerated to 1.5 MeV and 13.0 MeV.

A new, solid state RF generator was acquired for use with the weak field hyperfine transition cavity. The old generator was a home-built unit using vacuum tube technology. It was run open loop into a mismatched load which reflected 80% of the forward power. An impedance matching network was designed and installed in the cavity housing. A feedback controller using the rectified signal from a probe in the cavity was designed and built to drive the new amplifier and reduce drift in the RF drive signal. The probe signal is conditioned by an inverting amplifier with a short differentiation time constant. This signal is compared to a setpoint level which is keyed by the cavity flipping signal. The difference between the probe and the keyed setpoint is amplified and limited to stay within the acceptable input range of the RF unit. This signal is applied directly to the final mixer stage in the RF amplifier, bypassing the rise and fall delays required by the FCC for transceivers. The new system operates with less than 5% reflected power and less than 0.5% RF amplitude drift.

The cryopumps for the cesium gun region and neutralizer region of the source showed signs of wear after close to 8 years of operation. The pumps required frequent regeneration and pumped to unsatisfactory base pressures. Both pumps were sent to the factory for refurbishment and have been returned, installed, and are now working properly.

11.12 Tandem charging system update

C.E. Linder, T.A. Trainor and W.G. Weitkamp

The present belt has been running for well over a year with compound stainless steel shim belt charge applicators. The belt performance is indicated by the typical 1 μA rms corona current variations and 1 kV rms stripper voltage variations required to hold the terminal to a constant voltage within a few tens of volts. These noise figures are low enough that stable beam can be maintained within image slits without control except for occasional adjustment of the upcharge to correct for slow drifts. The stripper correction amplitude directly measures the roughness of the belt surface. The low correction plus visual inspection of the belt surface indicate that the shims are polishing the surface with time. We believe that belt lifetime is further enhanced by ensuring that the belt always falls to the inside belt guides (see below). This means that the outside belt surface will not be overcured and hardened by frictional heating which leads to cracks and accelerated belt failure.

We now routinely check two parameters of the belt positioning each time we are in the pressure tank. The first parameter is the static position of the belt. To measure accurately the distance from the outer surface of the belt to the belt guides, we hold a straight 1/8 in. drill rod vertically along the belt with a small magnet positioned half way up the belt. The second parameter we measure is the charging current at which the belt falls from its uncharged position to a position in which it is rubbing either on the inside or outside belt guides. This motion can easily be observed by looking down through the column at the midsection. We know that when the static position of the center of the outer surface is 0.230 in. from the outer belt guides, the belt sometimes falls inward and sometimes outward at a charging current of 280 μA. As the static position is moved in or out, the belt falls consistently in one direction and at a smaller current.

Throughout the year, we have had difficulty with the belt transferring charge onto the column near the quarterpoint. This shows up as anomalously high high-energy column current, as much as 60% higher than the low energy column current. The vertical position of the beam is affected because the additional column current disrupts the normal field gradient along the vertically-inclined-field beam tube. Since this is a phenomenon that we didn't observe until a few years ago we speculate that it is due to deteriorating belt guide insulators. We note that the electric field normal to the belt surface due to the upcharge is 75% of the axial column field (up to 1.8 MV/m), but that the surface distance across a belt guide insulator is only 3 mm. We are planning to upgrade some fraction of the column belt guide insulators in the near future.

12 COMPUTER SYSTEMS

12.1 Acquisition system developments

M.A. Howe, C.E. Hyde-Wright, R.J. Seymour, T.A. Trainor

Our principal data acquisition system consists of a Digital VAXStation 3200 running VMS v4.7a. We use VWS/UIS as the "windowing" software. The VAXstation supports a BiRa MBD-11 controlled CAMAC crate. The VAXStation's BA-23 cabinet is cabled into a BA-23 CC expansion cabinet, with a MDB DWQ11 Qbus to Unibus converter driving our old PDP 11/60's Unibus expansion bay. Our Qbus peripherals include an Aviv DFC 904 controller with a 760 megabyte Maxtor disk drive, a TTI CTS-8000 8mm tape system, a DEC IEQ11 IEEE-488 bus controller, and a DEC DRV11-J. The Unibus bay contains a DR11-C, our Printronix lineprinter controller and a Unibus cable to the MBD-11.

This main CAMAC system contains interface modules for our dozen Tracor Northern TN-1213 ADCs. Those ADCs and the CAMAC modules are controlled by an in-house built synchronization interface, which includes routing-Or capabilities, and 32 10-digit 75 MHz scalers.

Additional CAMAC space is available for our LeCroy 2249's, 2228's and 2551's. We are still beset by the LeCroys' problem with lockup if gates arrive during their Clear interval. We now have two FERA 4300B ADCs which move from system to system as needed.

Our acquisition software is based upon TUNL's XSYS, with major modifications to their DISPLAY program.

We have two additional VAX-based acquisition systems. They run as a VMS v4.7a two-member cluster. Each consists of a VAXstation 3200 with an Able Qniverter directly connecting to an MBD-11. There is no Unibus "drawer" required. One has two disk drives, and the other is a diskless satellite. They are both mounted in roll-around rack cabinets, and can be moved throughout the building as needed. Neither has the main system's complex external interfacing equipment.

Our PDP-11-based versions of MULTI/QDA and SINGLES are still running at TANDAR, Argentina's vertical tandem Van de Graaff center in Buenos Aires. Communication and visits keep us informed of their developments. They are preparing to install our version of XSYS next month.

12.2 Analysis and support system developments

M.A. Howe, C. Hyde-Wright, R.J. Seymour and T.A. Trainor

Our principal interactive system is still an 8 megabyte VAX 11/780 running VMS version 4.7, with connections to thirty-odd local terminals. Our in-house functioning VAX complement now includes the main 11/780, three VAXstation 3100/30's, a VAXstation 3100/38, five VAXstation 3200's, and a VAXstation 2000. There are three additional 3200's serving the Nuclear Theory group. One VAXstation II/GPX is currently located at SLAC. We have three independent clusters in the building, primarily to isolate missions, VMS versions, and interruptions. TGV's Multinet provides us with TCP/IP access to Internet. Our principal Internet address is npl.washington.edu. Bitnet access is via the campus central site's VAXes and IBM 3090 system.

TUNL's XSYS is our primary offline analysis package, although we also run two versions of LAMPF's Q on two VAXStations. Conversion programs for other data formats are written on an

as-needed basis.

Our color DECStation 3100, running Digital's Ultrix v4.2, is primarily used for Wolfram's Mathematica, but now we have also ported CERN's GEANT and PAW to it. Some Monte Carlo packages have also be implemented on it to make use of its speed advantage over our VAXstations.

The newest hardware is a pair of HP 9000/710 "Snake" systems. They were purchased for sheer numbercrunch power and compatibility with X-windowing tracking software being developed for the SVT project. See Section 12.3 for a report on pre-purchase acceptance testing.

As with any new system, the 710's arrival included a number of "hiccups" which slowed their full implementation, in part due to HP's delivery of an obsolete pre-installed version of their Unix product (HP-UX). Split shipments gave us our computers, but the CDrom drive to load the newer software is still some weeks away. The CDrom drive from the INT site (see below) has been pressed into service, and is working. The old version (8.05) of HP-UX does not support Exabyte 8mm drives. Version 8.07 doesn't "support" them, but does include a usable driver. We had successfully implemented the driver on the demonstration system and performed a week's worth of Monte Carlo runs. The as-delivered new 710's could not read those tapes.

A bug was found in an interaction between the Unix "tar" (tape archive) program and the 8mm driver HP supplied. It was reported to them via Usenet's comp.sys.hp. The "bug" was in part caused by the Exabyte 8200's response to a "write zero filemarks" command (used by HP to flush the drive's buffer). The Exabyte 8200 actually wrote a filemark. This symptom is Exabyte PROM-version dependent. We borrowed a newer Exabyte 8510 from R-Squared and demonstrated that they did not respond that way. HP has changed the driver for its release in version 9.0 of HP-UX.

An indication of the state of our 11/780 was the recent "gift" of another campus site's 11/780 containing twice the memory of our own machine. Parts shall be transplanted between the two systems to maximize performance.

The Nuclear Theory Group's installation grew by the addition of more campus-surplus equipment: four RA-81's and two RA-82 disk drives.

We also provide some system management services for the Institute for Nuclear Theory. That remote site now has three DECstation 5000/200's, each with 32 Mbytes of memory, color displays, and a total of 5 gigabytes of disk. Two 4mm DAT drives and a CDrom drive "float" throughout the installation. As their usage has grown, and to provide better expertise in Unix management, system management duties are now shared with the main Physics site.

12.3 A dual HP-710 RISC workstation system for high speed data analysis

J.G. Cramer, R.J. Seymour and D.J. Prindle

The Nuclear Physics Laboratory has recently received a capital equipment grant from the US Department of Energy. This grant is for the purchase of a fast RISC workstation and associated peripherals to be used primarily for the analysis of NA35 data from the Fall–1991 and Spring–1992 runs and for performing FRITIOF/GEANT simulations to predict detector response to relativistic heavy ion collisions.

The capital equipment proposal to the DOE, as it was originally structured, proposed the purchase of a single Hewlett-Packard 9000/720 RISC workstation, three 19" color X-terminals, disk and tape drives, and software. However, in the time interval between the submission and funding of the capital equipment proposal the HP 9000/710 workstation was announced. The HP 710 is rated at about 88% the speed of the HP 720 (or about 50 time the speed of a VAX 11/780) and is significantly cheaper than the HP 720. We found that two HP 710s and two 19" color X-terminals could be accommodated within the capital equipment budget, with a significant increase in net processing power and flexibility for the same expenditure. Therefore, we have purchased two HP 710 workstations along with two X-terminals, peripherals and software.

As an example of the flexibility of the resulting two workstation system, we plan to take one of the HP 710 workstations to CERN for 7 weeks during the Spring–1992 NA35 run for use in analysis of NA35 TPC data as it arrives. We will leave the other workstation in Seattle for use in simulations and program development. Since the two machines can be directly linked by telnet across 9 time zones, both data and programs can be freely transferred between systems while the experiment is in progress.

Although the new HP 710 workstations have not yet arrived in the laboratory at this writing (3/18/92), we have been able to borrow a demonstration HP 710 unit on which we have been running representative CPU/floating-point intensive programs to determine compatibility and running times. The following comparisons were generated using HP f77 Fortran operated with sufficient physical memory to avoid page swapping. Comparisons below, which were made with DEC Ultrix, used the DEC RISC Fortran compiler, (not the MIPS compiler).

Machine	Run Time	f77 Compiler Options Used	System
HP 710	92.6 sec	+E1 OP4 O3 Wl,-a,archive	8.07
HP 710	92.8 sec	+E1 OP4 OS O3 Wl,-a,archive	8.07
HP 720	90 sec	+E1 OP4 OS O3 Wl,-a,archive	8.05
HP 730	70 sec	+E1 OP4 OS O3 Wl,-a,archive	8.05
DECstation 5000/240	64 sec	(default)(-O4)	Ultrix 4.2
DECstation 5000/200	103 sec	(default)(-O4)	Ultrix 4.2
DECstation 3100	166 sec	(default)(-O4)	Ultrix 4.2
VAXstation 3100/38	455 sec	(default)	VMS 5.4-2
VAXstation 3100/30	786 sec	(default)	VMS 5.4-2

These results were disappointing. At this point we used InterNet to ask for suggestions from the international community of HP users. Bob Montgomery of Hewlett Packard suggested a slight

recoding of two subroutines of the test program which used multiple calls of the SIND and COSD routines, since the HP optimizer does not move repeated calls of SIND and COSD to a common sub-expression area. DEC's Ultrix Fortran and VMS Fortran both perform that optimization (and, in fact, VMS provides a routine which evaluates both SIN and COS in one call. The modified test program generated these new timings.

Machine	Run Time	f77 Compiler Options Used	System
HP 710	47.5 sec	+E1 OP4 O3 Wl,-a,archive	8.07
HP 720	51.2 sec	+E1 -O Wl,-a,archive	8.05
DECstation 5000/240	63.6 sec	-O5	Ultrix 4.2
DECstation 5000/240	69.5 sec	(default)(-O4)	Ultrix 4.2
DECstation 3100	170 sec	(default)(-O4)	Ultrix 4.2
VAXstation 3100/30	535 sec	(default)	VMS 5.4-2

Thus, with a slight modification of the code (changing about 6 lines of 500) we have improved the previous results with the HP 710 by more than a factor of three. It is interesting that the HP 710 appears to be slightly *faster* than the HP 720 in these tests.

We are grateful to Bo Thide of the Swedish Institute of Space Physics, who suggested the use of the "-Wl,-a,archive" option and provided the HP 720/730 timings.

13 APPENDIX

13.1 Nuclear Physics Laboratory personnel

Faculty

Eric G. Adelberger, Professor
John G. Cramer, Professor
Ludwig de Braeckeleer, Research Assistant Professor
George W. Farwell, Professor Emeritus
Cynthia A. Gossett, Research Assistant Professor[1]
Pieter M. Grootes, Research Associate Professor, Geological Sciences and Physics
Isaac Halpern, Professor
Blayne R. Heckel, Associate Professor
Charles E. Hyde-Wright, Assistant Professor
Alan M. Nathan, Visiting Professor[2]
Kurt A. Snover, Research Professor
Derek W. Storm, Research Professor; Director, Nuclear Physics Laboratory
Thomas A. Trainor, Research Associate Professor
Robert Vandenbosch, Professor
William G. Weitkamp, Research Professor; Technical Director, Nuclear Physics Laboratory

Research staff

Marc Frodyma, Research Associate[3]
Jens H. Gundlach, Research Associate
Mitchell Kaplan, Research Associate
Paul Magnus, Research Associate
David Sesko, Research Associate
Douglas Wells, Research Associate
Danzhao Ye, Research Associate
Xianzhou Zhu, Research Associate

Predoctoral research associates

John A. Behr[4]
Jeff Bierman
Thomas A. Brown
Nick Cabot
Aaron Charlop
Pakkin Chan
Ziad M. Drebi
Alejandro García[5]
Michael Harris
S. John Luke
Diane Markoff
Brian McLain
Douglas P. Rosenzweig
William Schief
Gregory Smith
Yue Su
Kenneth Swartz
Bruce Thompson[6]

[1]On leave at: High Technology Center, Boeing Space and Defense Group, Seattle, WA 98124.
[2]Permanent address: University of Illinois, Nuclear Physics Laboratory, Champaign, Il 61820.
[3]Now at: SLAC, Bin 44, PO Box 4349, Stanford, CA 94309.
[4]Now at: Graduate Physics Building, Center Drive, SUNY at Stony Brook, Stony Brook, NY 11794-3800.
[5]Now at: Lawrence Berkeley Laboratory, B-88, 1 Cyclotron Road, Berkeley, CA 94720.

Weidong Jiang

Professional staff

John F. Amsbaugh, Research Engineer
Gregory C. Harper, Research Engineer
Mark A. Howe, Research Engineer
Duncan Prindle, Research Scientist
Richard J. Seymour, Computer Systems Manager
Rod E. Stowell, Electronics Engineer/Electronics Shop Supervisor
H. Erik Swanson, Research Physicist
Timothy D. Van Wechel, Electronics Engineer
Douglas I. Will, Research Engineer

Technical staff

Dean T. Corcoran, Engineering Technician
James Elms, Instrument Maker
Louis L. Geissel, Instrument Maker, Student Shop Leadman
Carl E. Linder, Engineering Technician
Hendrik Simons, Instrument Maker, Shop Supervisor
John A. Wootress, Accelerator Technician

Administrative staff

María G. Ramírez, Administrative Assistant
Karin Hendrickson, Office Assistant

Part time staff

Hazen Babcock
Marshall Balick
Joyce Buchheit
Jan Chaloupka
Christopher Cochran
Erik Dybwad
James Evans
Qing Feng
Shawn Golliher
Christopher Lee
Caitlin Mitchell
Lawrence Norton
Manish Rohila
Todd Rudberg
Jim Vance
Eric Vandervort

[6]Now at: University of Washington, Physics Department, Seattle, WA 98195.

13.2 Degrees granted, academic year 1991–1992

Ph. D. Degrees:

"Giant Dipole Radiation and Isospin Purity in Highly Excited Compound Nuclei," John A. Behr, Ph. D. Thesis, University of Washington, (1991).

"Two Problems in Nuclear Astrophysics: The Efficiency of the ^{37}Cl Neutrino Detector and Explosive Hydrogen Burning," Alejandro García, Ph. D. Thesis, University of Washington (1991).

13.3 List of publications

Published papers:

"Inclusive inelastic scattering of 96.5 MeV π^+ and π^- by the hydrogen and helium isotopes," M.A. Khandaker, M. Doss, I. Halpern, T. Murakami, D.W. Storm, D.R. Tieger and W.J. Burger, Phys. Rev. C. **44**, 24, 1991.

"Analysis of multiparticle Bose-Einstein correlation in ultra-relativistic heavy ion collisions," J.G. Cramer, Phys. Rev. C **43**, 2798, (1991).

"Empirical density dependent effective interaction for nucleon-nucleus scattering at 500 MeV," B.S. Flanders, J.J. Kelly, H. Seifert, D. Lopiano, B. Aas, A. Azizi, G. Igo, G. Weston, C. Whitten, A. Wong, M.V. Hynes, J. McClelland, W. Bertozzi, J.M. Finn, C.E. Hyde-Wright, R.W. Lourie, B.E. Norum, P. Ulmer, B.L. Berman, Phys. Rev. C. **43**, 2103 (1991).

"Electroexcitation of negative-parity states in ^{18}O," D.M. Manley, B.L. Berman, W. Bertozzi, T.N. Buti, J.M. Finn, F.W. Hersman, C.E. Hyde-Wright, M.V. Hynes, J.J. Kelly, M.A. Kovash, S. Kowalski, R.W. Lourie, B. Murdock, B.E. Norum, B. Pugh and C. P. Sargent, Phys. Rev. C. **43**, 2147 (1991).

"Electron scattering from ^{9}Be," J.P. Glickman, W. Bertozzi, T.N. Buti, S. Dixit, F.W. Hersman, C.E. Hyde-Wright, M.V. Hynes, R.W. Lourie, B.E. Norum, J.J. Kelly, B.L. Berman and D.J. Millener, Phys. Rev. C. **43**, 1740 (1991).

"Spectrum of ^{9}Be from proton scattering," S. Dixit, W. Bertozzi, T.N. Buti, J.M. Finn, F.W. Hersman, C.E. Hyde-Wright, M.V. Hynes, M.A. Kovash, B.E. Norum, J.J. Kelly, A.D. Bacher, G.T. Emery, C.C. Foster W.P. Jones, D.W. Miller, B.L. Berman, Phys Rev C, 1990.

"Structure of ^{9}Be from proton scattering at 180 MeV," S. Dixit, W. Bertozzi, T.N. Buti, J.M. Finn, F.W. Hersman, C.E. Hyde-Wright, M.V. Hynes, M.A. Kovash, B.E. Norum, J.J. Kelly, A.D. Bacher, G.T. Emery, C.C. Foster W.P. Jones, D.W. Miller, and B.L. Berman, Phys. Rev. C. **43**, 1758 (1991).

"Carbon isotopic composition of atmospheric CH_4: fossil and biomass burning source strengths," P.D. Quay, S.L. King, J. Stutsman, D.O. Wilbur, L.P. Steele, I. Fung, R.H. Gammon, T.A. Brown, G.W. Farwell, P.M. Grootes and F.H. Schmidt, Global Biogeochemical Cycles **5**, 25 (1991).

"Accelerator mass spectrometry dates on bones from Old Crow Basin, Northwest Yukon Territory," R.E. Morlan, D.E. Nelson, T.A. Brown, J.S. Vogel and J.R. Southon, Canadian Journal of Archaeology **14**, 75 (1990).

"Accelerator Radiocarbon Dates from the NOGAP Archaeology Project," J.S. Vogel, T.A. Brown, J.R. Southon and D.E. Nelson, Canadian Archaeological Association Occasional Paper **1**, 143 (1991).

"T-violation experiments using Mössbauer transitions," A. Schäfer and E.G. Adelberger, Z. Phys. A - Hadrons and Nuclei 339, 305, 1991.

"β^+ decays of ^{37}Ca: implications for the efficiency of the ^{37}Cl solar ν detector," A. García, E.G.

Adelberger, P.V. Magnus and H.E. Swanson, O. Tengblad and Isolde Collaboration, D.M. Moltz, Phys. Rev. Lett. **67**, 3654, 1991.

"Is the weak axial-vector current renormalized in nuclei?," E.G. Adelberger, A. García, P.V. Magnus and D.P. Wells, Phys. Rev. Lett. **67**, 3658, 1991.

"Searches for new macroscopic forces," E.G. Adelberger, C.W. Stubbs, B.R. Heckel and W.F. Rogers, Ann. Rev. Particle and Nuclear Science **41** (1991).

"Statistical analysis of neutron interferometer detection systems," G.I. Opat, Rev. Sci. Instrum. **62** (1991).

"Stark effect for a rigid symmetric top molecule: exact solution," G.I. Opat and J.V. Hajnal J. Phys. B. Atomic, Molecular and Optical Physics **24**, 2799 (1991).

"The fall of charged particles under gravity," T. Darling, F. Rossi, G.I. Opat and G. Moorhead, Rev. Mod. Phys. **64**, 237 (1992).

"The precession of a Foucault pendulum viewed as a beat phenomenon of a conical pendulum to a coriolis force," G.I. Opat, Am. J. Physics **59**, 822 (1991).

"High spin and shape coexistence in ^{73}Se," M.S. Kaplan, J.X. Saladin, D.F. Winchell, H. Takai, J. Dudek, Phys. Rev. C. **44**, 668 (1991).

"Cluster-impact-fusion yields: no collective effect for small water clusters," R. Vandenbosch, T.A. Trainor, D.I. Will, J. Neubauer, and I. Brown, Phys. Rev. Lett. **67** 3567, 1991.

"Search for high energy γ rays from the spontaneous fission of ^{252}Cf," S.J. Luke, C.A. Gossett and R. Vandenbosch, Phys. Rev. C. **44**, 1548, 1991.

"The solution of a charging belt problem," W.G. Weitkamp, T.A. Trainor and C.E. Linder, in *Symposium of North Eastern Accelerator Personnel*, World Scientific, 1991, p. 69.

"Comparison of giant dipole resonance decay in stiff ^{92}Mo and soft ^{100}Mo excited nuclei," M. Kicinska-Habior, K.A. Snover, J.A. Behr, C.A. Gossett, J.H. Gundlach and G. Feldman, Phys. Rev. C. **45**, 569 (1992).

Papers submitted or to be published:

"Angular momentum distributions in sub-barrier fusion reactions," R. Vandenbosch, submitted to Annual Reviews of Nuclear Science.

"Radiocarbon AMS dating of pollen extracted from peat samples," T.A. Brown, G.W. Farwell, P.M. Grootes and F.H. Schmidt, Radiocarbon (1992), in press.

"Intra-annual variability of the radiocarbon content of corals from the Galapagos Islands," T.A. Brown, G.W. Farwell, P.M. Grootes, F.H. Schmidt and M. Stuiver, submitted to Radiocarbon.

"Interpreting the small isotope signal," P.M. Grootes, submitted to Radiocarbon.

"Measurements of the electric and magnetic form factors of the proton from $Q^2 = 1.75$ to 8.83 $(\mathrm{GeV/c})^2$," P.E. Bosted, L. Clogher, A. Lung, L. Stuart, J. Alster, R.G. Arnold, C.C. Chang,

F.S. Dietrich, R. Gearhaert, J. Gomez, K. Griffioen, R. Hicks, C.E. Hyde-Wright, C. Keppel, S. Kuhn, J. Lichtenstadt, R. Miskimen, G. Petratos, S. Rock, S. Rokni, W. Sakumoto, M. Spengos, K. Swartz, Z. Szalata, L.H. Tao, and W. Dodge, Submitted to Phys Rev Lett, March 1992.

"Photon scattering for ^{4}He: the charge symmetry problem revisited," D.P. Wells, D.S. Dale, R.A. Eisenstein, F.J. Federspiel, M.A. Lucas, K.E. Mellendorf, A.M. Nathan and A.E. O'Neill, submitted to Phys. Rev. C.

"Evidence for a phase transition in the nuclear shape at finite temperature and rapid rotation," M. Kicinska-Habior, K.A. Snover, J.A. Behr, C.A. Gossett, Y. Alhassid and N. Whelan, submitted to Phys. Rev. Lett.

Published conference proceedings and invited talks:

"Open problems in sub-barrier fusion," R. Vandenbosch, Eighth Winter Workshop on Nuclear Dynamics, Jackson Hole, Wyoming, 1992.

"Interplay between pion absorption and inclusive-inelastic scattering on hydrogen and helium isotopes for 96.5-MeV kinetic energy pions," D.W. Storm, Mesons and Light Nuclei V, Prague, Few-Body Syst., Suppl. **5**, 219, 1992.

"Nucleon radiative capture and the inverse reaction at intermediate energies," I. Halpern, Beijing International Symposium on Fast Neutron Physics, Beijing, China, 1991.

"Charged pion Hanbury-Brown-Twiss interferometry with large ultra-relativistic sources," J.G. Cramer, Spring APS Meeting, Washington, DC, April 22–25, 1991.

"Compton scattering on the proton," C.E. Hyde-Wright, SLAC Workshop on High Energy Electroproduction and Spin Physics, Feb. 5–8, 1992.

Abstracts and other conference presentations:

"Inclusive photoproduction of π^+ on nuclei at 215 MeV," D.P. Rosenzweig, M. Frodyma, I. Halpern, D.W. Storm, K.G. Fissum, J.C. Bergstrom, H.S. Caplan, M. Doss, K. Garrow, E.L. Hallin, G.V. O'Reilly, D.M. Skopik, J.M. Vogt, Bull. Am. Phys. Soc. (1992).

"Nuclear Rainbow Scattering in ^{6}Li + ^{12}C at 14.5 MeV/nucleon," J.G. Cramer, S.J. Luke, B.T. Mclain, D.J. Prindle and W.J. Braithwaite, Bull. Am. Phys. Soc. (1992).

"Isospin purity in intermediate mass compound nuclei," D.P. Wells, K.A. Snover, J.A. Behr, Z.M. Drebi and M.S. Kaplan, Bull. Am. Phys. Soc. **36**, 2116 (1991).

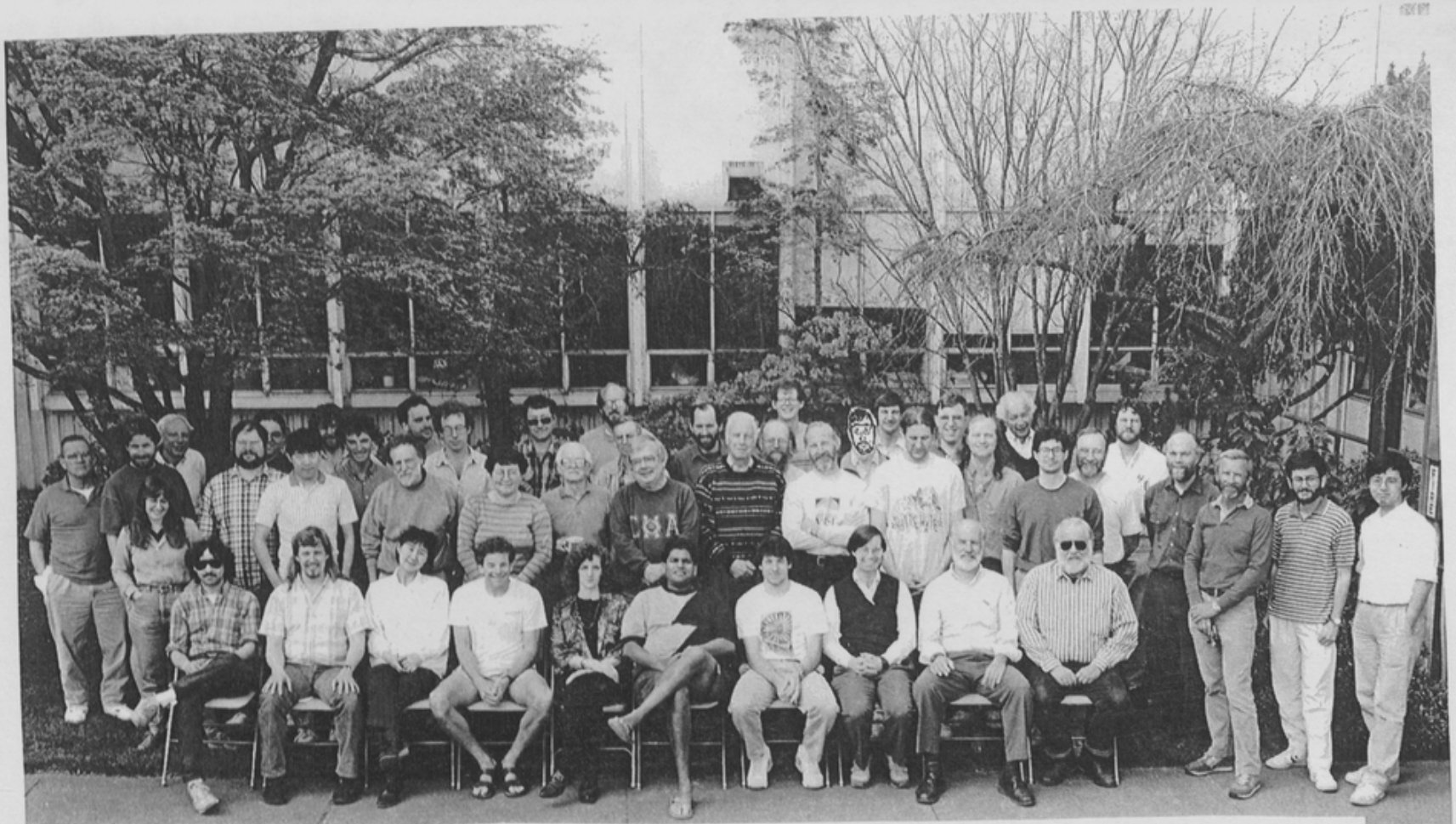

Front row: M. Kaplan, A. Charlop, Y. Su, W. Schief, K. Hendrickson, S.J. Luke, K. Swartz, C. Hyde-Wright, W. Weitkamp, C. Linder

Second row: D. Markoff, W. Jiang, E. Swanson, M. Ramirez, L. Geissel, R. Stowell, G. Farwell, P. Grootes, G. Harper, D. Rosenzweig, D. Storm, K. Snover, Z. Drebi, D. Ye

Third row: J. Wootress, D. Sesko, R. Vandenbosch, N. Cabot, 1/2 of J. Bierman, 1/2 of T. Brown, J. Gundlach, D. Wells, M. Harris, J. Elms, M. Howe, H. Simons, T. Van Wechel, R. Seymour, G. Smith, T. Trainor, B. Mclain, D. Corcoran, D. Prindle, I. Halpern, D. Will, J. Amsbaugh